

Autonomous Augmentation of Audio

Perception: Au³

(Thesis format: Monograph)

by

Thomas E. Doyle

Faculty of Engineering Science
Department Electrical and Computer Engineering

Submitted in partial fulfillment
of the requirements for the degree of
Doctor of Philosophy

Faculty of Graduate Studies
The University of Western Ontario
London, Ontario, Canada

© Thomas E. Doyle 2006



Library and
Archives Canada

Bibliothèque et
Archives Canada

Published Heritage
Branch

Direction du
Patrimoine de l'édition

395 Wellington Street
Ottawa ON K1A 0N4
Canada

395, rue Wellington
Ottawa ON K1A 0N4
Canada

Your file Votre référence

ISBN: 978-0-494-30696-3

Our file Notre référence

ISBN: 978-0-494-30696-3

NOTICE:

The author has granted a non-exclusive license allowing Library and Archives Canada to reproduce, publish, archive, preserve, conserve, communicate to the public by telecommunication or on the Internet, loan, distribute and sell theses worldwide, for commercial or non-commercial purposes, in microform, paper, electronic and/or any other formats.

The author retains copyright ownership and moral rights in this thesis. Neither the thesis nor substantial extracts from it may be printed or otherwise reproduced without the author's permission.

AVIS:

L'auteur a accordé une licence non exclusive permettant à la Bibliothèque et Archives Canada de reproduire, publier, archiver, sauvegarder, conserver, transmettre au public par télécommunication ou par l'Internet, prêter, distribuer et vendre des thèses partout dans le monde, à des fins commerciales ou autres, sur support microforme, papier, électronique et/ou autres formats.

L'auteur conserve la propriété du droit d'auteur et des droits moraux qui protègent cette thèse. Ni la thèse ni des extraits substantiels de celle-ci ne doivent être imprimés ou autrement reproduits sans son autorisation.

In compliance with the Canadian Privacy Act some supporting forms may have been removed from this thesis.

Conformément à la loi canadienne sur la protection de la vie privée, quelques formulaires secondaires ont été enlevés de cette thèse.

While these forms may be included in the document page count, their removal does not represent any loss of content from the thesis.

Bien que ces formulaires aient inclus dans la pagination, il n'y aura aucun contenu manquant.


Canada

THE UNIVERSITY OF WESTERN ONTARIO
FACULTY OF GRADUATE STUDIES

CERTIFICATE OF EXAMINATION

Supervisor

Dr. Zdenek Kucеровsky

Supervisory Committee

Examiners

Dr. William Greason

Dr. Gerasimos Moschopoulos

Dr. Argyrios Margaritis

Dr. John Makaran

The thesis by

Thomas E. Doyle

entitled:

Autonomous Augmentation of Audio Perception: Au3

is accepted in partial fulfillment of the
requirements for the degree of
Doctor of Philosophy

Date _____

Chair of the Thesis Examination Board

Abstract

The control and communication in man and the machine has been an active area of research since the early 1940's and since then the usage of the computing machine for the augmentation or rehabilitation of man has been broadly investigated. One active area of such research is the interface of the human brain to the computer; brain-computer-interfacing (BCI). The current few successful examples of functional BCI control the computer screen cursor movement, but require extensive subject training and significant, if not full, cognitive focus. Our model proposed an alternative approach to implementing the BCI for the application of controlling a digital hearing aid by autonomously modifying the speech signal based on the identification of electrophysiological response, or an affective state. The speech communication channel was studied and the individual's hearing threshold tested while the brain activity measured using surface skin electrodes and the author's designed bioelectric amplifier. The subject acknowledgement was used as reference for which a response had previously just occurred. Using the response from a threshold 8-kHz audio tone a set of data samples is extracted for the training of a statistical learning method; the support vector machine (SVM) classifier. The SVM has the ability to produce a very high classification accuracy on small training sets of data by mapping input attribute data to span across a higher order feature space and using the features space to calculate a non-linear soft decision boundary (hypersurface) for classification. The training data output distribution was uncertain in the respect that a response had occurred, but its precise time of occurrence and duration is a component of our the investigation. The SVM is *taught* using several output approximations and their results compared using an independent testing set of data. The reduction of data dimensionality was investigated using a Laplacian electrode array for source density estimation and the θ , α , β , and γ frequency ranges were also extracted from the Laplacian for model analysis. The results of our model were very encouraging with successful binary classification greater than 90% for raw electroencephalographic, raw Laplacian, and filtered Laplacian testing measurements. Our model successfully demonstrated the efficacy of autonomous single trial identification of affective states as an alternative or additional method of hearing prosthetic control at a communication transfer rate of 240 bits/second.

Acknowledgements

The author would like to acknowledge his chief advisor, Dr. Z. Kucеровsky, for his continuous motivation, guidance, and support. The knowledge gathered from a life of learning is better consumed with good coffee.

I would like to sincerely thank Dr. W. D. Greason for his suggestions and support and to my colleagues Adrian Ieta, Martin Flatley, Damian Trybus, Duane Jacques, and Raymond Chokelal for enriching my graduate experience. I would also like to thank the electronic shop and Mr. Gerrit Aartsen for his time and technical expertise.

My friends and family, your support has been truly appreciated.

To my Allie, your voice of reason was there when my own was silent. You are my favourite affective state.

Contents

Certificate of Examination	ii
Abstract	iii
Acknowledgements	iv
Contents	v
List of Tables	viii
List of Figures	ix
Nomenclature	xi
1 Introduction	1
1.1 Scope of Research	11
1.2 Overview	15
2 Theoretical Section	16
2.1 The communication channel	16
2.1.1 Production	17
2.1.2 Transmission: sound and vibration	20
2.1.3 Reception and Perception	21
2.2 Hearing impairment	23
Types of Loss	23
Determining Loss	23
Psychological Affect of Hearing Loss	26
2.2.1 Methods of correction	26
2.3 Electrophysiology	29
2.4 Electrophysiological Signals of Interest	29
2.4.1 The eye and electrooculography (EOG)	30

	Electrooculography	30
	Vector Positioning	32
2.4.2	The brain and electroencephalography (EEG)	32
	The human brain	32
	Standard electrode placement	37
	Alternative electrode placement	37
2.5	Data processing	39
2.5.1	Filter design	41
	Frequency sampling filter	43
2.5.2	Data reduction	51
	Source density analysis	51
2.6	Data attributes and classification	55
2.6.1	Support vector machine classification	56
3	Experimental Section	66
3.1	Subject preparation	66
3.2	Subject positioning	68
3.3	Data acquisition	69
3.4	Hardware	70
3.4.1	Electrophysiological Amplifier	70
	Interface	73
	Filtering and amplification	74
	Output and isolation	74
3.4.2	Microcontrollers	74
3.5	An electroocular computing interface	75
3.5.1	Objective	75
3.5.2	Background	75
3.5.3	Procedure	75
3.5.4	Observation	76
3.5.5	Discussion	77
3.6	Electrophysiological Response to Auditory Tones: Threshold	78
3.6.1	Objective	78
3.6.2	Background	78
3.6.3	Procedure	79
3.6.4	Observation	80
3.6.5	Discussion	80
4	Model and Analysis	83
5	Discussion, Conclusion, and Recommendations	98

Appendix A: Subject A Experimental Results	102
Appendix B: Threshold Data Analysis Files	123
Appendix C: Single Channel Schematic of Electrophysiological Amplifier	125
Bibliography	127
Vita	138

List of Tables

2.1	Brain Rhythm Frequency Ranges	33
4.1	Minimum and maximum correct SVM classification	88
4.2	Best classification for least computational cost	88
4.3	Laplacian source density approximation minimum and maximum correct SVM classification (250 ms, $\sigma = 0.5$)	96
4.4	Filtered θ <i>vs.</i> α Laplacian source density approximation minimum and maximum correct SVM classification (250 ms, $\sigma = 0.5$)	96
4.5	Filtered α <i>vs.</i> β Laplacian source density approximation minimum and maximum correct SVM classification (250 ms, $\sigma = 0.5$)	97
4.6	Filtered $\alpha\beta$ <i>vs.</i> γ Laplacian source density approximation minimum and maximum correct SVM classification (250 ms, $\sigma = 0.5$)	97

List of Figures

1.1	A Time Line of Digital Electronic Computing	2
1.2	The Neuron and Synaptic Structure	6
1.3	Dual Feedback for Autonomous Augmentation	12
2.1	Speech Articulators	18
2.2	Motion of a Tuning Fork	21
2.3	Components of the human ear	22
2.4	Author's audiogram	25
2.5	The Three Categories of Hearing Aids: a) Analogue, b) Digitally Programmable Analogue, c) Fully Digital.	28
2.6	Electrooculography: changes in electric field due to eye movement. (a) centered, (b) movement from center towards negative electrode, (c) movement from center towards positive electrode	31
2.7	Electrooculography electrode placement. Electrodes $x+$ and $x-$ measure the horizontal, and $y+$ and $y-$ measure the vertical movement.	31
2.8	Horizontal, Vertical and Resultant Vectors	31
2.9	Classification of brain activity research	35
2.10	Sensory associated regions of the human brain	36
2.11	The standard 10-20 electrode placement	38
2.12	An alternate electrode placement by Vidal <i>et al.</i>	40
2.13	An alternate electrode placement by Doyle <i>et al.</i>	40
2.14	Traditional N-tap non-recursive FIR filter structure	42
2.15	N-section frequency sampling filter structure	42
2.16	Type-II frequency sampling filter magnitude response (β filter)	50
2.17	Type-II frequency sampling filter phase response (β filter)	50
2.18	Source density approximation using a vanishingly small volume unit	54
2.19	Source density analysis: unit Laplacian electrode arrays	54
2.20	Analogue source density computation	55
2.21	SVM diagram	60

3.1	Subject positioning	71
3.2	Data acquisition system overview	71
3.3	Overview of single channel electrophysiological biological amplifier components: 1) interface, 2) filtering and amplification, and 3) output and isolation	72
3.4	Electrophysiological amplifier frequency response for fixed input of $4 \mu V_{pp}$	72
3.5	Horizontal (x -axis) DC record of eye movement	78
3.6	Subject-A hearing threshold response	81
3.7	Subject-B hearing threshold response	81
3.8	Subject-C hearing threshold response	82
3.9	Author's hearing threshold response	82
4.1	Experimental trials and their relation to training and testing data	87
4.2	Support vector machine training input and output	87
4.3	Subject-A parametric plot using 250 ms classification window	90
4.4	Subject-A parametric plot using 500 ms classification window	91
4.5	Subject-B parametric plot using 250 ms classification window	92
4.6	Subject-B parametric plot using 500 ms classification window	93
4.7	Subject-C parametric plot using 250 ms classification window	94
4.8	Subject-C parametric plot using 500 ms classification window	95

Nomenclature

$\langle x, y \rangle$	vector coordinate
α/μ	brain frequency band 8–13 Hz
β	brain frequency band 13–22 Hz
δ	brain frequency band 0.5–4 Hz
γ	brain frequency band 22–30 Hz
\mathfrak{R}^n	Data generator of n dimension
\mathbf{x}	input \ attribute space vector
\mathbf{z}	feature space vector
∇	Divergence - partial derivative
∇^2	Laplacian - second order partial derivative
Ω	ohm, SI unit of resistance or impedance
Ψ	electric flux
ρ_v	volume charge density
\mathbf{D}	electric flux density vector
\mathbf{E}	electric field intensity vector
\mathbf{H}	horizontal vector
\mathbf{R}	resultant vector
\mathbf{S}	closed surface

\mathbf{V}	vertical vector
θ	brain frequency band 4–8 Hz
Φ	attribute to feature space mapping function
$d(\mathbf{x})$	decision hypersurface function
$i_F(\mathbf{x})$	indicator function
K	Kernel function
L	Lagrangian
v	volume
10-20	International standard method for surface electrode placement
A	Ampere, SI unit of electric current (C/s)
ADC	Analog to Digital Converter
BCI	Brain Computer Interface
BP	Bereitschafts potential
C	coulomb, SI unit of electric charge
CNV	Contingent Negative Variation
DAC	Digital to Analog Converter
DARPA	United States Defense Advanced Research Projects Agency
ECG/EKG	Electrocardiogram
EEG	Electroencephalogram
EMG	Electromyogram
EOG	Electrooculogram
ERP	Event Related Potential
F	farad, SI unit of capacitance
FIR	Finite Impulse Response

FSF	Frequency Sampling Filter
$h(n)$	time domain transfer function
$H(z)$	frequency domain transfer function
Hz	cycles per second
IIR	Infinite Impulse Response
MEG	Magnetoencephogram
NLS	oN-Line System
Q	electric charge
s	second, SI unit of time
SI	Système International d'Unités
SVM	Support Vector Machine
TTD	Thought Translation Device
V	Volt, SI unit of electric potential difference
$v(n)$	time domain difference equation
$V(z)$	frequency domain difference equation
VEP	Visual Evoked Potential

Chapter 1

Introduction

The improvement, augmentation, and rehabilitation of human attributes through technology has ever been a primary goal of science and engineering. These enhancements must not only be scientifically and physically sound, they must also achieve a social acceptance before being widely adopted. Notable examples of such assistive technologies are corrective eye wear and the hearing aid. Both serve to compensate for deficiencies in these primary senses as a result of maltreatment, ailment, age, or heredity.

Corrective eye wear use glass and plastic lenses to change the incident angle of light as it enters the eye to strike the correct focal point (the retina). With the exception of research to restore sight to the blind using a retinal implant [1], this process remains analogue and it fully performs its task as such.

Hearing assistive devices have traditionally amplified sound into the region in which a subject can hear using analogue electronics. Hearing aid technology has been analogue over the last hundred years [2]. However, it is believed that the analogue method of hearing correction may have reached a rehabilitative

limit and that more advanced digital signal processing will be needed to improve a user's hearing. The digital hearing aid has matured to the point where it offers greater computational complexity density [3] than its analogue predecessor, but unfortunately, almost all except the most recent commercially available digital hearing aids were no more than digital implementations of the analogue device and provide little, if any, further processing.

The increased computational density of the digital hearing aid is representative of the decreasing physical size and increasing computational power of electronic computers in general. For reference, a time-line of digital electronic computing has been provided in Figure 1.1. From the first electronic computers in the 1940's, the Anastoff-Berry Computer¹ (ABC) and the Electronic Numeric Integrator and Calculator² (ENIAC), that filled entire buildings to the present, where devices of similar and greater computational ability may be carried on our person.

As the benefits and abilities of these early computers were explored, their implications were met with some trepidation. In his 1947 treatise of Cyber-

¹The ABC was developed at Iowa State University for solving large numbers of simultaneous equations

²The ENIAC was developed by the United States military to compute World War II ballistic firing tables

Electronic Computers	Batch Processing	Time Sharing Systems	Private/Industrial Computing	Personal Computing and Connectivity	Increasing Computational Density
1945	1950	1965	1975	1980	1990 present
Vacuum Tubes	Transistors	Integrated Circuit Technology	Supercomputers	Graphical User Interface	Laptops/Palmtops/Digital Assistants
Machine Language Programming	Magnetic Core Memory	Operating System Software	Microcomputers	IBM PC (desktop)	Wireless networking
ENIAC	Assemblers	Teleprocessing	Workstations	Portable Computing	GHz Microprocessors
	Compilers	Microprocessors	Apple II (desktop)	LAN/WAN/WWW	Technology Convergence
	UNIVAC 1		Altair/IMSAI		Wearable Computing
	IBM 704				

Figure 1.1: A Time Line of Digital Electronic Computing

netics: or Communication and Control in the Animal and Machine [4] Norbert Wiener described the use of the computer as the modern industrial revolution that would “devalue the human brain”. Although Wiener’s comments were meant to underscore the social implications of the technology, his prediction has seen some truth today.

The application of electronic computing machines was initially very specialized because of fixed pathways for data and instructions; these pathways were hardwired. The proposals of the mathematician John von Neumann to use the computer’s own memory to create these pathways (making them “softwired”) and the fundamental computer architecture³ of how memory, the central processing unit, and input/output were interconnected and organized electronic computing machines for endless possible applications.

As a young engineer, Douglas Engelbart came to the realization that man’s ability to process large and/or complex volumes of information was falling behind the ever increasing rate of new information. In 1963, Engelbart [6] proposed a conceptual model for the computer augmentation of man’s intellect to enhance or extend his innate capabilities. His system divided *augmentation* into four basic categories:

1. Artifacts - physical objects designed to provide for human comfort, and the manipulation of both physical objects and symbolic information.
2. Language - the way in which the individual classifies the picture of their world into the concepts that their mind uses to model that world, and the symbols they attach to those concepts and uses in consciously ma-

³It is of interest to note that von Neumann studied in the workings of the human brain in comparison to digital electronic computers [5]. It is this author’s belief that von Neumann’s computer architecture was derived from his research into the organization and operation of the human brain.

nipulating the concepts (“thinking”).

3. Methodology - the methods, procedures and strategies with which an individual organizes thier goal-centered activity.
4. Training - the conditioning needed by the individual to refine thier skills to the point where they are operationally effective.

Engelbart’s proposal foreshadowed much of his future research [7–9] in the augmentation of the human intellect by organizing shared information across computer communications systems (“Bootstrapping”). By present technological and communication standards, this concept may appear rudimentary, but Engelbart’s demonstration of this work, the NLS (oN-Line System), pre-dates the United States Defense Advanced Research Projects Agency’s (DARPA) similar initiative; the ARPANET, or the “internet” predecessor. In fact Engelbart’s NLS (also known as AUGMENT) was the precursor to ARPANET and was its second host computer [10]. Many of our modern computer interfaces such as the mouse and WYSIWYG word processing [11] can be traced back to Engelbart’s research.

The computer interface has been an active area of research for as long as there have been computing devices. One such interface research path has been the direct coupling of the human brain to a computer; the brain computer interface (BCI). In 1973, Vidal published a “modest experimental program” [12] that outlined a systematic attempt on direct brain-computer communication using the electroencephalogram (EEG) and the theory of both voluntary and event related potentials (ERP). Vidal outlined three basic assumptions fundamental to the program’s success:

1. Mental decisions can be probed using observable bioelectric signals, in

particular using the fluctuations of electroencephalographic potentials from the human scalp.

2. All meaningful electroencephalographic phenomena should be viewed as a complex structure of elementary wavelets that sequentially represent individual cortical events that create a stream of neuroelectric messages.
3. Operant conditioning procedures can increase the reliability and stability of these time signatures and patterns.

Vidal noted that these assumptions did not completely agree with the then contemporary literature, but that extensive experimental data supported his assumptions. Vidal concluded his program would require several years of maturity before suitable computational electronics would become available. Referring to Figure 1.1, the reader may observe that it was not until about 1975 that general purpose digital computers were becoming more prevalent. In 1977 Vidal presented his work on detecting and classifying individual evoked responses (“a single epoch”) in real-time by using the computer as an impartial observer to classify the evoked response [13]. Most research at this time was focussed on averaging the ERPs from repeated evoking stimulus of a single electrode site because of technical limitations. Although averaging is a valid and efficient method of signal recovery from noise, it can also mask short or singular events of relevant data. Under experimental conditions, Vidal’s system had a correct classification of greater than 90%.

Vidal described the early work presented by H. Berger’s 1929 demonstration of the possibility of recording the electrical activity of the brain from the surface of the skull. The brain is a complex chemical and electrical structure composed of nerve cells (neurons). Each neuron consists of a body (soma),

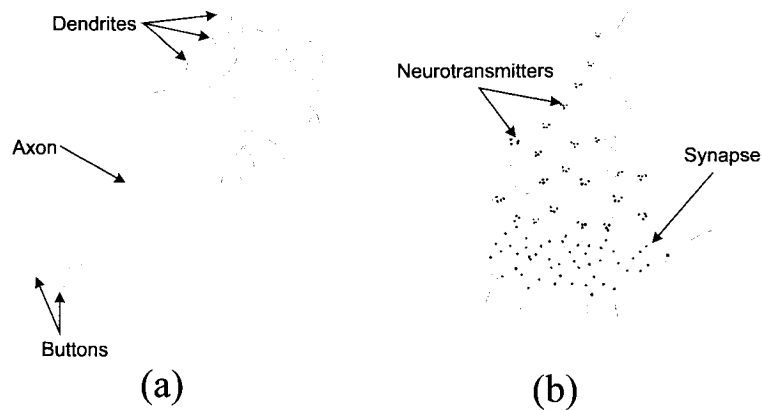


Figure 1.2: The Neuron and Synaptic Structure

several short input channels (dendrites) and a long output channel (axon). Neurons may be interconnected one-to-one, one-to-many, many-to-many, and many-to-one. This array of connections function similarly to digital logic AND-OR circuitry. The neuronal connection interface is electrically unidirectional and the transmission of the nerve impulse may be described in three parts:

1. Presynaptic - Dendritic input potentials sum at the presynaptic membrane neuron interface. When the threshold potential (approximately -70 mV) is reached the nerve excitation begins a change (depolarization) in membrane permeability producing an ionic exchange across the synaptic junction. This initiates the action potential output along the axon
2. Action potential - The action potential propagates along the axon causing the nerve to become negative to adjacent regions and to “sink” current from adjacent nerves. This in turn causes the adjacent nerves to

become negative relative to their surrounding regions and propagating their self-excitation. Duration of the action potential is typically 1 ms.

3. Postsynaptic - After the action potential the nerve must reestablish ionic equilibrium. This is a prolonged period of positive potential (repolarization). Duration is typically 15 to 200+ ms.

Previously, it was believed that the action potential was being measured on the scalp, but in fact its duration and penetration are small relative to the postsynaptic potentials that are summed at the surface of the brain (pyramidal cell membrane) and measured on the scalp surface with the electroencephalogram (EEG). One might expect that the measurement of these alternating polarization and depolarization of such a complex and interwoven structure would produce a Gaussian white noise, however, this is not the case. This “spontaneous” activity contains low frequency rhythmic potentials [14–18]. The correlation of these rhythms to physical or emotional properties is an ongoing research area, but it has been well established that there are distinct rhythms; this agrees with Vidal’s second assumption.

From the time of Vidal’s work researchers have attempted to utilize various properties of the EEG [19–38] to implement a brain-computer interface using surface electrodes. Although successful research exists on subdural and surface-cortical brain-computer interfaces, it is considered too invasive for most applications.

Wolpaw et al. [20] presented work on an EEG-based brain-computer interface for cursor control. Their research was intended to be used by individuals with motor deficits as a neural prosthesis. Wolpaw et al. trained subjects to voluntarily change the amplitude of a specific frequency range of brain rhythm (μ) for control of a one-dimensional cursor. This result was significant be-

cause it demonstrated the ability of a subject to quickly and accurately change the amplitude of a specific frequency range of their brain current. This research was further extended to two-dimensional cursor control [21, 23, 24, 31, 35] and binary (yes/no) responses to spoken questions [25].

Birbaumer et al. [27–29, 39] have focussed on subjects that are completely locked-in with amyotrophic lateral sclerosis (ALS). These subjects suffer complete paralysis while maintaining completely intact cognitive and sensory functions. These researchers have successfully implemented a spelling interface (SI) for the paralyzed using voluntary control of slow cortical potentials (SCP) to control a two-dimensional cursor or a binary selection using a modified Huffman’s algorithm. This research was further extended to the “Thought Translation Device” (TTD) where instead of continually selecting letters the subject could select common words or icons to increase the communication bandwidth. Birbaumer et al. [40] published research on the psychophysiological structure of emotion with some clinical perspectives. They present their case against a basic set, or a fundamental set, of emotions (e.g. joy, anger, fear, etc.) because their classification was subjective; however, the use of positron-emission tomography (PET) for the visualization of neural activity of the functioning awake human brain combined with measurement of the electrical (EEG) and magnetic (MEG) activity demonstrated a clear cortical separation between emotional responses from non-emotional “cold” cognitive operations. The implicit implication here is that although classification into a fundamental set of emotions is not tractable, the electrical or magnetic emotional response within the brain is measurable. This agrees with Vidal’s first assumption.

However, measurement of emotional response is not restricted to brain current. Heart rate, respiration, skin conduction, muscular contraction, a focus of gaze, an angry frown, and/or joyful gesture are all examples of measurable

reactions with physiological properties that reflect emotional states. Picard et al. [41–46] proposed an alternative computer interface which employs affective patterns. The interface does not identify general basic emotions, but instead classifies emotional, or affective, responses incorporating both physical and cognitive aspects of emotion. The classification of emotional response is not limited to a single physical or cognitive characteristic; it may combine several. As a simple example, consider the two characteristics of arousal/attention (high and low) and valence (positive and negative) that may be mapped to a vector in two-dimensional space:

1. High arousal and positive valence - e.g. successful completion of a Ph.D. dissertation,
2. High arousal and negative valence - e.g. news of a local disaster,
3. Low arousal and positive valence - e.g. stopping to smell the roses,
4. Low arousal and negative valence - e.g. visiting a local cemetery.

The use of affective states provides a powerful interface for medical monitoring, assistive, and/or personal electronics. These types of electronics are normally smaller, more personal devices adorned about the user’s body and commonly referred to was *wearable computing*. Two specific examples of an affective interface to a wearable computer are the “Startlecam” [41] that records an image of user’s environment upon sudden emotional stress (“startle”) and the quantification of stress during the operation of an automobile [46].

Research into wearable computing has matured quickly, accelerated by the increased computational density of digital electronics. Two of the more prominent researchers in the field of wearables, Starner [47–54] and Mann [55–57], have developed functional systems which they employ for both personal and

professional augmentation with interfaces that are more conventional based. Concurrent with the interface research are the practical computing aspects of generation of power [58, 59], thermoregulation [60], and communications through the skin (Personal Area Network - PAN) [59, 61].

The Wright Patterson Air Force Base's Research Laboratory (AFRL) in Dayton, Ohio, researches and evaluates alternative methods of man-to-machine interface and control [62–64]. These researchers' objective was to provide alternative control of “hands-busy” applications by using wearable computing devices. They have found success in both voluntary and evoked EEG control. As of 2000, the US military started incorporating wearable computing into a soldiers combat gear [65].

Wearable computing is finding application in more mainstream commercial and medical areas. An example of such an application was demonstrated with IBM's prototype Wearable PC [66] which has the power of a Thinkpad⁴ laptop in the size of a portable personal stereo. The incorporation of electronics into textiles (e-broidery) is producing wearable motherboards, physiologically aware “SmartShirts”, and even electronic wallpaper with thermally sensitive inks [67]. Ambulatory medical applications include wireless heart-rate stress monitoring [68], electroencephalography for epilepsy patients [69], and dynamic suppression of upper-limb tremor in Parkinson's patients [70]. The immediate benefit of wearable computing to medicine is the ability to remotely monitor, record, and analyze the patient in their natural and more familiar environment. The real benefit of wearables to medicine will be their integration into augmentative and rehabilitative prosthetics.

The range of wearable computer assisted applications and implementations

⁴In early 2005, IBM sold its personal computer division, including the Thinkpad laptop line, to Lenovo.

is truly an exciting and expanding field. From excitation for posture control [71] to electroocular wheelchair guidance [72], to implanted functional electric stimulators (FES) to restore standing and walking for the paraplegic [73] and to aid in corrective walking [74].

Researchers have employed electrophysiological signals in an effort to enhance, augment or regain subsystems of the body [12,20,28,75,76]. Others have attempted to replicate natural electrophysiological subsystem inputs [77,78].

The hearing aid is perhaps one of the most common prosthetic today; however, it has benefitted relatively little from the advances in brain-computer interfaces and wearable computing. Given its programmability, processing capability, and normal proximity to a wide array of electrophysiological signals, it would appear to be an ideal candidate.

1.1 Scope of Research

Most, if not all, forms of rehabilitative or assistive devices attempt to aid the user by replacing a damaged attribute with a corrective prosthetic. If this augmentation attempts any processing, it normally reduces the attribute to a simplified transfer function with feedback for stability. This leaves the user out of the loop, so to speak. Traditionally, the prosthetic or augmentation is a technological crutch that acquires little, if any, input from it's user. For the individual that has experienced a post-"learned" loss of a normal or innate attribute, this is often ineffectual and frustrating.

Rather than replacing an attribute, we propose to employ the post-"learned" and innate characteristics that remain from the damaged attribute or are associated with it. Our proposed prosthetic could then aid in the user's self-regulation, or internal feedback and at the same time use those characteristics

in its own feedback. In effect, we have two systems, each using the other for stability of its own feedback as illustrated in figure 1.3.

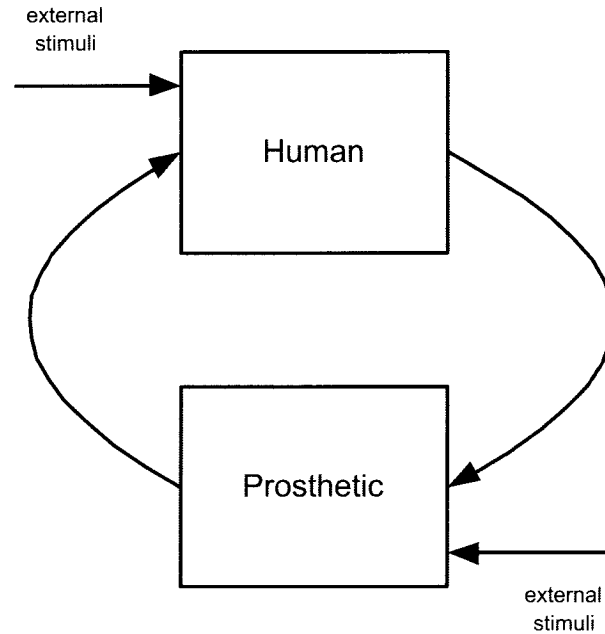


Figure 1.3: Dual Feedback for Autonomous Augmentation

The challenge is to monitor, or observe, the post-“learned” and innate characteristics with as little conscious intrusion as possible. In most cases it would be preferable to perform the observations *in vivo*, however this is not practical for most ambulatory *in situ* measurements. As a result, *in vitro* methods of measurement are necessary. These external measurements are predominantly of the mechanical and electrical subsystem characteristics.

Mechanical subsystem measurements can be restrictive and cumbersome and result in the measurement not being from the natural, original, or appropriate position. However, by placing electrodes on the skin’s surface observa-

tion of the electrical subsystem may be performed with minimal obtrusiveness by measurement of the present electrophysiological signals.

Electrophysiological signals are electrical phenomena related to a physiological event, such as a heart beat or muscular contraction. These signals can be divided into voluntary and involuntary. Depending on the signal or event of interest, there are several types of measurements which may be taken. Some of these measurement types are the Electrocardiogram (ECG or EKG), Electroencephalogram (EEG), Electromyogram (EMG), and Electrooculogram (EOG).

The author's research is focused on an alternative computing interface that incorporates an affective response into the double feedback mechanism to provide an "awareness" of its users internal electrophysiological environment. By looking inward, we have a device which is more responsive to its user, thus creating a truly personal computing device.

Our research proposes a system to augment a hearing impaired subject's audio perception by using the electrophysiological signals related to hearing physiology and affective state of healthy adults. Our application is restricted to the loss of hearing condition called presbycusis. Presbycusis is the gradual hearing loss normally associated with aging; typically the higher frequencies are more effected. Presbycusis is usually a sensorineural hearing disorder, but as with any hearing loss it is a unique combination of damage which is the cause [79]. Independent of the cause, this particular hearing damage effects an increase of the hearing threshold. To reduce the variability in subject hearing damage, our research will approximate the hearing damage on normal hearing and healthy adults by measuring their hearing threshold and presenting the audio of interest below that threshold. The processing, or augmentation, of the audio data shall be to determine when a change to the audio amplification

should occur such that it will be increased above the hearing threshold.

To better understand the problem we will investigate the communication channel from speech production to perception. With the hearing aid normally worn about the ear, our research will focus on the collection and observation of slow cortical potentials and their affective properties. The collection of these signals require the development of a multichannel bioelectric amplifier and data acquisition system suitable for both micro- and milli-volt amplification. Although analysis of this work will be done off-line, our focus is on data processing methods and algorithms for a class of less power computing devices (e.g. a digital hearing aid). This required the use of efficient signal processing, but also reduction of data complexity.

Similar to Vidal's assumptions, this research has three assumptions to its success based upon literature review:

1. Emotional responses, or affective patterns, can be probed using observable bioelectric signals, in particular using the fluctuations of electroencephalographic potentials from the human scalp.
2. All meaningful electroencephalographic phenomena should be viewed as a complex structure of elementary rhythms that have correlation with underlying processes.
3. Although operant conditioning procedures could increase the reliability and stability of these time signatures and patterns, the loss of a normal or innate attribute would invoke a reliable and measurable affective pattern.

This research seeks to prove the efficacy of such a system as an alternative or additional method of hearing prosthetic control. Thus audio processing algorithms based on such control is beyond the scope of this thesis.

Wiener [4] presented a treatise on Cybernetics; the study of control and communication in the animal and the machine. This thesis aims to present the ground work for the area of study of control and communication *between* the animal and the machine; Cybranetics.

1.2 Overview

Chapter 1 provides an introduction and rationale for our research. This chapter describes the intersection of several diffuse areas of study and how we propose their union. This chapter concludes the scope of research and an overview of this document.

Chapter 2 presents the theoretical framework and background material.

Chapter 3 is the experimental work and observations.

Chapter 4 employs the experimental data and presents the result of our off-line processing model.

Chapter 5 is the discussion, conclusion and recommendations.

Chapter 2

Theoretical Section

The theoretical section will provide the framework and background material related to the proposed research. This section will address:

1. the communication channel from the point of speech production to the physiological process of perception,
2. hearing impairment and classical methods of correction,
3. the measure of the electrophysiological signals in general,
4. specific properties of the electrophysiological signals of interest,
5. data processing, and
6. data attributes and classification.

2.1 The communication channel

The human communications system consists of speech, sound, and hearing and as with any communication system, it can be divided into a transmitter,

a transmission medium, and a receiver. The physical and physiological process of human communication is well understood, but the mechanisms that control the speech articulators and hearing comprehension are somewhat of a mystery.

2.1.1 Production

Speech is composed of a collection of sequential complex sounds. The syntax and protocol of these sounds are governed by the rules of grammar that form symbols to convey information based on a cognitive lexicon. The formulation of these sounds is beyond the scope of this research; however, it has been proposed that we are born with the ability to rapidly acquire a meaning for innate concepts and that we use those meanings to develop a lexicon to communicate, using a universal grammar [80]. Rabiner states that the production of these sounds may be modeled with a time-varying linear system [81] that according to Parsons can be divided into two functions; excitation and modulation [82].

Production of speech requires energy. Speech energy is supplied from the expiratory phase of the breathing mechanism. Air flowing out of the lungs generates a steady flow of energy in one direction causing, initially, the vocal cords to oscillate, and then the air particles surrounding them. Fry best describes this as the vibration of a musician's lips on a brass wind instrument [83].

Referring to figure 2.1 we describe the physical flow of air used to produce speech. Air is forced out of the lungs into the trachea. The vocal cords block the passage of air from the trachea to the pharynx. Air pressure (subglottal pressure) increases behind the vocal cords until it overcomes the opposing muscular and elastic forces holding them together. Once open, the ligaments and muscles that make up this region attempt to return to their initial position and do so rapidly, with the aid of the Bernoulli effect, and the pressure building

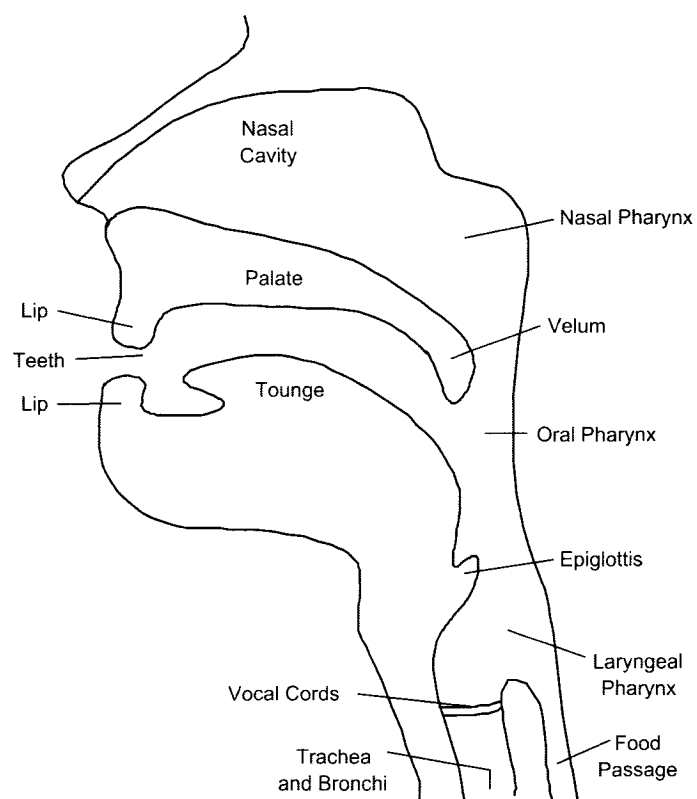


Figure 2.1: Speech Articulators

cycle begins again. This pressure cycle results in continuous pulses of air being released into the space above the larynx which is the basis for sound production, or excitation.

However, the excitation function does not explain the means by which we are able to control the frequency of the sound produced. By manipulating the mass, length, and tension of the vocal cords and the larynx, there are infinite possible configurations and modes of vibration, or modulation.

The pulsed sound waves from the larynx have still to travel outward through the pharynx, oral cavity, past the teeth and lips (vocal tract) and into the air.

The path of nasal cavity through to the nostrils is opened by the lowering of the soft palette, or velum. This segment of the vocal tract is forced into vibration because of the pulsed sound waves from the larynx. The radiated sounds from the lips and nostrils are a result of the changes to the larynx sound wave imposed by the configuration of the remaining pathway(s). The tongue plays the most significant role in acoustically filtering the pulsed sound waves.

The vocal tract may be modeled as a column of air that has a resonant, or fundamental, frequency. The column will have harmonic frequencies that are integer multiples of the fundamental frequency. By manipulating the vocal tract the fundamental frequency is also changed. For speech the average fundamental frequency for men is 120 Hz, for women is 225 Hz, and for children is 265 Hz, with a range from 60 Hz to 500 Hz [83].

The description of speech production becomes more complex because it can be described on three different levels:

1. Linguistic: study of the structure and nature of human speech (i.e. morphology, syntax, dialectology, phonology, etc.).
2. Acoustic: differences in the acoustic levels are due to dialect, physiological characteristics, and speaker mannerisms. These differences may be so great that it is not practical, or possible, to record the actual sounds. So instead, speech is characterized in terms of articulatory gestures. Alternatively, a spectrogram is used.
3. Articulatory: removes the physical characteristics, which cause the differences in acoustic levels, and allows the representation of speech to be done using a formal set of symbols (IPA - International Phonetic Alphabet).

A further confusion is the terminology relating these levels. At the linguistics level, a speech unit is called a *phoneme*, which is translated by an articulatory gesture into a *phone* at the acoustic level. The phoneme is the intended unit of language and the phone is the sound produced.

2.1.2 Transmission: sound and vibration

The propagation of speech sound waves is analogous to the sound produced when a tuning fork is struck. The vibration of the tuning fork produces a displacement of the immediate air particles forcing them into vibration. However the tuning fork will emit a single pure tone, or single frequency, while the human voice is composed of an infinitely possible combination of “tuning forks” producing complex tones, or mixture of frequencies.

There are two types of vibratory wave motion a particle can assume: transverse and longitudinal.

The transmission of sound through air is often compared to the ripple effect a pebble would produce on a still pond. If we consider the pebble in the pond effect along a radial line we see that the individual particle moves up and down, perpendicular to the outward motion of the wave; this is a transverse wave. This type of vibratory motion appears at first to resemble that of a tuning fork as shown in figure 2.2. However, this type of vibration can only occur on the surface of a liquid or in a solid, but it cannot occur in a gas, thus it cannot create sound waves (audible vibration) in air.

The vibration of the tuning fork causes compression and rarefaction of the contiguous air particles, causing them to oscillate along the line of travel; this is a longitudinal wave.

The compression and rarefaction motion of a single particle in a longitu-

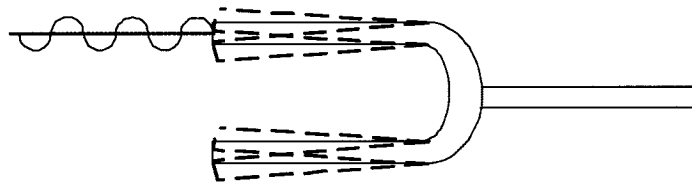


Figure 2.2: Motion of a Tuning Fork

dinal wave causing the rise and fall of air pressure will produce a sinusoidal waveform. However, sound travels omni-directionally from the source; expanding radially.

Any sound that reaches the ear drum is the result of compression and rarefaction of the air particles of a longitudinal waveform.

2.1.3 Reception and Perception

The information contained in human speech comes from more than the words that are used to convey our thoughts. Our auditory system must process speech by translating sound pressure waves into a sequence of electrical impulses that are passed through the nervous system into the brain. Different sounds in our language produce different frequencies of vibration in the ear and these vibrations contain information. The processing of this information is so automatic that we can not consciously be aware of the different vibrations and the information they contain.

The human ear consists of three main parts as illustrated in figure 2.3:

1. Outer ear: the visible part, the auditory canal and the eardrum,
2. Middle ear: the hammer, the anvil, and the stirrup bones, and
3. Inner ear: the cochlea, and auditory nerves.

Sound (compression and rarefaction) enters the auditory canal and strikes the eardrum. The hammer, anvil and stirrup bones convey eardrum vibrations to the cochlea in the inner ear. These vibrations cause pressure waves to travel down the cochlea making the cochlea's tiny hair cells bend creating action potentials. The hair cells are attached to the auditory nerves and this information is transmitted to the brain.

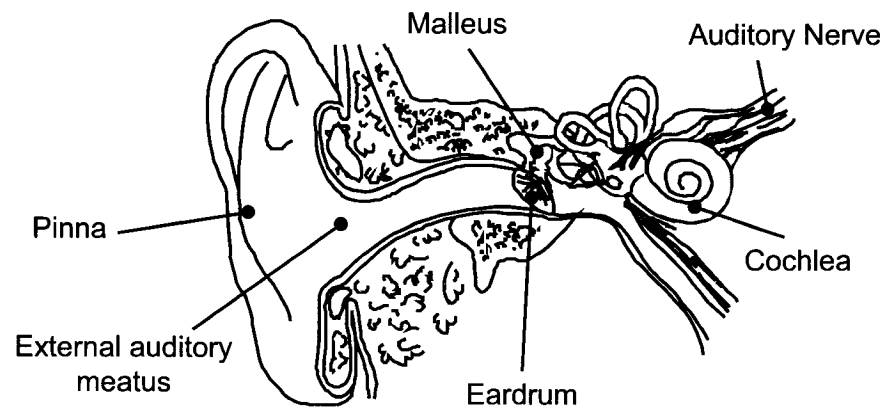


Figure 2.3: Components of the human ear

2.2 Hearing impairment

Simply stated, hearing impairment can be described as a spectrum analyzer with a damaged channel [3]. Admittedly, this definition does not provide a sense of the many types and forms of hearing impairment, but it does give us insight to the resultant problem. The most common form of hearing loss is the mixed type of conductive and sensorineural damage. The degree of hearing impairment varies according to the division of the mix and by the method which the damage occurred.

Types of Loss

Hearing loss can be divided into three general types [84]:

1. Conductive: damage to the outer or middle ear,
2. Sensorineural: impairment to the inner ear or nerves of hearing, and
3. Mixed: a combination of conductive and sensorineural.

If we restrict our impairment definition to presbycusis, then it is the progressive increase of upper frequency threshold of hearing. As the threshold floor rises, the intelligibility of high frequency speech components is reduced. However, it has been suggested that presbycusis is actually the result of long term exposure to our modern environmental noise. A study of an isolated and relatively noise free tribe in the Sudan revealed almost no signs of presbycusis [85]. Presbycusis is primarily a sensorineural impairment.

Determining Loss

Once the physical factors are ruled out, there are a basic set of audiometric tests to determine the type and degree of hearing impairment [79]:

Air Conduction Test evaluates the air conduction pathways because a problem in the pathway could restrict sound waves entering the ear canal.

Weber Tuning Fork Test evaluates lateralization using a 250 or 500 Hz tuning fork tapped into vibration and its stem placed on the frontal bone. It is then determined which ear perceives the sound: right, left, or midline. Based on perception, a clinician can better focus further diagnostic tests based on an preliminary diagnosis of normal, conductive, sensorineural, or mixed loss.

Rinne Tuning Fork Test evaluates intensity using a 250 or 500 Hz tuning fork tapped into vibration and places it on the mastoid process (bone behind the ear at the base of the skull) or near the external auditory meatus. Depending which location sound is more intense the clinician can better focus further diagnostic tests based on a preliminary diagnosis of normal, conductive, sensorineural, or mixed loss.

Audiogram is a graph of hearing threshold values. There is some disagreement in the field as to the order of frequency testing, but consistency is considered the optimum standard. It is common to start with the better ear at 1000 Hz and then present higher frequencies up to 8000 Hz (1000, 2000, 3000, 4000, 6000, and 8000 Hz) and then return to 1000 Hz and evaluate the lower frequencies (1000, 500, and 250 Hz). The patient responds to pure tone audiometry by pressing a button or raising a hand on a positive response. The tone presentation should range from 500 ms to 1000 ms and the time span between stimuli should be varied, but not shorter than the test tone duration. Figure 2.4 is the author's audiogram [86].

Bone Conduction evaluates the bone conduction pathways by direct mechanical vibration to the mastoid process or frontal bone that will send the vibration directly to the cochlea where the energy is converted to fluid vibration.

The method of testing for an audiogram is fairly coarse when the variability of hearing impairment is considered. More individualized response curves would obviously be advantageous, but the increased time and subjectiveness of user responses makes it clinically impractical. However, by employing involuntary electrophysiological response we can achieve an objective analysis. It has also been proposed that the usage of neural networks for individualized responses could produce an improved audiological fit [87].

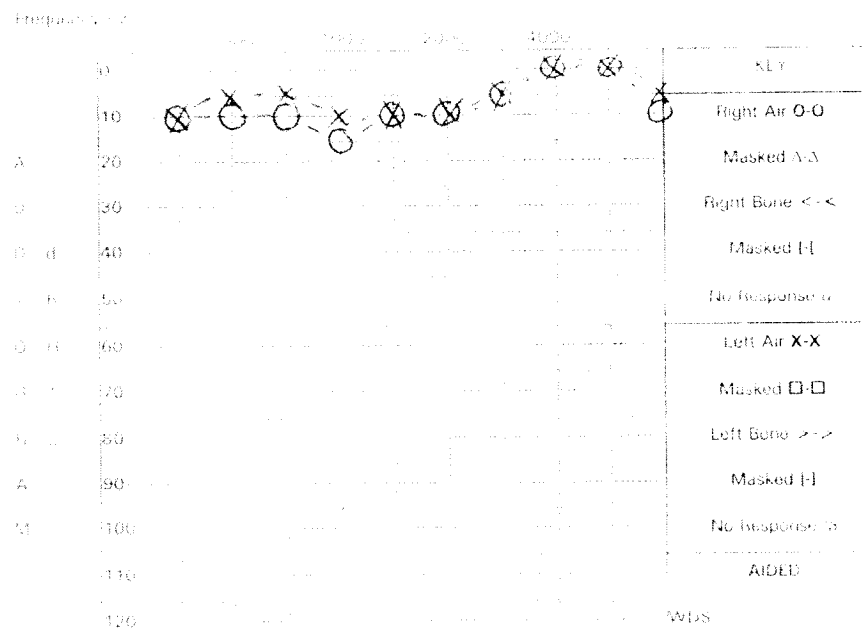


Figure 2.4: Author's audiogram

Psychological Affect of Hearing Loss

The type, method, severity, and age of onset of hearing loss has both psychological and social implications. The limited empirical literature finds hearing loss is associated with elevated rates of depression and anxiety [88]. Clinical study and experience suggest that because loss of hearing effects the unconscious and primitive level of hearing [89] and appeared to cause increased stress [90]; especially in adults with acquired hearing loss, in comparison to prelingually deaf. Also, the author's own observations indicate a strong correlation between a hearing impaired individual's increased emotional stress and an instance of miscommunication; often this increased stress goes unnoticed by the impaired.

2.2.1 Methods of correction

The goal of a hearing aid is to increase discrimination between speech sounds by pushing the input signal into the hearing range of the user. A users hearing range is the difference between a lower threshold and an upper limit of hearing for a particular frequency.

Hearing aid technology has a long history [79,91] and the analogue model has been predominant. Although early model analogue hearing aids did little for speech sound discrimination, due to clipped sound input and high frequency distortion, the technology has progressed to offer a number of styles and categories.

There are six main styles of hearing aids, ordered most to least used [79]: in-the-ear (ITE), behind-the-ear (BTE), in-the-canal (ITC), completely-in-the-canal (CIC), eyeglass, and body worn. The CIC is the fastest growing style, while collectively the eyeglass and body worn account for less than 1% of

hearing aids currently worn.

Hearing aid technology also falls into several categories. However, since there is no standardization of these categories, the author has chosen to define three main categories of hearing aids:

1. Analogue: considered the traditional hearing aid which are mainly fixed frequency gain and selective amplification,
2. Digitally Programmable Analogue: perform more advanced analogue signal processing than the analogue category, but has digitally programmable parameters, and
3. Digital: programmable and fully digital signal processing¹.

It has been questioned whether analogue hearing aid technology is suitable for all sound environments and if it has reached its limit of benefit. It is believed that in order to improve the quality of these devices, they will have to perform further processing on board, which only the digital category can provide [3, 93, 94].

Figure 2.5 illustrates how each category functions by showing a generalized flow diagram. Part a) shows the Analogue category flow diagram. Sound enters the microphone (MIC) and is amplified (Amp) and/or filtered, then the signal is processed using analogue circuitry (such as filter banks), then it is recombined, amplified and/or filtered again, and then output through the receiver (REC). Part b) shows the Digitally Programmable Analogue category flow diagram. This category functions the same as part a); however, it has more complex signal processing and digitally programmable parameters (i.e.

¹The Cochlear Implant is a hearing assistive device which would fall under the category of a Digital hearing aid, however, this device is far more invasive and perhaps requires it's own category. For a review of cochlear implants, refer to Loizou [92].

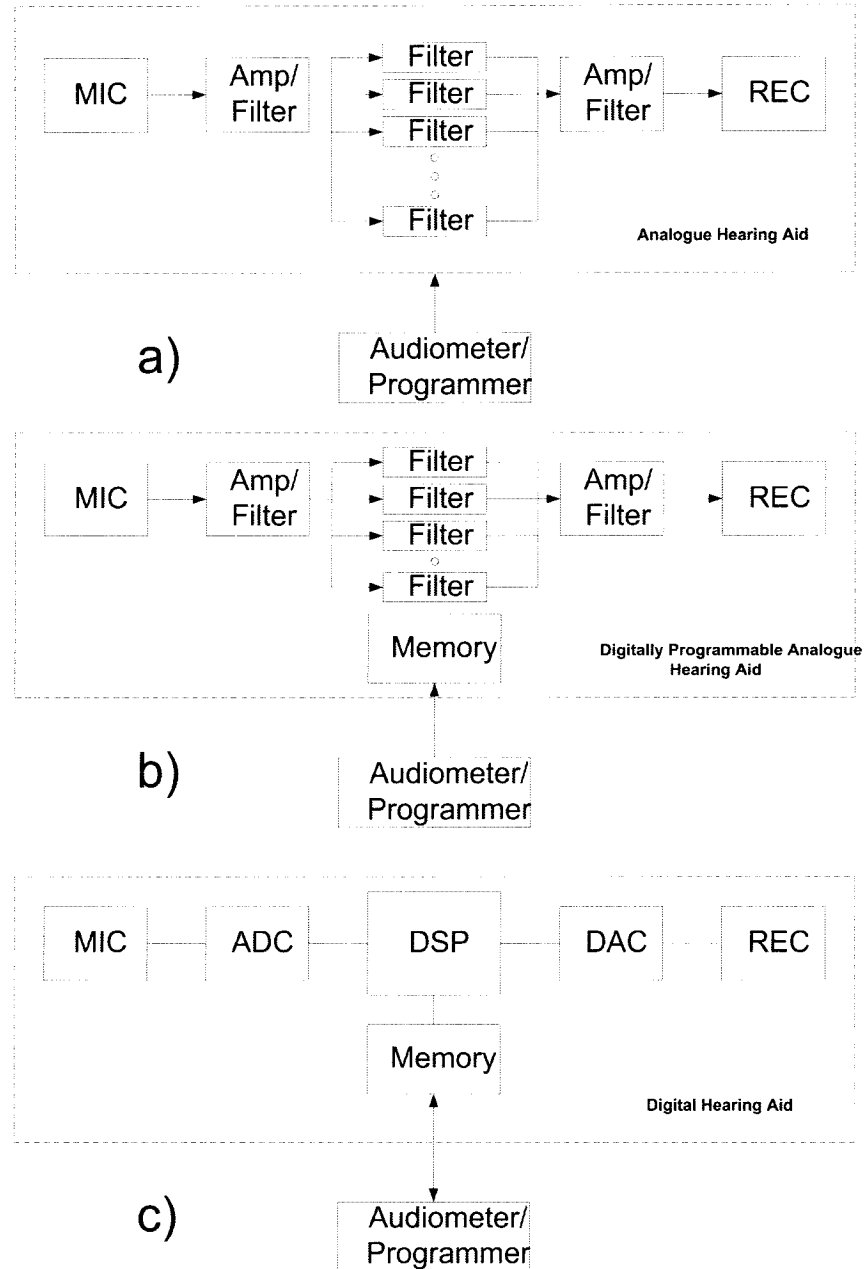


Figure 2.5: The Three Categories of Hearing Aids: a) Analogue, b) Digitally Programmable Analogue, c) Fully Digital.

amplifier gain). Part c) shows the digital flow diagram. Sound enters the microphone (MIC) and is then converted to a digital representation using the analogue-to-digital converter (ADC), then the digitized signal is processed using the digital signal processor (DSP) and then converted back to analogue by the digital-to-analogue converter (DAC) before being output through the receiver (REC).

2.3 Electrophysiology

An electrophysiological signal is an electrical phenomena related to a physiological event, such as a heart beat or muscular contraction. These signals can be divided into voluntary and involuntary. Depending on the signal, or event of interest there are several types of measurements which may be taken:

1. Electrocardiogram (ECG or EKG): measures electrical impulses that are triggered by the heart beat,
2. Electroencephalogram (EEG): measures electrical impulse of the brain,
3. Electromyogram (EMG): measures electrical impulses that are triggered from muscular contraction, and
4. Electrooculogram (EOG): measures electrical impulses generated by eye movement.

2.4 Electrophysiological Signals of Interest

We have restricted our scope to electrophysiological signals that are in close proximity to where a modern hearing aid would be worn. Specifically, we

investigated the usage of electrical waveforms generated by the human eye (electrooculography) and the human brain (electroencephalography). All signals were measured using surface electrodes. Surface electrodes were chosen because they are the least invasive method of measuring the electroocular and electroencephalographic signals.

2.4.1 The eye and electrooculography (EOG)

The human retina consists of an electrically-charged nerve membrane [95]. As a result, the measured potential between the cornea and the optic nerve is between 2 to 20 millivolts. This potential is constant value for a given adaptation without stimulation; it is the retinal resting potential. The retinal resting potential causes an electric field around the eyeball, centered on the optical axis, which can be measured by placing electrodes near to the eye. As a result, the motion of the eye causes a measurable change of DC voltage amplitude between the electrodes.

Electrooculography

Electrooculography (EOG) is the technique of using electrodes to measure the electrical potential generated by the motion of the eye. Figure 2.6 illustrates the EOG measurement as a result of eye movement and Figure 2.7 shows a common electrode arrangement for the EOG. The EOG can be used to record eye movements up to $\pm 70^\circ$ with a typical accuracy of 1.5° to 2.0° [96]. The EOG provides an advantage over other measurements of eye movement because head movements do not hinder recording.

Typical applications of the EOG include the measure of saccadic eye movements, smooth pursuit eye movements, nystagmus, and blinking [97]. Uenoyama

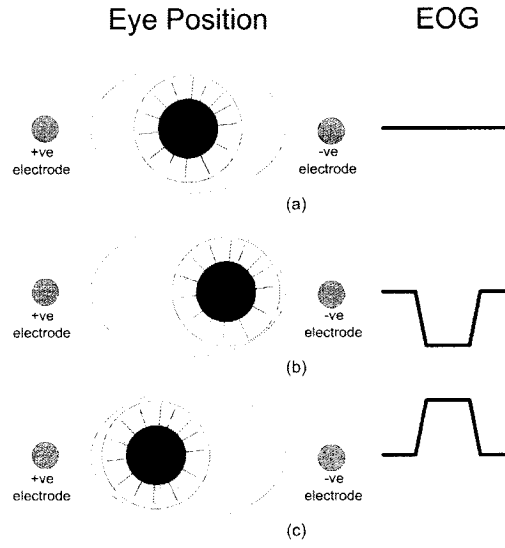


Figure 2.6: Electrooculography: changes in electric field due to eye movement. (a) centered, (b) movement from center towards negative electrode, (c) movement from center towards positive electrode

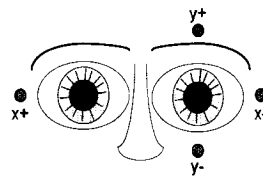


Figure 2.7: Electrooculography electrode placement. Electrodes $x+$ and $x-$ measure the horizontal, and $y+$ and $y-$ measure the vertical movement.

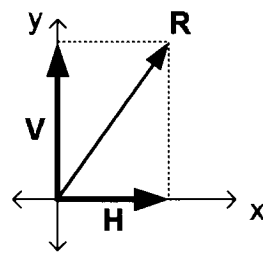


Figure 2.8: Horizontal, Vertical and Resultant Vectors

et al. [98] used the *vector*-EOG to control the x and y deflection of an electron-gun in a cathode-ray-tube (CRT) to clinically study the motion of the eye.

Vector Positioning

Eye movement measured using the EOG provides an electrical vector along the horizontal $\mathbf{H} = \langle x1, y1 \rangle$ and vertical $\mathbf{V} = \langle x2, y2 \rangle$ axis. The resultant vector

$$\mathbf{R} = \mathbf{H} + \mathbf{V} \quad (2.1)$$

where,

$$\mathbf{R} = \langle x1, y2 \rangle .$$

As illustrated in figure 2.8, the resultant vector (R) provides the eye's position from the axial center.

2.4.2 The brain and electroencephalography (EEG)

The human brain

Brain current research has five well defined frequency bands, or rhythms [14, 17, 99, 100]: $\alpha, \beta, \gamma, \delta$, and θ . Table 2.1 shows these frequency ranges and their associated cognitive and emotional attributes.

Table 2.1: Brain Rhythm Frequency Ranges

Rhythm	Frequency [Hz]	Attribute
Delta (δ)	0.5 - 4	Deep Sleep
Theta (θ)	4 - 8	Emotional Stress
Alpha/Mu (α/μ)	8 - 13	Focus of Attention
Beta (β)	13 - 22	Increased Mental Activity
Gamma (γ)	22 - 30	Attentional States and consciousness

The research into brain activity may be broadly classified into spontaneous and event related. Event related can be considered to have been invoked or evoked, and each of those may be further defined as shown in figure 2.9 and described below.

Expectation (CNV) - contingent negative variation, is the electrical activity of the brain prior to motor action. It is named descriptively CNV based on the negative voltage shift associated with an anticipated response to an expected stimulus.

Preparation (BP) - Bereitschaftspotential, a readiness potential associated with motor action.

Exogenous (VEP) - visual evoked potential, a reflex action associated with a stimulus.

Endogenous (P300) - positive peak 300 ms after stimulus, is a voltage peak associated with the cognitive processing of a stimulus event. Also referred to as slow cortical potential.

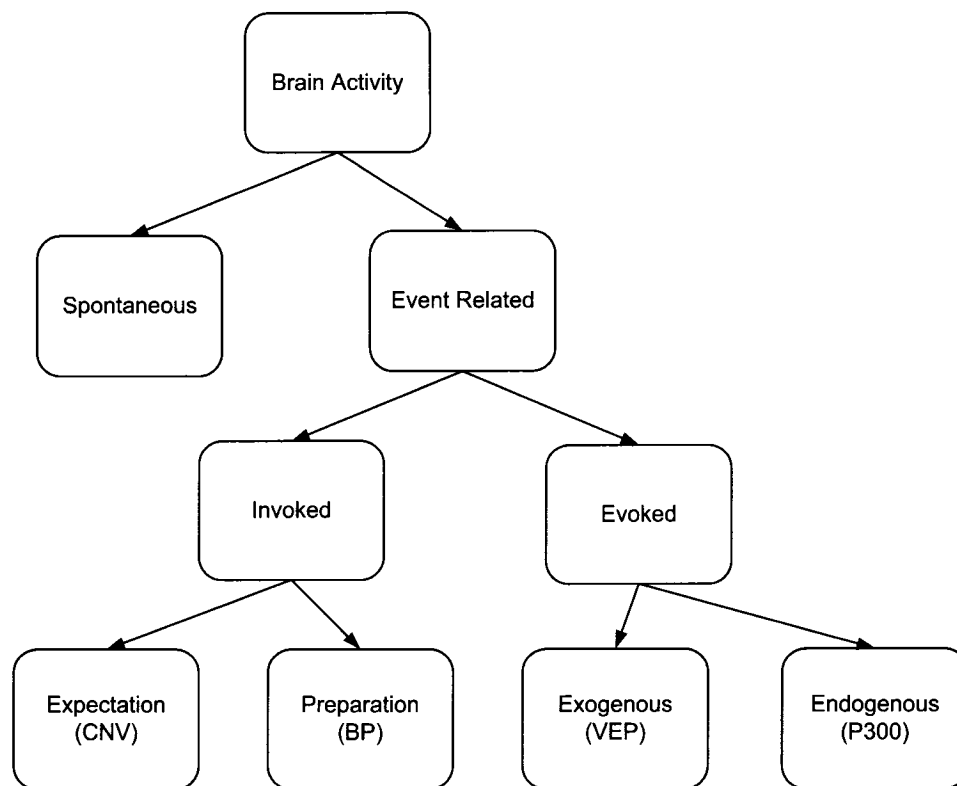


Figure 2.9: Classification of brain activity research

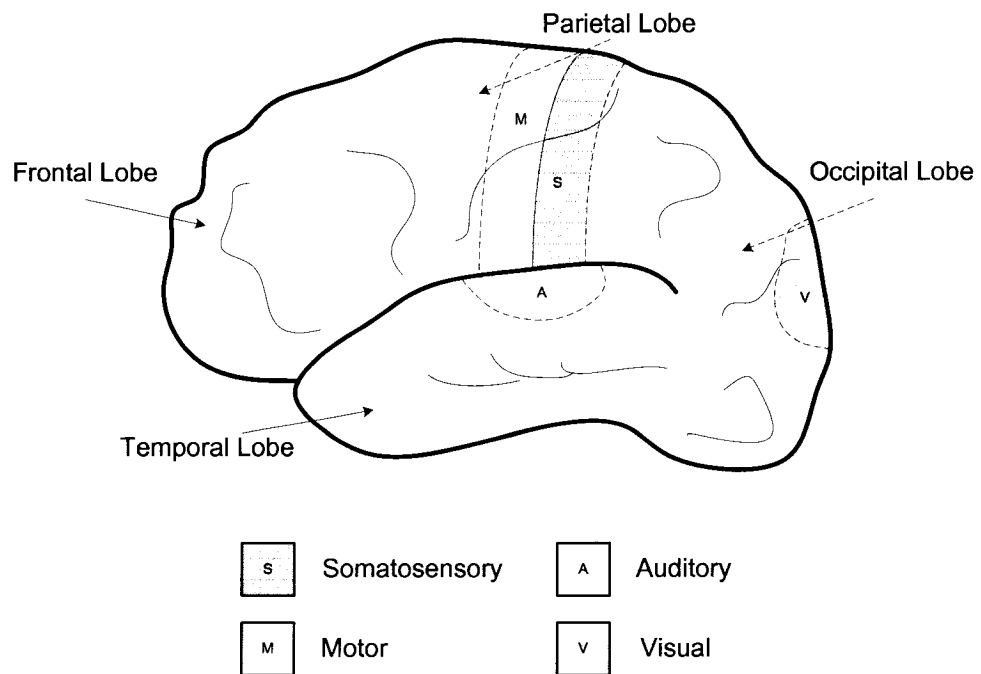


Figure 2.10: Sensory associated regions of the human brain

Standard electrode placement

Using scalp electrodes, past attempts to isolate brain current for singular cognitive functions has proven difficult, if not impossible. This is due to the diffuse nature of the brain's electrical signals through the organic medium of the scalp. More recent research takes a generalized approach (affective patterns) to classifying electrophysiological patterns, perhaps taking it's cue from the classification of the rhythms.

The measurement of brain current is done mostly in the study of epilepsy and seizures to try to isolate both temporal and spatial abnormal electrical activity. The 10-20 system is an international standard of scalp electrode placement [18, 101] which is used to perform consistent recording of the electroencephalogram. The name 10-20 refers to the 10% and 20% inter-electrode distance of the individual's skull measurement.

However, the 10-20 is not the only system used in the measurement of brain current. Although not internationally standardized, there are alternative placements for measurement during sleep and ambulatory needs [102].

It should be noted that the EEG being examined is of an adult, or at least considered adult. The EEG is different for children through stages of their development, and it is not until approximately thirteen years of age that an EEG has all the "adult" characteristics.

Alternative electrode placement

However, the 10-20 system is not the only method of placing electrodes. For systems that require ambulatory monitoring there are various electrode montages that may be selected based external sympathetic restrictions, such as placement outside the hairline [69, 102]. Typically these montages are config-

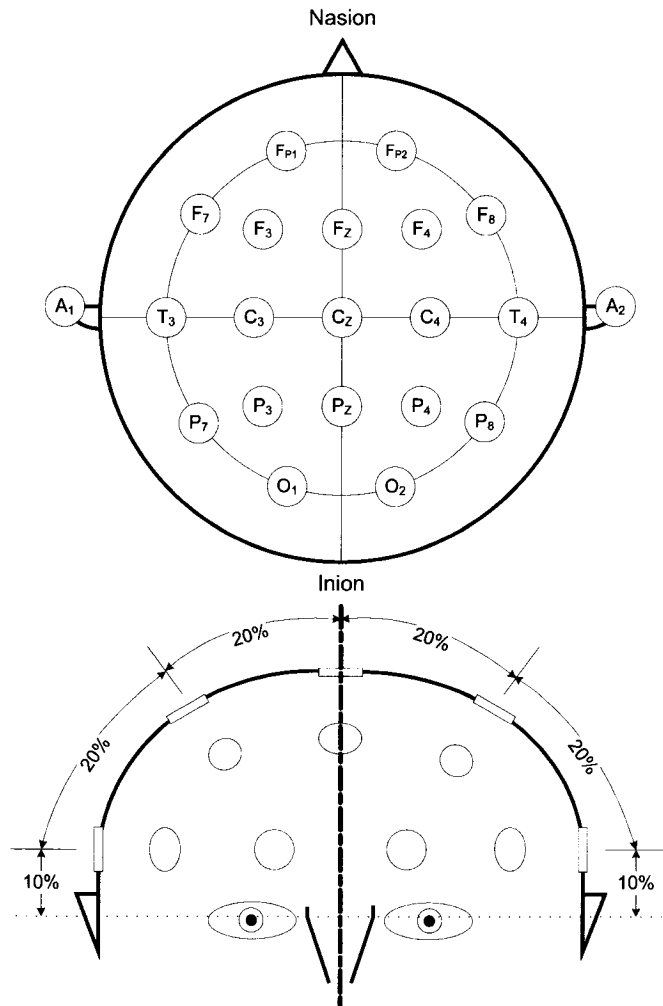


Figure 2.11: The standard 10-20 electrode placement

ured for spatial and temporal observation of brain current anomalies.

The design of a brain-computer-interface (BCI) does not require the highest spatial and temporal resolution, but rather an educated placement using as few electrodes permissable to collect the signal(s) of interest. Figure 2.12 illustrates the alternate electrode placement used by Vidal *et al* for their functional BCI used for a single dimension cursor control based on the subject's control of their α/μ rhythm. The montage was selected such that four of the electrodes were situated about the occipital-parietal areas of the brain which is primarily responsible for visual system, while the fifth electrode is placed over the frontal lobe for the removal of facial muscular artifacts. The electrode montage selected for our research was based upon the success of Vidal's approach and is shown in figure 2.13. Our electrode locations conform to the 10-20 system of positioning and we have expanded the horizontal range of the montage to reduce the influence by the occipital region (visual subsystem) and to increase the influence of the somatosensory (sensation) region of the brain. Regions of the brain are shown in figure 2.10.

2.5 Data processing

Processing of data was performed off-line using Intel-CPU class computers. Processing was primarily performed on a laptop with Intel Pentium-M 1.1 GHz (ULV), 2 MB cache, with 1.2 GB of primary memory and a desktop Intel Pentium-III 733 Mhz, 512 kB cache, with 1.2GB of primary memory. However, the proposed application of this research was for much less powerful platforms such as the Motorola digital signal processor DSP56300 or the Motorola microcontroller HC9S12.

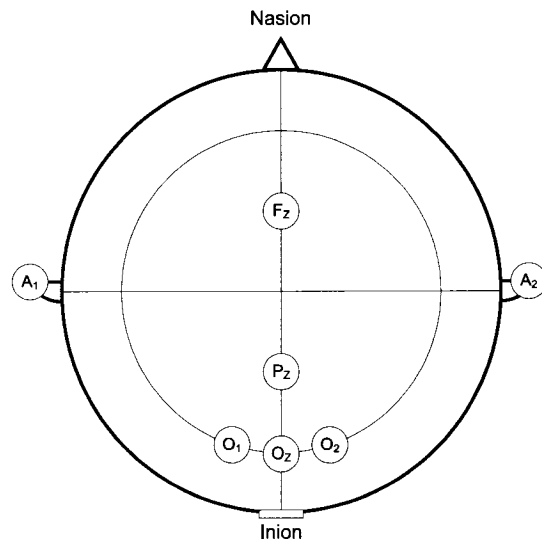


Figure 2.12: An alternate electrode placement by Vidal *et al.*

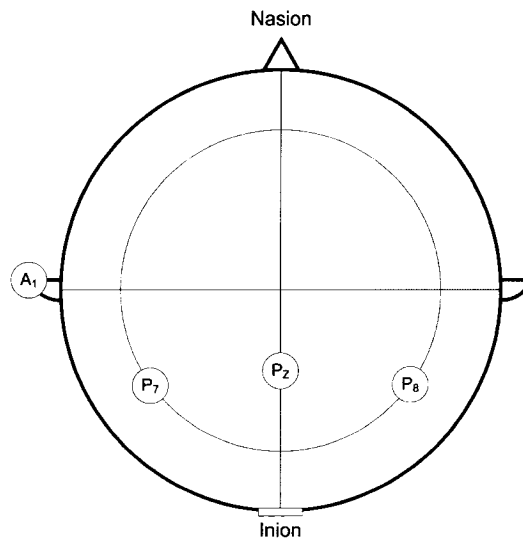


Figure 2.13: An alternate electrode placement by Doyle *et al.*

2.5.1 Filter design

The designer is faced with a task of choosing the best filter for the application. The well established field of analogue electronic filter design and implementation has direct use in the digital domain and is often chosen because the designer has experience with the subject. The choice of analogue design methodology may also have to do with the focus of modern literature on these methods based on the primary criterion of obtaining the narrowest filter transition band. The current computational capability of the general desktop computer makes a filter's transition band the primary and *a priori* concern. However, for a slower and/or less powerful system, the computational efficiency must take precedence.

Analogue design methods offer recursion as a more efficient means of implementation; however, this comes at the expense of the filtered signal having non-linear phase and infinite impulse response (IIR). It is perhaps inferred by the designer from current literature that the only method of achieving a resultant linear phase and finite impulse response (FIR) is by non-recursive means. Although it is true that all FIR filters can be realized non-recursively, there exists a class of filters that are recursive FIR filters which can be more efficient than traditional analogue design.

Figure 2.14 illustrates a traditional N-tap non-recursive FIR filter structure.

Employing digital domain principles of the comb filter and digital resonator an equivalent, but completely digital, filter structure may be realized. Figure 2.15 illustrates this combination with the comb filter driving a bank of parallel resonators to make an equivalent filter to figure 2.14. This is the principle of the frequency sampling filter (FSF).

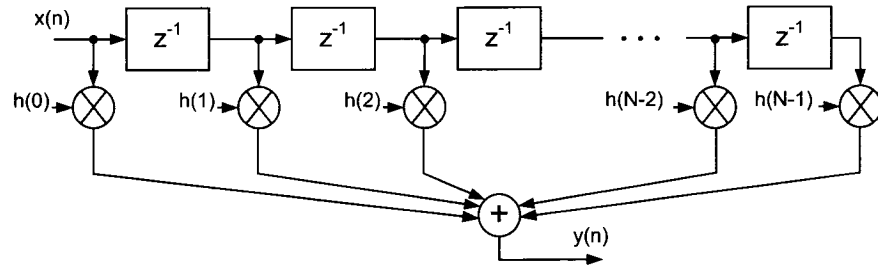


Figure 2.14: Traditional N-tap non-recursive FIR filter structure

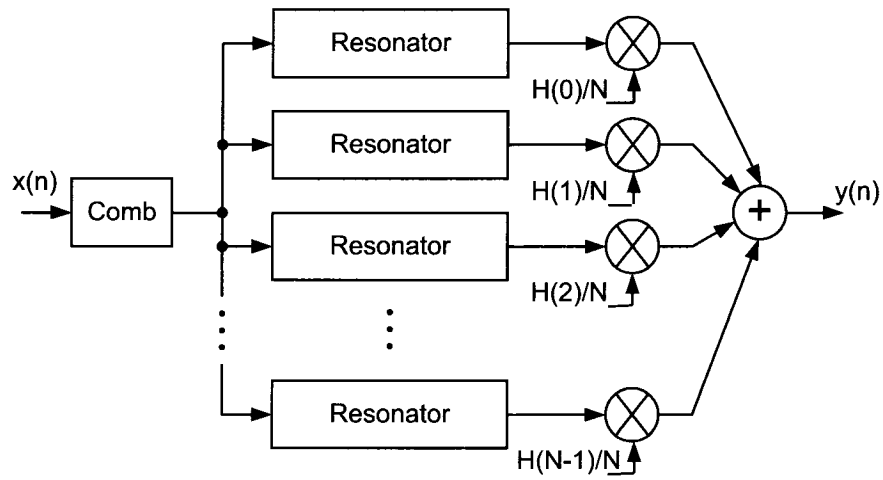


Figure 2.15: N-section frequency sampling filter structure

Frequency sampling filter

The frequency sampling/selection filter is composed of two stages: 1) the digital comb filter, and 2) an N -section bank of parallel digital resonators. Each stage will be described individually and then combined.

Comb filter

The non-recursive comb filter is given by the time-domain difference equation

$$v(n) = x(n) - x(n - N), \quad (2.2)$$

that has the z -domain transform of

$$V(z) = X(z) - X(z)z^{-N}, \quad (2.3)$$

which may be used to determine the z -domain transfer function of the comb filter,

$$H(z) = \frac{V(z)}{X(z)}, \quad (2.4)$$

$$H(z) = \frac{X(z)(1 - z^{-N})}{X(z)}. \quad (2.5)$$

Thus the comb filter z -domain transfer function is

$$H_{comb}(z) = \frac{V(z)}{X(z)} = 1 - z^{-N}. \quad (2.6)$$

This places N equally spaced zeros around the z -domain's unit circle.

For the frequency response of equations 2.6 we substitute $e^{j\omega}$ for z because $re^{j\omega}$ defines the unit circle when $r = 1$ in the z -domain. The substitution yields,

$$H_{comb}(z)|_{z=e^{j\omega}} = 1 - e^{-j\omega}. \quad (2.7)$$

We factor out the exponential term $e^{-j\omega N/2}$ to employ the Euler's identity of $\sin \theta = \frac{e^{j\theta} - e^{-j\theta}}{2j}$

$$H_{comb}(e^{j\omega}) = 2je^{-j\omega N/2} \sin(\omega N/2). \quad (2.8)$$

Combining the imaginary portion into exponential term ($j = e^{j\pi/2}$) produces the frequency response,

$$H_{comb}(e^{j\omega}) = 2e^{-j(\omega N - \pi)/2} \sin(\omega N/2). \quad (2.9)$$

The real magnitude response of the comb filter is,

$$|H_{comb}(e^{j\omega})| = 2|\sin(\omega N/2)|. \quad (2.10)$$

Complex resonator

The complex resonator's time domain difference equation is,

$$y(n) = v(n) + e^{j\omega_r} y(n-1), \quad \text{where } -\pi \leq \omega_r \leq \pi. \quad (2.11)$$

The angle ω_r determines the resonant frequency.

The z -domain transform of the difference equation is given by,

$$Y(z) = V(z) + e^{j\omega_r} Y(z)z^{-1} \quad (2.12)$$

The z-domain transfer function for the complex resonator is,

$$H_{resn}(z) = \frac{Y(z)}{V(z)} = \frac{1}{1 - e^{j\omega_r} z^{-1}}. \quad (2.13)$$

Frequency sampling filter using single section complex resonator

The combination of comb filter and single resonator forms the basis for the frequency sampling filter. The z-domain transfer function of the frequency sampling filter (FSF) is the product of the individual transfer functions and a gain coefficient $H(k)$.

$$H(z) = H_{comb}(z)H_{resn}(z)H(k), \quad (2.14)$$

$$H(z) = \frac{1 - z^{-N}}{1 - e^{j\omega_r} z^{-1}} H(k). \quad (2.15)$$

In order to align the resonator poles and the comb zeros for their cancellation the resonant frequency must be restricted by,

$$\omega_r = \frac{2\pi k}{N}, \quad \text{where } k = 0, 1, 2, \dots, N-1. \quad (2.16)$$

Using this restriction, the the single section complex resonator's z-domain transfer function becomes,

$$H(z) = \frac{(1 - z^{-N})H(k)}{1 - e^{j2\pi k/N} z^{-1}} \quad (2.17)$$

By combining multiple resonators in parallel we may sum their individual z-domain transfer functions using the principle of super-position to create easily customizable filters with little extra effort.

Stability

The FSF description to this point has assumed pole/zero cancelation on the z -domain unit circle. In practice, base representational error and finite precision errors may result in poles located outside the unit circle causing instability. Unless implemented on an integer based machine the poles and zeros should be moved slightly inside the unit circle to a radius r . A value of $r < 1$ causes a decayed/damped impulse response, widens the filter transition band, and cause non-linearity in the phase response. For these reasons stability must be balanced against performance.

In general, the damping factor is incorporated by substituting the product rz for each occurrence of z .

Frequency Sampling Filter Using Multiple (N) Section Real Resonator

Expanding upon the case of the single section complex resonator into a parallel bank of single section complex resonators the bank of resonators has a z -domain transfer function of the sum of their individual transfer functions. This is given by,

$$H(z) = (1 - z^{-N}) \sum_{k=0}^{N-1} \frac{H(k)}{1 - e^{j2\pi k/N} z^{-1}}. \quad (2.18)$$

From equation 2.18 it is noted that there may be up to N parallel resonators in the bank, but in practice only a few are required for a narrow-band filter.

It is possible to obtain real valued coefficients by requiring the complex multi-section resonator to have complex conjugate poles at all non-zero gain factors $H(k)$ and $H(N - k)$ where $H(k) = H^*(N - k)$. This requires complex conjugate poles at $\pm 2\pi k/N$ radians.

Incorporating the stability damping factor, the complex multisection FSF

is

$$H(z) = (1 - r^N z^{-N}) \sum_{k=0}^{N-1} \frac{H(k)}{1 - (r e^{j2\pi/N}) z^{-1}} \quad (2.19)$$

The summation is split into two parts; one for each half of the conjugate pair. Assuming N is even², the 2 cases of $H(0)$ and $H(N/2)$ must be addressed separately. If N were odd then the cases of $H(N/2)$ would not exist and a high-pass filter could not be realized.

Dividing up the summation produces

$$H(z) = (1 - r^N z^{-N}) \left[\frac{H(0)}{1 - r z^{-1}} + \frac{H(N/2)}{1 - r z^{-1}} + \sum_{k=1}^{N/2-1} \frac{H(k)}{1 - [r e^{j2\pi/N}] z^{-1}} + \sum_{k=N/2+1}^{N-1} \frac{H(k)}{1 - [r e^{j2\pi/N}] z^{-1}} \right]. \quad (2.20)$$

Using the symmetry of the z -domain unit circle the summations may be combined by changing the second summation's index from k to $(N - k)$. Forming a common denominator between the two summation expressions and then expanding them out produces (focussing on just the summations),

$$H_{summ}(z) = \sum_{k=1}^{N/2-1} \frac{H(k)(1 - r e^{j2\pi(N-k)/N} z^{-1}) + H(N - k)(1 - r e^{j2\pi k/N} z^{-1})}{1 - r e^{j2\pi(N-k)/N} z^{-1} - r e^{j2\pi k/N} z^{-1} + r^2 e^{j2\pi(k+N-k)/N} z^{-2}}. \quad (2.21)$$

Defining $H(N - k) = H^*(k)$ requires all poles to have conjugate pairs. This requirement produces a frequency sampling filter with real coefficients. Collecting common terms gives us,

²The case where N is even will be explored as the author's FSF design uses an even N .

$$H_{summ}(z) = \sum_{k=1}^{N/2-1} \frac{H(k) + H^*(k) - (H(k)re^{-j2\pi k/N} + H^*(k)re^{j2\pi k/N})z^{-1}}{1 - r(e^{-j2\pi k/N} + e^{j2\pi k/N})z^{-1} + r^2z^{-2}} \quad (2.22)$$

Converting each complex $H(k)$ to polar form and adding their polar form

$$\begin{aligned} H(k) &= |H(k)|[\cos \phi_k + j \sin \phi_k] \quad \text{and} \\ H^*(k) &= |H(k)|[\cos \phi_k - j \sin \phi_k] \end{aligned}$$

to produce

$$H(k) + H^*(k) = |H(k)| \cos \phi_k \quad (2.23)$$

Substituting equation 2.23 and Euler's identity

$$\cos \alpha = \frac{e^{j\alpha} + e^{-j\alpha}}{2}$$

results in the frequency sampling filter transfer function

$$\begin{aligned} H(z) &= (1 - r^N z^{-N}) \left[\frac{H(0)}{1 - rz^{-1}} + \frac{H(N/2)}{1 - rz^{-1}} + \right. \\ &\quad \left. 2 \sum_{k=1}^{N/2-1} \frac{|H(k)|[\cos \phi_k - r \cos(\phi_k - 2\pi k/N)z^{-1}]}{1 - [2r \cos(2\pi k/N)]z^{-1} + r^2z^{-2}} \right] \quad (2.24) \end{aligned}$$

This is referred to as a Type-I real frequency sampling filter.

The Type-I FSF resonator structure can be simplified by setting all ϕ_k

phase angle offset of each non-zero gain coefficient to 0 and moving the gain factor within the resonator. The transfer function can be further simplified by setting all non-zero gain factors $H(k) = 1$; however, as will be shown, this gain factor can improve the performance of stop-band attenuation. Instead of defining the phase angle for each non-zero gain factor, a linear phase multisection FSF can be realized by using just the magnitude $|H(k)|$ values and incorporating a $(-1)^k$ alternating term. This alternating term makes each single section π -radians out of phase with its adjacent sections. These simplifications result in the Type-II frequency sampling filter with z-domain transfer function

$$H_{Type-II}(z) = (1 - r^N z^{-N}) \left[\frac{H(0)}{1 - rz^{-1}} + \frac{H(N/2)}{1 - rz^{-1}} + \sum_{k=1}^{N/2-1} \frac{(-1)^k |H(k)| [2 - 2r \cos(2\pi k/N) z^{-1}]}{1 - [2r \cos(2\pi k/N)] z^{-1} + r^2 z^{-2}} \right]. \quad (2.25)$$

Transition band coefficients

To this stage, it has been assumed that any non-zero gain coefficient of the frequency sampling filter has a value of 1. Although a convenient approximation, it has the effects of decreasing stop-band attenuation and injecting high-frequency elements into the original signal's spectrum due to Gibbs phenomenon. By defining gain coefficient(s) in the transition band these effects can be significantly reduced. The cost of this improvement is a widening of the filter transition band and the extra computation of an additional FSF section for each coefficient. The transition band coefficients may be calculated empirically or referenced from design tables [103–105].

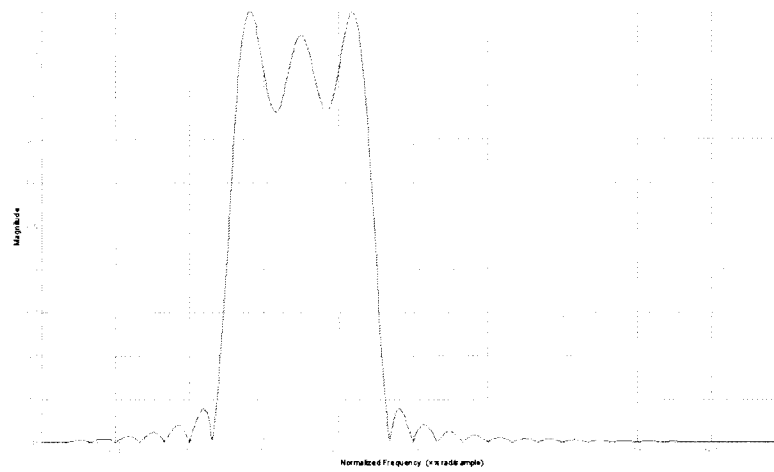


Figure 2.16: Type-II frequency sampling filter magnitude response (β filter)

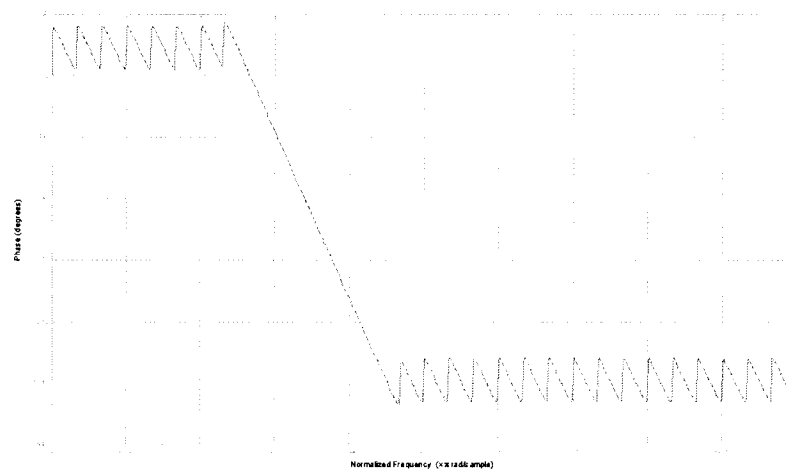


Figure 2.17: Type-II frequency sampling filter phase response (β filter)

2.5.2 Data reduction

The choice of electrode site to focus upon, whether montages should be bipolar or monopolar, and the selection of a reference all add to the complexity of measuring brain current. An obvious approach may be to collect measurements with as high an electrode resolution possible; however, this only serves to increase the complexity and time of interpretation.

For practical purposes, a brain-computer-interface require as few electrode sites possible and method(s) of data reduction. One method of analysis and reduction [106] is an approximation based on the Poisson's theorem.

Source density analysis

If we consider the electrode arrangement ΔS and apply Gauss's law, where the electric flux passing through any closed surface is equal to the total charge enclosed by that surface, then the total flux passing through ΔS is,

$$\Delta\Psi = \mathbf{D}_S \cdot \Delta\mathbf{S} \quad (2.26)$$

$$\begin{aligned} \Psi &= \int d\Psi \\ &= \oint \mathbf{D}_S \cdot d\mathbf{S} = Q \quad \text{charge enclosed.} \end{aligned} \quad (2.27)$$

Total charge enclosed assumes the skull to be volume conductor. If we wish to evaluate the flux density we may consider it per unit volume,

$$\frac{\oint \mathbf{D}_S \cdot d\mathbf{S}}{\Delta v} = \frac{Q}{\Delta v}. \quad (2.28)$$

As the volume shrinks to infinitesimally small,

$$\lim_{\Delta v \rightarrow 0} \frac{\oint \mathbf{D}_S \cdot d\mathbf{S}}{\Delta v} = \lim_{\Delta v \rightarrow 0} \frac{Q}{\Delta v}, \quad (2.29)$$

we observe Maxwell's first equation, that states that the electric flux per unit volume leaving a vanishingly small volume unit is exactly equal to the volume charge density there. This is illustrated in figure 2.18. Equation 2.30 is Maxwell's first equation:

$$\nabla \cdot \mathbf{D} = \rho_v. \quad (2.30)$$

The definition of \mathbf{D} is

$$\mathbf{D} = \epsilon \mathbf{E} \quad (2.31)$$

and the gradient relationship

$$\mathbf{E} = -\nabla V. \quad (2.32)$$

By substituting equations 2.31 and 2.32 into equation 2.30 we produce

$$\nabla \cdot \mathbf{D} = -\nabla \cdot (\epsilon \nabla V) = \rho_v \quad (2.33)$$

$$\nabla \cdot \nabla V = -\frac{\rho_v}{\epsilon} \quad \text{where } \epsilon \text{ is constant} \quad (2.34)$$

Equation 2.34 is Poisson's equation which states that the source density of an potential field distribution is proportional (e.g. $\frac{1}{\epsilon}$) to $\nabla^2 V$.

Expanding 2.34 in cartesian coordinates provides

$$\nabla^2 V = \frac{\partial^2 V}{\partial x^2} + \frac{\partial^2 V}{\partial y^2} + \frac{\partial^2 V}{\partial z^2}. \quad (2.35)$$

Normally ∇^2 is expressed in orthogonal coordinates, but as an approximation to scalp current density it has found application in EEG analysis and evoked potential research. The source density analysis provides several advantages:

1. the measurements may be more easily visualized,
2. may provide a higher spatial resolution,
3. has less vulnerability to common-mode interference, and
4. solves the problem of choosing a reference electrode.

Conceptually, the Laplacian may be understood as an operator that subtracts from the infinitesimally small volume potential the average potential of its adjacent electrodes. The conventional Laplacian electrode array, shown in figure 2.19a), uses a rectangular grid, but in principle the adjacent electrodes are not required to be orthogonally arranged. Figure 2.19b) illustrates a triangular grid which is more economical and has reported effective [107–109].

Applying this concept and a triangular grid electrode array to analogue electronics, the current from each adjacent electrode is converted to a voltage and then summed and averaged across a resistor network. The average of the adjacent electrodes is subtracted through the negative feedback path and the result amplified,

$$V_{Laplacian} = n(V_a - \frac{\text{sum of adjacent electrodes}}{n}), \quad (2.36)$$

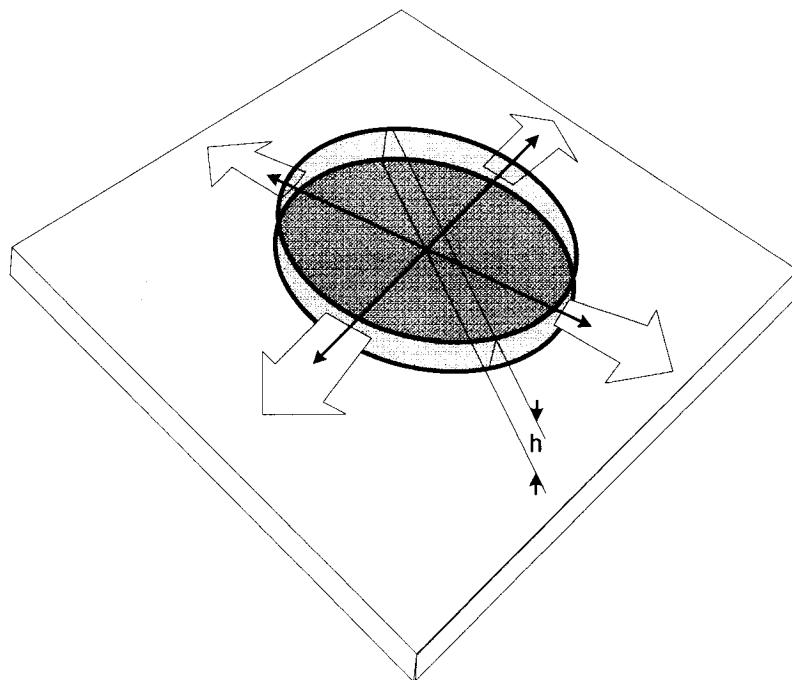


Figure 2.18: Source density approximation using a vanishingly small volume unit

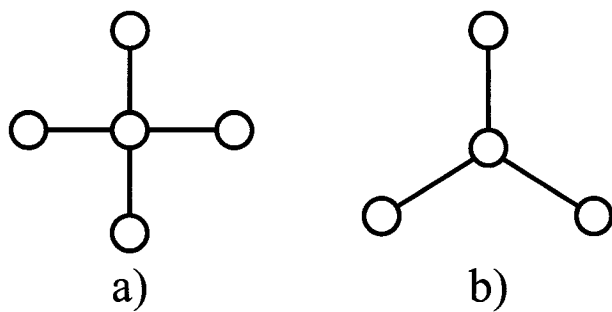


Figure 2.19: Source density analysis: unit Laplacian electrode arrays

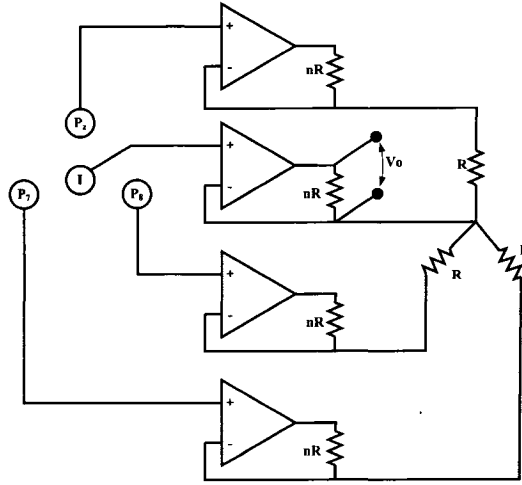


Figure 2.20: Analogue source density computation

where n is the number of adjacent electrodes. Figure 2.20 illustrates the circuitry.

Analogue implementation is preferred because it reduces analog to digital conversion overhead, but post-processing computation is achieved using equation 2.36.

2.6 Data attributes and classification

The choice of data attribute(s) on which to focus is an active and broad area of brain-computer-interface research. There are however, some well defined frequency bands that have been associated with cognitive and emotional attributes.

These defined frequency ranges will be referred to in general as *narrow-band* (e.g narrow-band- α) and contiguous combinations will be *wide-band* (e.g. wide-band- $\alpha\beta$). These defined frequency ranges had their power spectral den-

sity calculated and results recorded.

Researchers have achieved functional BCI using purely frequency domain data by training the subject to accurately manipulate the μ -band (Vidal and Wolpaw et al.). However, as noted by Mensh [110], this ignores the available time domain data of slow-cortical potential (P300) that researchers have also exhibited BCI success (Birbaumer et al.).

Regardless of the attribute(s) selected, the visualization and classification of such data becomes an increasing challenge that may be considered proportional to dimensionality. Fundamental to the classification problem is the unknown distribution of the data, which is further complicated with the fact that real-world, experimental data of this nature are often not linearly separable without significant misclassification error.

2.6.1 Support vector machine classification

Often data is inseparable using a linear classifier. This may be overcome by permitting some data to be misclassified, or by the use of a nonlinear classifier. A support vector machine (SVM) may be used to create nonlinear classification boundaries (hypersurfaces) by using a mapping (Φ) from input (attribute) space (\mathbf{x}) to feature space (\mathbf{z}) and creating hypersurfaces in feature space.

Generally, for an n -dimension input vector (\mathbf{x}) an SVM classifier will apply a mapping to calculate an f -dimension feature vector and then generate a nonlinear separating hypersurface in feature space. This separating hypersurface is used to determine classification.

To design of a nonlinear SVM will begin with a linear SVM for classification. Given the data generator \mathbb{R}^d , where d is the dimension, the input

vectors

$$\mathbf{x} \in \mathbb{R}^n$$

are mapped into vector \mathbf{z} of a higher dimensional feature space

$$F(\mathbf{z}) = \Phi(\mathbf{x}) \quad (2.37)$$

where Φ represents the fixed and chosen mapping $\mathbb{R}^n \mapsto \mathbb{R}^f$. For our classification we assign two output states: $\mathbf{y} \in \{-1, 1\}$. To produce the mapping in this feature space:

$$\mathbf{x} \in \mathbb{R}^n \mapsto \mathbf{z}(\mathbf{x}) = [\phi_1(\mathbf{x}), \phi_2(\mathbf{x}), \dots, \phi_n(\mathbf{x})]^T \in \mathbb{R}^f$$

The mapping Φ objective is to produce linearly separable images of \mathbf{x} in feature space. Once mapped, we use the decision hyperplane

$$d(\mathbf{x}) = \mathbf{w}^T \mathbf{z} + b, \quad (2.38)$$

where \mathbf{w} is a weighting vector and b is a bias in feature space. The calculation of weighting vector \mathbf{w} is performed during the learning stage and will be further described shortly. After evaluating the decision function, an indicator function is applied to determine the set in which the decision lies. For the case of output states $\mathbf{y} \in \{-1, 1\}$:

$$i_F(\mathbf{x}) = \text{sign}(d(\mathbf{x})) \quad (2.39)$$

The indicator function is a linear classifier in feature space (\mathbf{z}) and creates

a nonlinear separating hypersurface in the original input space (\mathbf{x}).

Consider a case of system with input attribute vector $\mathbf{x} = [x_1 x_2 x_3]$ ($n = 3$) with mapping Φ . Based on the mapping, the feature vector is

$$\mathbf{z}(\mathbf{x}) = [\phi_1(\mathbf{x}) \phi_2(\mathbf{x}) \dots \phi_9(\mathbf{x})]^T \in \mathbb{R}^9.$$

The mapping order is determined by

$$f = \frac{n(n+3)}{2}, \quad (2.40)$$

with the feature space mapping set as

$$\begin{aligned} z_1 &= x_1, \quad \dots \quad z_n = x_n \\ z_{n+1} &= (x_1)^2, \quad \dots \quad z_{2n} = (x_n)^2 \\ z_{2n+1} &= x_1 x_2, \quad \dots \quad z_f = x_n x_{n-1}. \end{aligned}$$

Thus for our system $\phi_i(\mathbf{x})$ is given as

$$\begin{aligned} \phi_1(\mathbf{x}) &= x_1, & \phi_2(\mathbf{x}) &= x_2, & \phi_3(\mathbf{x}) &= x_3, \\ \phi_4(\mathbf{x}) &= x_1^2, & \phi_5(\mathbf{x}) &= x_2^2, & \phi_6(\mathbf{x}) &= x_3^2, \\ \phi_7(\mathbf{x}) &= x_1 x_2, & \phi_8(\mathbf{x}) &= x_1 x_3, & \phi_9(\mathbf{x}) &= x_2 x_3. \end{aligned}$$

Referring to equation 2.38 the decision function produces a second order poly-

nomial hypersurface given by

$$\begin{aligned}
 d(\mathbf{x}) &= [w_1 \ w_2 \ w_3 \ w_4 \ w_5 \ w_6 \ w_7 \ w_8 \ w_9] \times \\
 &\quad [x_1 \ x_2 \ x_3 \ (x_1)^2 \ (x_2)^2 \ (x_3)^1 \ x_1x_2 \ x_1x_3 \ x_2x_3]^T + b \\
 &= w_1x_1 + w_2x_2 + w_3x_3 + w_4(x_1)^2 + w_5(x_2)^2 + w_6(x_3)^2 + \\
 &\quad w_7x_1x_2 + w_8x_2x_3 + w_9x_1x_3 + b.
 \end{aligned}$$

The mapping from three-dimensional input space to nine-dimensional feature space ($\mathbb{R}^3 \mapsto \mathbb{R}^9$) is shown in figure 2.21. To calculate a value from the decision function, the weighting vector (\mathbf{w}) and bias b need to be solved. The goal when calculating an SVM decision boundary (hypersurface) is to maximize the margin M between boundary adjacent training data (support vectors). First consider the point P in feature space, the distance D from P to a hyperplane is given by:

$$\begin{aligned}
 D &= \frac{|\mathbf{w}\mathbf{x}_p \pm b|}{\|\mathbf{w}\|} \\
 &= \frac{|w_1x_{1p} + w_2x_{2p} + \dots + w_nx_{np} \pm b|}{\sqrt{w_1^2 + w_2^2 + \dots + w_n^2}}.
 \end{aligned} \tag{2.41}$$

Now, consider that the maximum hyperplane margin lies exactly halfway between the projected normal of data points from different output sets. Thus having equal projected distances from the plane,

$$M = \frac{q - (-q)}{\|w\|} \tag{2.42}$$

$$= \frac{2q}{\|w\|}. \tag{2.43}$$

The distance from either of the two points to the plane would be half of the

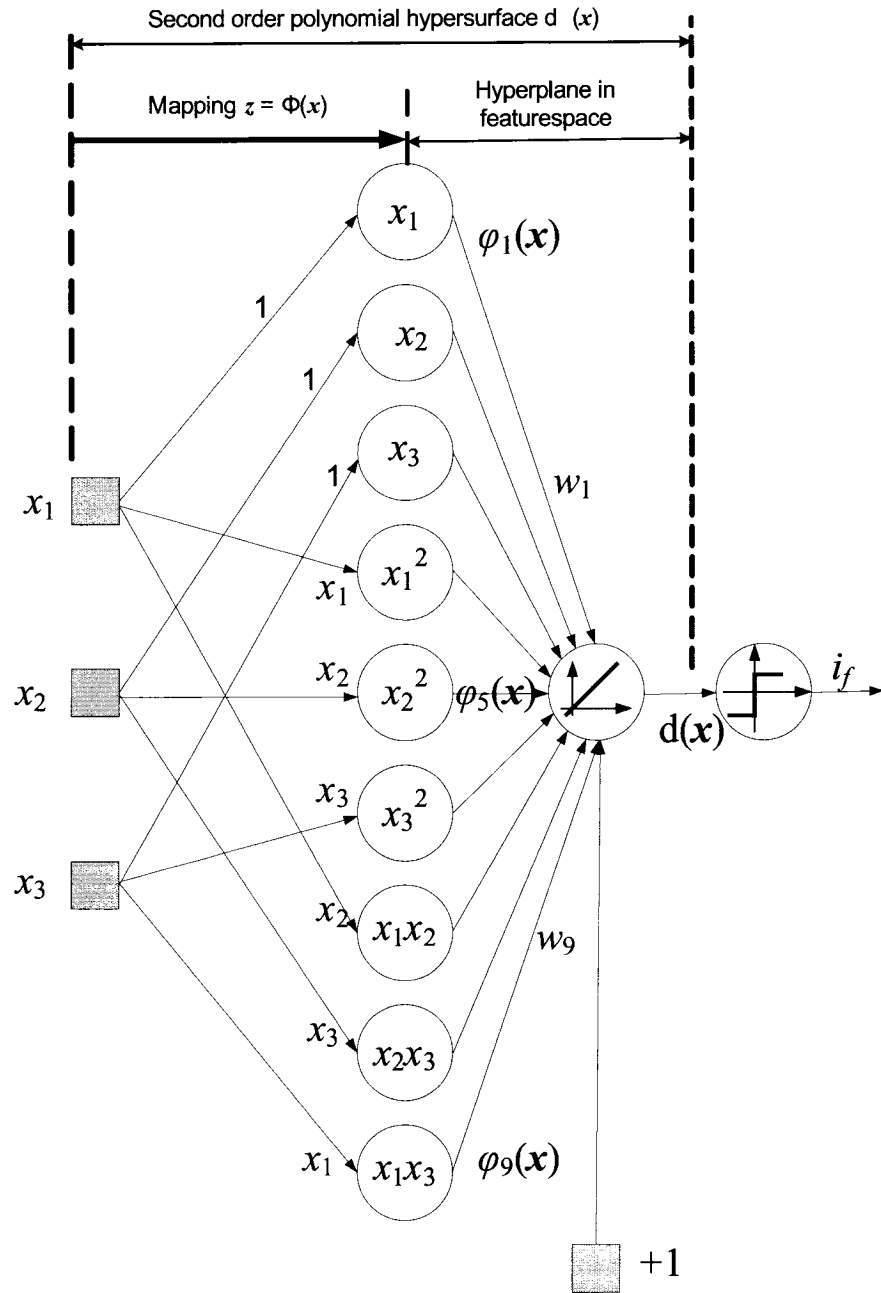


Figure 2.21: SVM diagram

value calculated in equation 2.43.

$$D = \frac{M}{2} \quad (2.44)$$

$$= \frac{|\mathbf{w}\mathbf{x} + b|}{\|w\|} \quad (2.45)$$

$$= \frac{q}{\|w\|} \quad (2.46)$$

Thus observing equation 2.46 it is noted that to maximize the distance between the hyperplane and the boundary data points that \mathbf{w} must be minimized.

In defining the hyperplane, it is necessary to impose the restriction

$$\min_{x_i \in X} |\mathbf{w}^T \mathbf{x}_i + b| = 1 \quad (2.47)$$

to ensure the use of a canonical plane. This requirement restricts how a hyperplane can be defined to ensure its description is unique. Given equation 2.47's restriction, equation 2.46 may be rewritten as

$$D = \frac{1}{\|w\|}. \quad (2.48)$$

This defines the optimal canonical separating hyperplane (OCSH) with the largest margin M and the adjacent training data (support vectors) specified by $y_j[\mathbf{w}^T \mathbf{x}_j + b] \equiv 1$, where $j = 1, \dots, \text{nsv}$. Thus all remaining training data must satisfy

$$y_j[\mathbf{w}^T \mathbf{x}_j + b] \geq 1, \quad i = 1, \dots, l, \quad (2.49)$$

where l is the number of training data and nsv is the number of support vectors.

Therefore the decision equation is a nonlinear function in feature space

that requires optimization of its parameters to determine the optimal canonical separating hyperplane. The learning machine must minimize $\|w\|$ to maximize M based on the restrictions stated. This problem is a nonlinear optimization with inequality constraints that may be solved using the Lagrangian saddle point. The Lagrange function is given as

$$L(\mathbf{w}, b, \alpha) = \frac{\mathbf{w}^T \mathbf{w}}{2} - \sum_{i=1}^l \alpha_i (y_i [\mathbf{w}^T \mathbf{x}_i + b] - 1), \quad (2.50)$$

where α_i are the Lagrangian multipliers. The α_i values will be used as weighting values in feature space. The Lagrangian must be minimized with respect to \mathbf{w} and b , and maximized with respect to α_i ($\alpha_i \geq 0$). The partial derivatives with respect to \mathbf{w} and b will be zero when the saddle point is found. Thus,

$$\frac{\partial L}{\partial \mathbf{w}_0} = 0, \text{ or } \mathbf{w}_o = \sum_{i=1}^l \alpha_i y_i \mathbf{x}_i, \quad (2.51)$$

$$\frac{\partial L}{\partial b_0} = 0, \text{ or } \sum_{i=1}^l \alpha_i y_i = 0. \quad (2.52)$$

Classical Lagrangian duality permits transformation of the primal space (\mathbf{w} and b) into Lagrangian space (α_i) which is more easily solved. The Lagrangian dual is:

$$L_d(\alpha) = \sum_{i=1}^l \alpha_i - \frac{1}{2} \sum_{i=1}^l \sum_{j=1}^l y_i y_j \alpha_i \alpha_j \mathbf{x}_i^T \mathbf{x}_j. \quad (2.53)$$

The Lagrangian dual is significant because it is expressed in terms of training data (\mathbf{x}), but perhaps most importantly, the result of $\mathbf{x}^T \mathbf{x}$ is a scalar product.

Reviewing equation 2.38 and incorporating the necessary condition of determining the Lagrangian saddle point from equation 2.52, the decision func-

tion may be rewritten for feature space (\mathbf{z}) as:

$$d(\mathbf{x}) = \sum_{i=1}^l \alpha_i y_i \mathbf{z}^T(\mathbf{x}) \mathbf{z}(\mathbf{x}_i) + b. \quad (2.54)$$

It is clear that given the mapping function Φ and its dimensionality, the amount data can quickly become unmanageable, even considering the scalar product term. However, the feature space F may be expressed using a kernel function K , defined in input space as,

$$K(\mathbf{x}_i, \mathbf{x}_j) = \mathbf{z}_i^T \mathbf{z}_j = \Phi^T(\mathbf{x}_i) \Phi(\mathbf{x}_j). \quad (2.55)$$

The use of a kernel function to define the feature space avoids the potentially unmanageable computation required of a high dimension problem. The choice and application of the kernel function remains an active research area in many diverse fields. Researchers currently use empirical methods to evaluate kernel performance. A popular kernel function that is considered suitable for noisy experimental data is the Gaussian Radial Basis function, defined as:

$$K(\mathbf{x}_i, \mathbf{x}_j) = e^{-\frac{|\mathbf{x}_i - \mathbf{x}_j|^2}{2\sigma^2}}. \quad (2.56)$$

The use of a Gaussian kernel removes the equality constraint of equation 2.52 because Gaussian basis functions do not require a bias term. Thus the Lagrangian may be rewritten with the kernel function as

$$L_d(\alpha) = \sum_{i=1}^l \alpha_i - \frac{1}{2} \sum_{i=1}^l \sum_{j=1}^l y_i y_j \alpha_i \alpha_j K(\mathbf{x}_i, \mathbf{x}_j), \quad (2.57)$$

subject to the condition

$$\alpha_i \geq 0, \quad i = 1, \dots, l,$$

where l is the number of data points.

Maximizing L_d requires solving for α_i which may be done using standard quadratic numerical programming methods [111,112]. The result will be an α_i for $i = 1, \dots, l$, where l is the total number of data points. Fortunately, only the data points used as support vectors will be nonzero values and in practical application the number of support vectors should be small percentage of the total data set.

To this point, a “hard” margin hypersurface classifier has been defined. In practice, particularly on noisy data, a degree of acceptable misclassification permits a better generalization of the data, producing a better classifier; this is called a “soft” margin (C). The only change that results from the soft margin is a limit on the upper bound of the α_i :

$$C \geq \alpha_i \geq 0, \quad \text{where } i = 1, \dots, l. \quad (2.58)$$

The final result is a nonlinear hypersurface that describes the soft margin division between sets of linearly nonseparable data. The primary advantages of such a system are that it may be used for the classification of data where the distribution of this data is unknown and/or the dimensionality of the attribute (\mathbf{x}) space is too large for classical visualization methods.

The decision hypersurface function is now defined as,

$$d(\mathbf{x}) = \sum_{i=1}^l y_i \alpha_i K(\mathbf{x}, \mathbf{x}_i) + b, \quad (2.59)$$

and the indicator function is

$$i_f(\mathbf{x}) = \text{sign}(d(\mathbf{x})) = \text{sign}\left(\sum_{i=1}^l y_i \alpha_i K(\mathbf{x}, \mathbf{x}_i) + b\right). \quad (2.60)$$

Using a Gaussian kernel function reduces the constraints on the calculation of Lagrangian multipliers (α_i) , feature space weights, to

$$C \geq \alpha_i \geq 0.$$

The values of upper weighting bound C and Gaussian kernel σ parameters are empirically chosen.

Chapter 3

Experimental Section

This chapter will present the general experimental setup, an overview of the relevant hardware and software design, and the two primary investigative experiments.

The same setup was used for both experiments. These experiments were run sequentially. The set up will be described in three sections: 1) subject preparation, 2) subject positioning, and 3) the experimental data acquisition system.

The battery operated bioelectric amplifier was designed and built by the author for the future implementation of a portable BCI with online, realtime processing. All software for control, experimental operation, data acquisition, and measurement were designed and written by the author.

3.1 Subject preparation

The experiments require a total of ten surface electrodes to be placed on the subject. This includes the earlobe reference and bias current sink locations.

The placement of the electrodes are done in accordance with the skin preparation and equipment decontamination procedures of the College of Physicians and Surgeons of Ontario [113]. All electrode locations are first cleansed with alcohol swabs to remove oils, abraded to lower site impedance, and cleaned again with an alcohol swab. The electrodes are affixed using a small ball of conductive electrode paste, covered with a 1 inch² gauze pad, and secured with several strips of surgical tape (the subject's hair may also be used to help secure the EEG electrodes).

A set of five electrodes, with one shared reference electrode, are attached for the measurement of eye motion; the electrooculogram (EOG). The chosen electrode arrangement is illustrated in figure 2.7. While seated and focussed on point that both vertically and horizontally centers the eye pupil, the electrode are placed as near they as possible aligned with the centering axes.

A set of six electrodes, with one shared reference electrode, are attached for the measurement of brain activity; the electroencephalogram (EEG). The chosen electrode arrangement is illustrated in figure 2.13. Although not a standard montage, the individual electrode locations conform to the international 10-20 system. The standardized names for the chosen locations are: Inion, Pz, P7, and P8. The method of measuring individual subject's for the 10-20 system of electrode placement is explained in Fisch's EEG primer [17].

The subject was presented with both visual and audio instructions. The visual instructions were presented on the computer screen and provided an introduction to the experiments, requested identification information, and required approval for the publication of results. Audio information proceeded each experiment and was presented using a closed circumaural headphone.

Apparatus required for subject preparation:

1. surface skin electrode discs (Rochester Electro-Medical EverLast 9 mm gold-plated cup electrodes and reference ear clip),
2. general purpose alcohol swabs,
3. gauze padding,
4. surgical tape,
5. abrasion tape (3M Red Dot Trace Prep),
6. electrode paste (Grass-Telefactor electrode paste, type EC2),
7. cloth measuring tape,
8. distilled water and soft toothbrush for electrode washing, and
9. a closed circumaural pair of headphones.

3.2 Subject positioning

The subject was seated in a high-back computer arm chair which was well cushioned. The chair was inclined to a fixed position and the height of the chair was adjusted such that the subject's forward gaze is aligned level with the center of the computer monitor. The subject's feet were rested on a elevated platform approximately 20 cm off of the floor. Arms were placed relaxed on the chair arm rests and an acknowledgement button was placed in the left hand. A relaxed and comfortable seating position was necessary to reduce any extraneous movement that may have created signal artifacts in our data recording.

The positioning of a subject is illustrated in figure 3.1.

3.3 Data acquisition

The data acquisition system was designed, built, and programmed by the author. Each component was modular and could be tested independently. An overview of the system is illustrated in figure 3.2, however, only data connections are included; ground, reference, and control connections have been omitted for clarity.

The data acquisition system is built around the 8 channel electrophysiological amplifier which is described further in section 3.4. Each channel is reconfigurable for the amplification of either microvolts or millivolts to volts. The amplification may be fine adjusted to the appropriate voltage level for the data capture microcontroller's analog to digital converters (ADC). The sampled data and user acknowledgement data are (9 channels) streamed serially to the electrophysiological measurement capture computer. This computer's purpose is the collection and storage of the experimentally measured EEG and EOG data.

The EOG difference amplifier performs the difference between single axis electrodes. The differential of horizontal and vertical motion are output to the electrophysiological amplifier for scaling and recording. Referring to figure 3.2, the radio transmitter (TX) and receiver (RX) were employed for independent testing of the electroocular component.

A critical component of human feedback experiments is the choice and implementation of an acknowledgement system for a non-technical subject. A verbal and motion response are not an option as they are possible contaminants to EEG data. Fixed position buttons on control panels create confusion and physical discomfort. The use of a computer keyboard can potentially disrupt the software operating the experiment. The final choice was a momen-

tary push button housed in a cylindrical case that was comfortably held and easily actuated. The acknowledgement button was attached to the subject feedback microcontroller that was serially connected to the personal computer executing the series of stimuli. The feedback microcontroller also forwards the acknowledgement response to the data capture microcontroller for inclusion in the measurements. This acknowledgement response is used to synchronize the independently collected data.

The overall system was designed to perform the parallel tasks of presenting experiment stimuli, recording of the subject responses, and recording of the associated measurement data with no communication or control conflict.

Each set of experiments was video recorded for a complete record of the event.

3.4 Hardware

This section will describe the design of electrophysiological amplifier and the usage of the peripheral microcontrollers.

3.4.1 Electrophysiological Amplifier

The 8-channel electrophysiological amplifier was designed to allow each channel to be quickly reconfigured between an expected input of microvolt range ($5\ \mu\text{V}$) and millivolt range ($10\ \text{mV}$). These two ranges correspond well with the EEG (μV) and EOG or EKG (mV).

The design of the amplifier is divided into three components: 1) interface, 2) filtering and amplification, and 3) output and isolation. The related issues of shielding and grounding will be described as it relates to each component.

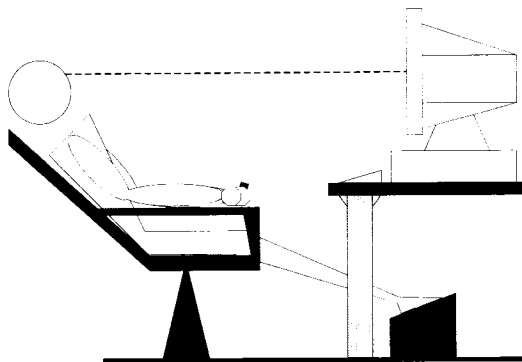


Figure 3.1: Subject positioning

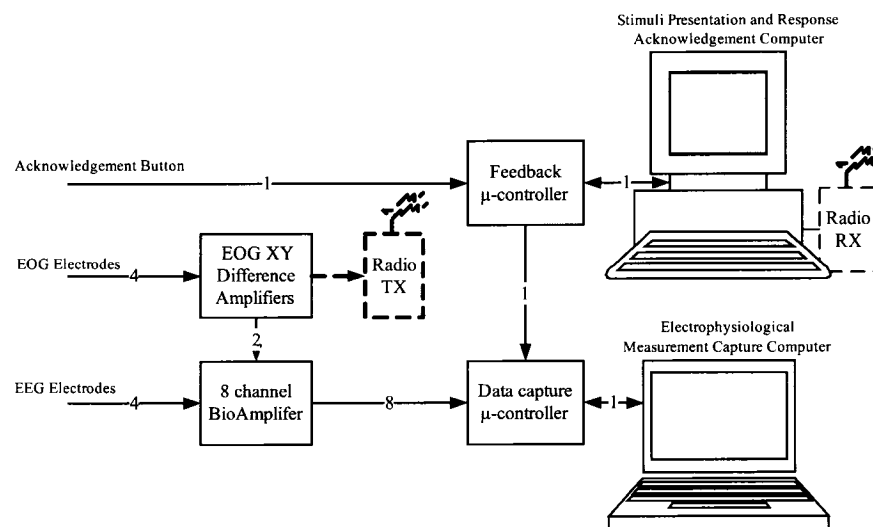


Figure 3.2: Data acquisition system overview

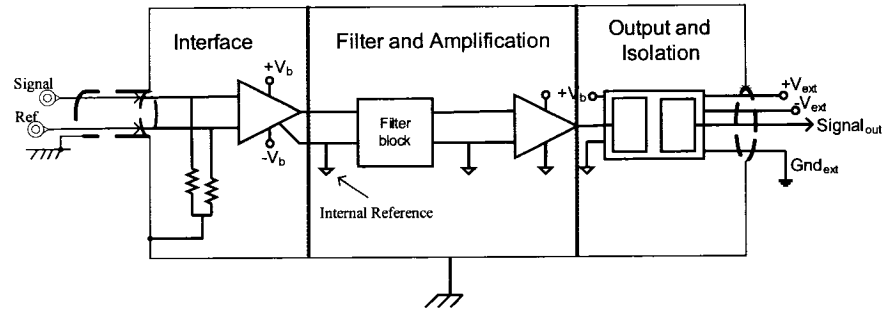


Figure 3.3: Overview of single channel electrophysiological biological amplifier components: 1) interface, 2) filtering and amplification, and 3) output and isolation

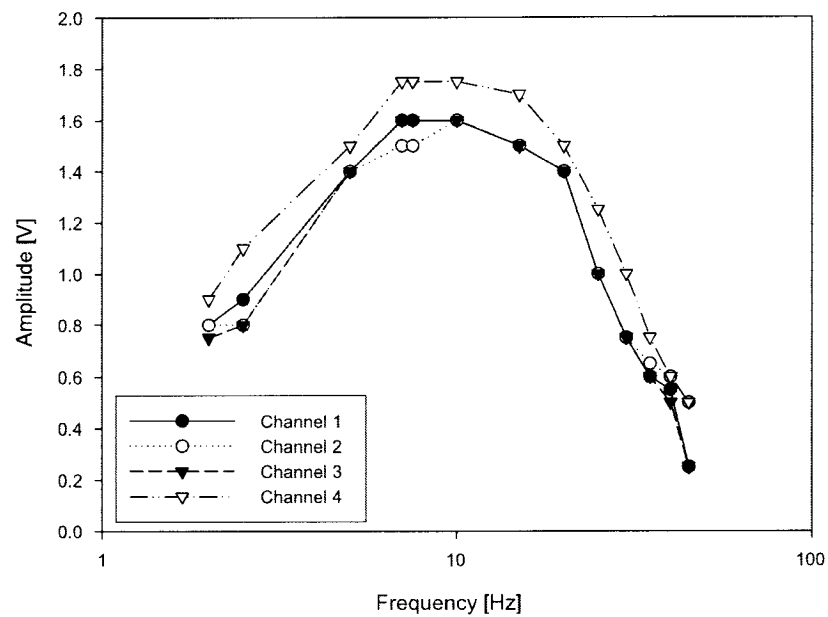


Figure 3.4: Electrophysiological amplifier frequency response for fixed input of $4 \mu V_{pp}$

Interface

The interface begins at the surface electrode locations. Each electrode is attached to the skin using a conductive electrode cream, as described in section 3.1. The site is prepared this way to lower electrode-skin impedance. The electrode material is chosen such that it will not interact chemically with electrolytes of the skin. Common choices of material for the electrode coatings are gold, silver-chloride, tin, or platinum. Each coating will produce a slightly different electrical reaction to the electrode cream, making it important to use the same electrode material for all electrodes. Based on communication with the London Health Sciences Centre's [114] epilepsy unit, gold-plated electrodes were chosen. The electrodes are connected to a shielded cable that carries their signal into one of eight channels of the electrophysiological amplifier. Each electrode measurement is referenced to an electrode clip placed on the left earlobe of the subject. The earlobe is a commonly used reference site because it is in the same region as the other EEG/EOG electrodes, but it is relatively isolated electrically from the signals of interest.

For each channel, the reference electrode voltage is subtracted from one signal electrode voltage using a precision instrumentation amplifier. The hardware chosen was the Burr-Brown (Texas Instrument) INA114, primarily for its operating range (minimum ± 2.25 V), common-mode rejection ratio (minimum 115 dB), and its very small input bias current (2 nA). The output of this amplifier presents the amplified voltage difference to the next stage. The output of this stage is referenced to an isolated signal ground.

Filtering and amplification

The signal is notch filtered to remove 60 Hz noise and then low pass filtered with a second order Butterworth filter. The hardware chosen is a general purpose, single-supply amplifier. The filtered signal is presented to the next and final stage.

Output and isolation

The final output stage electrically isolates the data acquisition electronics of microcontrollers and personal computers from the filtering and amplification stage. This isolation allows the internal signal voltages to float independent of the hardware to which it is connected. The hardware chosen was the Burr-Brown isolation amplifier ISO122.

3.4.2 Microcontrollers

The microcontroller selected was the Motorola 16-bit H9S12C32. The selection of this micro was based on three attributes:

1. speed - 25 MHz,
2. memory - 2 kB RAM and 32 kB flash, and
3. 8-channel with 10-bit resolution analog to digital converters (ADC).

The highest frequency of interest for these experiments is 30 Hz. Based on the Nyquist Sampling Theorem [115],

$$\Omega_S \geq 2\Omega_N \quad (3.1)$$

where Ω_N is the maximum frequency contained in our signal of interest (Nyquist frequency) and Ω_S is the Nyquist rate which must be at least twice Ω_N , our Nyquist rate must be greater-than or equal to 60 Hz. Our chosen sampling rate is 100 Hz. The maximum ADC input voltage is configurable, and chosen to be 2.56 V. Given that the ADC has a precision of 8-bits, this results in a resolution of 0.01 V.

To facilitate the timely transfer of recorded data measurements the micro-controller communicates serially (RS232) with the personal computer at rate of 115.2 kbps.

3.5 An electroocular computing interface

3.5.1 Objective

To investigate the suitability of the electrophysiological measurement of eye motion for the application of computer interfacing and/or control.

3.5.2 Background

In order to use the electrooculogram for our system, we need to characterize its parameters. According to Stern *et al.*, our system must be capable of amplifying signals in the range of 15 to 200 μV and be able to reproduce signals of up to 15 Hz for the accurate measurement of eye position.

3.5.3 Procedure

We performed two single-axis (x and y) experiments to verify the efficacy of the system concept.

The electrode positions, as illustrated in figure 2.7, were prepared according to section 3.1. The EOG amplifier block was then calibrated to the subject's range of eye motion.

The experiment required the subject to focus on the center of the computer screen from a distance of 1 m, then follow a horizontal line to the subject's left edge of the computer screen, then follow the line back to the center and on to the subject's right edge of the screen (screen width of 32.5 cm). This was repeated for the vertical axis.

Rather than directly connecting the microcontroller to the personal-computer, it was observed that the operation of a common computer mouse was based on the same 2-D vector principle as our electroocular device. The advantage of using standard hardware was the availability of software and drivers which are widely supported. We chose to employ a common and inexpensive 3-button computer mouse that used optical encoders to determine its x - and y -axis vectors. Once the internal operation of the computer mouse was reverse-engineered, its usage for this experiment was the matter of replacing the outputs of the optical encoders with output from the microcontroller to mimic "mickeys". A single "mickey" represents the smallest increment of movement along an axis for the mouse.

3.5.4 Observation

A partial record of the DC horizontal (x -axis) eye movement is shown in figure 3.5. The vertical (y -axis) movement was similar, but with a smaller amplitude. The position of the eye is easily observed in figure 3.5, however the range of values are less than desirable for a 2.5-V ADC range.

Based on the geometric arrangement of the experiment, the range of motion

of the eye on the x -axis was $\pm 9.2^\circ$ causing a voltage difference of 0.45 V. This resulted in a resolution of 24.5 mV/ $^\circ$.

Longer duration data records reveal a non-periodic oscillation, or shift, of the signal average. Although calibrated, this shifting results in a saturation of amplifier inputs causing outputs to vary beyond the power supply capability.

3.5.5 Discussion

The efficacy of the interface is confirmed, however, the longer duration data measurements show a non-periodic average shift of the measured signal causing amplifier saturation. Initial troubleshooting investigated the appearance of a floating electrical ground reference, however, the testing the system with an isolated electrical model eye of the human eye produced the correct and expected results which were within the limits of the amplifier design.

The exclusion of the amplifier from the source of oscillation indicates the recorded data is the result of a real electrical response from the eye. The cause of this is believed a combination of the eye responding to changes in light intensity and focus (“adaptation”).

Although the use of eye motion is an intuitive method of control, the issue of adaptation is not easily overcome. As a result, implementation of this control method was suspended for future research.

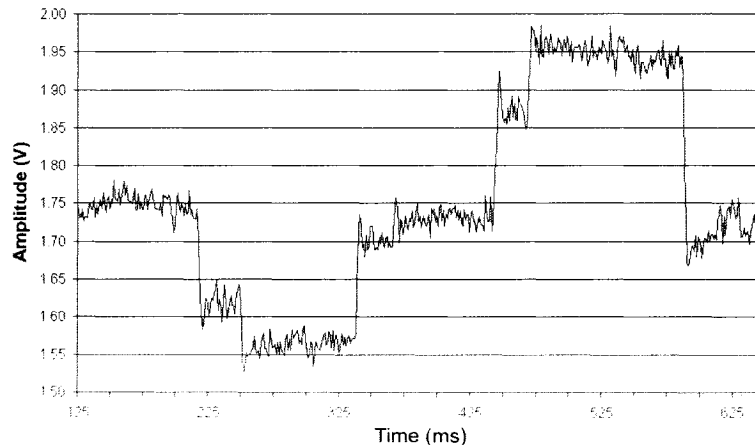


Figure 3.5: Horizontal (x -axis) DC record of eye movement

3.6 Electrophysiological Response to Auditory Tones: Threshold

3.6.1 Objective

To investigate if audiological threshold detection generates a consistent and measurable response in the subject's electroencephalogram and can this response be used as a binary state indicator for the control of an assistive computing device.

3.6.2 Background

When a hearing test is performed, one of the audiologist's measurements is the subject's hearing threshold. The threshold is determined by the subject's acknowledgement (or lack of) to series of short tones. The tones span the frequency range of human hearing and vary in amplitude. If a subject is

deficient in any portion of their threshold response then they generally require a hearing assistive device.

A hearing assistive device, such as a hearing aid, will amplify the incoming sound signals of the deficient frequency range beyond the subject threshold and into the subject's hearing range. There are two primary concerns here:

1. An individual with hearing impairment, that does not use a hearing assistive device has difficulty in communication because of corruption of incoming sound information; loss of intelligibility.
2. A common complaint among subjects with hearing aids is the lack of discrimination of the amplified sound information. Many users claim not to wear their aid as a result. Subjects that must wear their aid for prolonged periods will eventually further damage their hearing due to the constant amplification.

From observation, an individual experiencing difficulty in communication due to a loss of audiological intelligibility exhibits an unconscious emotional response; an affective state.

The electroencephalogram is a measure of brain current. A synchrony of oscillating brain currents have been correlated various brain activity. Several of those correlated oscillations have well defined frequencies in brain research.

3.6.3 Procedure

The electrode positions, as illustrated in figure 2.7, were prepared according to section 3.1.

The experiment required the subject sit back in a reclined chair and to close their eyes. All instruction and stimuli would be presented through the

headphones. Audio instruction explains the format of the experiment, the method of acknowledgement, and the anticipated duration of the experiment. The subject pressed the acknowledgement button to begin and is presented with an initial ten seconds of silence. The subject is presented with 3 sets audio tones. Each set presents the series of 100 Hz, 250 Hz, 500 Hz, 1 kHz, 2 kHz, 3 kHz, 4 kHz, 5 kHz, 8 kHz, 10 kHz, 12.5 kHz, and 15 kHz. The order of presentation, intra-, and inter-tone durations are varied. Each tone is presented in discrete, but increasing steps of amplification. When a tone is detected, the user presses the acknowledgement button. The EEG data and acknowledgement responses are collected by the data acquisition system.

3.6.4 Observation

Each experiment produced several mega-bytes of electrophysiological data. The frequency- and time-domain results of one subject and his/her threshold response to selected audio tones (8 kHz, 10 kHz, 12.5 kHz, 15 kHz) is included in Appendix A. Each set of figures examines the data for the two second duration preceding the subject's threshold acknowledgement.

3.6.5 Discussion

The visual inspection of EEG data may be performed by trained doctors and clinicians, but it is generally for the identification of abnormalities. With repeated response to the same stimulus, an averaged result may provide a consistent wave form. However, the identification of single trial response is not tractable using these methods, nor can they be effectively implemented in a personal computing device.

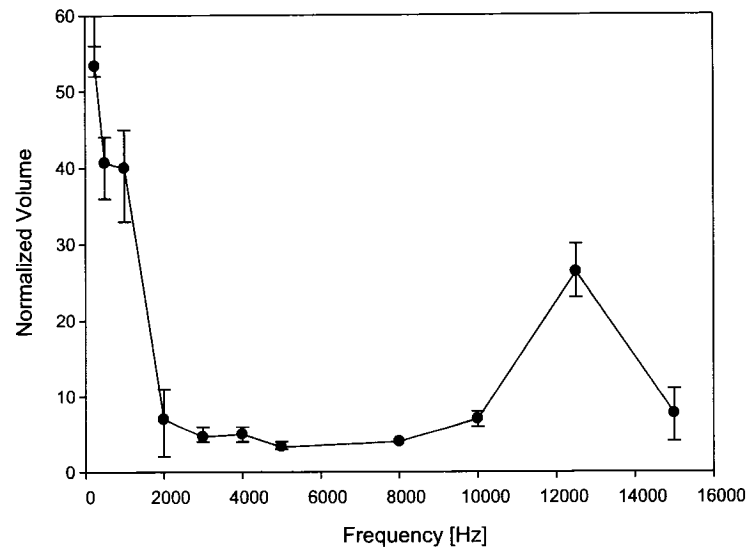


Figure 3.6: Subject-A hearing threshold response

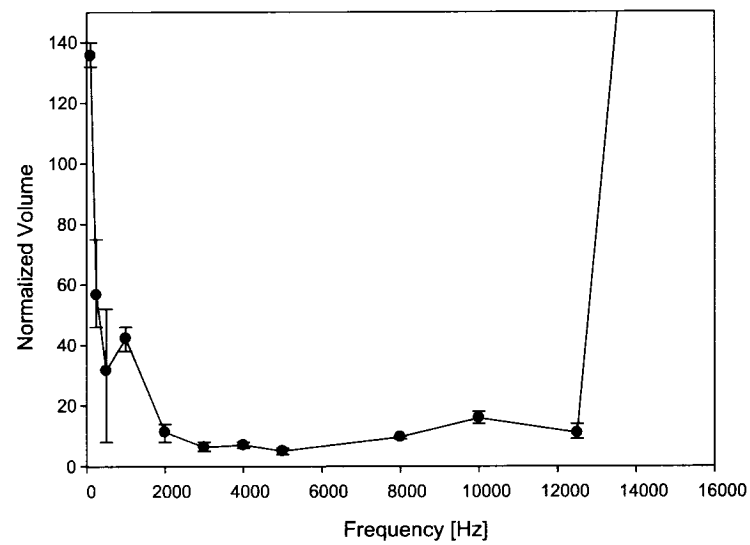


Figure 3.7: Subject-B hearing threshold response

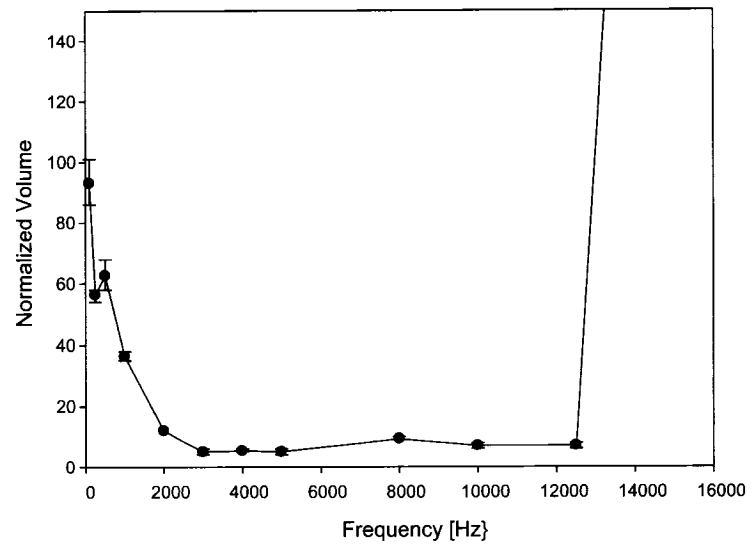


Figure 3.8: Subject-C hearing threshold response

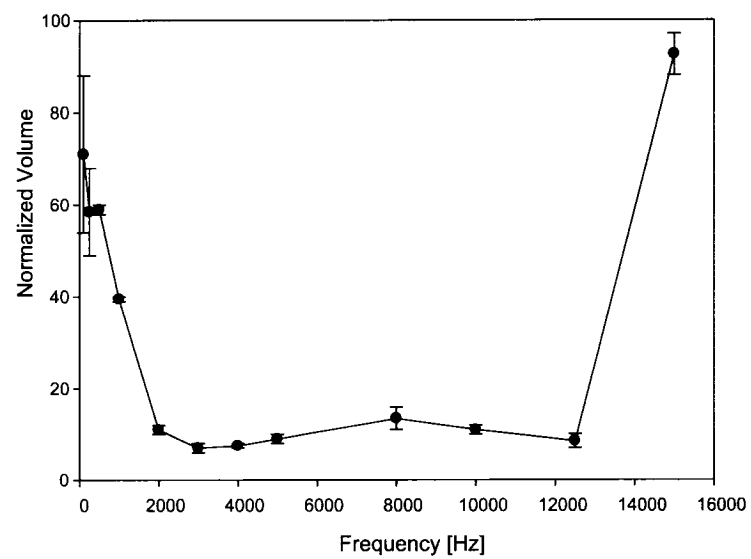


Figure 3.9: Author's hearing threshold response

Chapter 4

Model and Analysis

A successful system requires the application of a rule set that has good generalization properties and permits some error, but can be specific enough for selective activation; in our case binary classification. These requirements are not without conflict of each other.

The selection of data attributes to formulate a good rule set can be attempted using various methods of visualization, but this method is generally not well suited for data sets that have a dimensionality beyond three. Formulation of a rule set for data sets of high dimension is further complicated if the distribution of that data is the object of study; the distribution is unknown.

One method of handling such data sets is the use of an approximation to reduce the dimensionality. For our EEG data set (Inion, Pz, P7, P8) we have chosen to employ a Laplacian electrode array to estimate the source density current. The result was a reduction to a single dimension from four. If sufficient, this approximation will allow for visualization, reduce the effect(s) of non-common interference, and relax the difficulty in choosing a reference electrode location.

The post-processing and/or off-line processing of signal data filtering has an associated high computational cost; however, if the selection of specific components of the data can help improve the formulation or success of a classification rule set then that filtering may be implemented in analog electronics or possibly online processing. The choice of what to filter presented a more difficult question. The act of comprehension is performed unconsciously and is achieved, in part, by the redundancy in our speech [79]. It is only when this process fails that we begin to become aware of it, or rather, its failure. Before exhibiting a response externally, we respond internally; invoking an emotional state. By observation and introspection, a loss of comprehension will be followed by confusion (emotional stress), a focus of attention, and increased mental activity. There are a number of electrophysiological processes which may be correlated to these reactions, however, in the measure of brain current there are four frequencies that are well correlated:

alpha (θ) - emotional stress,

alpha (α) - focus of attention,

beta (β) - increased mental activity, and

gamma (γ) - attentional states.

There has been success using a wide band of $\alpha\beta$ in a functional brain-computer-interface [32]. Our off-line filtering was designed using a frequency sampling method that significantly reduced the computational cost of filtering making it suitable for online processing with smaller, less powerful processors.

For our model we have chosen to investigate:

1. the raw EEG measurements from the four electrodes (Inion, Pz, P7, P8),

2. the raw EEG Laplacian source density approximation,
3. the filtered Laplacian source density analysis (θ vs. α)
4. the filtered Laplacian source density analysis (α vs. β), and
5. the filtered Laplacian source density analysis ($\alpha\beta$ vs. γ).

The investigation requires knowledge of when a response is evoked. Our hearing threshold experiments prepared and positioned a subject to acknowledge when an audio tone was detected. What must be considered is that inherent in a subject's acknowledgement is the latency of human reaction time. This presents an uncertainty that cannot easily be overcome in the study of perception. Rather than attempt to define when a response is evoked, we chose to use the subject acknowledgement as the fixed reference and examine the preceding (2 seconds or 200 samples) data that prompted the acknowledgement. Unfortunately, even with a fixed reference the distribution of data relevant to the event was not sufficiently evident by visual inspection. An example of this data is provided in Appendix A. Developing a rule set based on visual inspection proved an unreliable method of classification and posed significant difficulties for individual subject implementation.

Support vector machines (SVM) have the capability of classifying nonlinearly separable data by "learning" from training data sets. The SVM takes the selected data attributes and spans them across a higher dimension feature space. The mapping from attribute space to feature space is performed using a kernel function. Based on the training output values, the SVM forms a decision, or classifier, boundary(ies) in feature space. This decision boundary is "*soft*", such that it permits misclassification in order to allow for better generalization. SVMs are well suited to our needs for two primary reasons.

First, training of the SVM may be performed with small data sets and yield high classification success, and second, the distribution of the output need not be known prior to training.

The implementation of the SVM requires the selection of several parameters: kernel function, associated kernel parameters, and a permissible margin of error. Each parameter is selected empirically and currently there are no better methods of selection. Our model used a Gaussian kernel because it has been accepted in machine learning theory literature [116–118] to be well suited to noisy experimental data and also because of the nature of a Gaussian function it relaxes the boundary restrictions of the SVM design.

The training data is extracted from the 8 kHz hearing threshold experiment in the first trail. This is illustrated in figure 4.1. The selected window of observation is two seconds, or 200 sampling points. To “*teach*” the SVM we require both input and output training data. However, we do not know the distribution of the output, but given the subject’s acknowledgement we know that a response has just occurred. The subject is presented with several hearing threshold trials, of which we have labeled two such trails in figure 4.1. From the first trail the *training input* is extracted and for our *training output* we have partitioned it into fifteen possible segments as shown in figure 4.2. Training output partitions numbered 1 - 7 were used to investigate a response duration of 500 ms, and partitions 8-15 were investigated a refined response duration of 250 ms. The SVM is trained using all fifteen possible outputs. The training will formulate the decision boundary (hypersurface) using a small number of training data points; support vectors. With the assertion that a response has occurred and that its occurrence is measurable, we evaluate a *testing set* of data. As illustrated in figure 4.2 the testing set of data is the entire second trial which is independent of the first trial. Each subject acknowledgement in

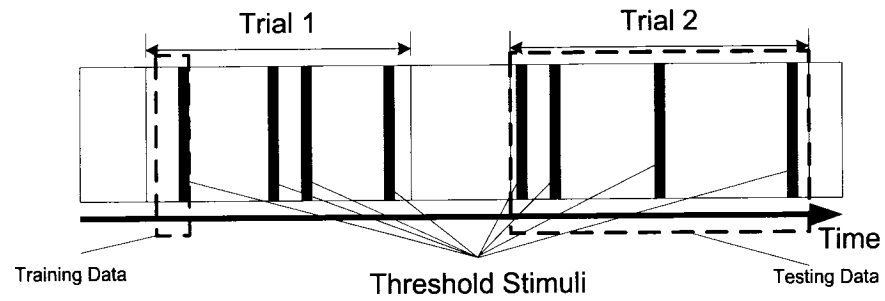


Figure 4.1: Experimental trials and their relation to training and testing data

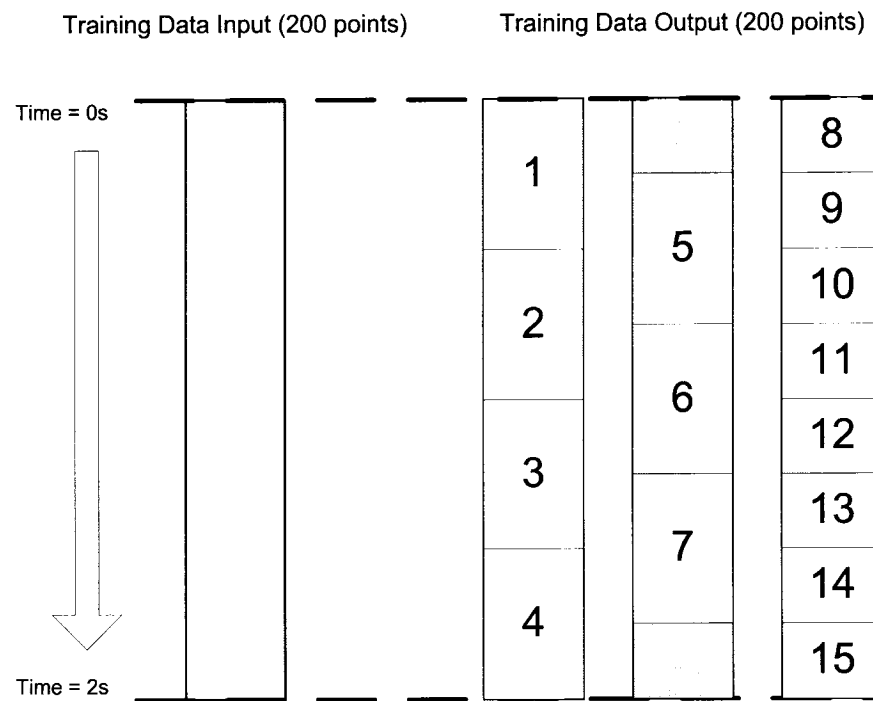


Figure 4.2: Support vector machine training input and output

Table 4.1: Minimum and maximum correct SVM classification

Subject	Duration (ms)	σ	C	NSV	Classifications	Correct(%)
A_{min}	250	0.25	10	57	14501	86.23
A_{max}	250	1.00	5	113	14501	98.79
B_{min}	500	0.25	10	141	2688	76.30
B_{max}	250	0.50	10	77	2688	93.49
C_{min}	500	0.25	10	158	1673	66.53
C_{max}	250	1.00	1	77	1673	90.79

Table 4.2: Best classification for least computational cost

Subject	Duration (ms)	σ	C	Correct(%)	NSV (%)	$\frac{\text{correct classification}}{\text{no. of support vectors}}$
A	250	0.50	1	98.79	26.5	3.73
B	250	0.50	5	92.93	37.0	2.51
C	250	0.50	5	90.32	36.0	2.51

the testing data is extended back in time (P) to accommodate subject reaction latency. If our training data created a good general classifier (binary classifier or dichotomization) then we may expect that the testing data would have had very high percentage of correct classification.

Using the four electrode locations (Inion, Pz, P7, P8) raw EEG measurement, our parametric search examined all combinations of outputs data (1-15), subject reaction latency (P: 500 and 250 ms), upper limit on classification error (C: 1, 5, and 10), and the Gaussian kernel radial bias function (σ : 0.25, 0.50, and 1.00). Table 4.1 presents the minimum and maximum classification results. Note that NSV is the number of support vectors required for the SVM classifier and that "Classifications" is the total number of points processed by the SVM classifier. Plots of the parametric searches are shown in figures 4.3 to 4.8.

The SVM classification has an associated computational cost that is directly related to the number of support vectors the machine requires to form

the decision boundary. The higher the percentage of support vectors, the higher the computational cost and often a poorer generalization for the classifier. Figures 4.3 to 4.8 were used to evaluate the classification results relative to computational cost. Table 4.2 summarizes the best classification for the relatively least computation cost.

Our model also investigated using the Laplacian source density approximation to reduce the data dimensionality. The SVM applied to this approximation using the above parameters for best classification results are presented in table 4.3.

Specific frequency components of the Laplacian signal were also analyzed. The θ *vs.* α frequency bands, α *vs.* β frequency bands, and the $\alpha\beta$ *vs.* γ frequency bands were each used for set of attribute space inputs. The classification results are presented in tables 4.4, 4.5 and 4.6, respectively.

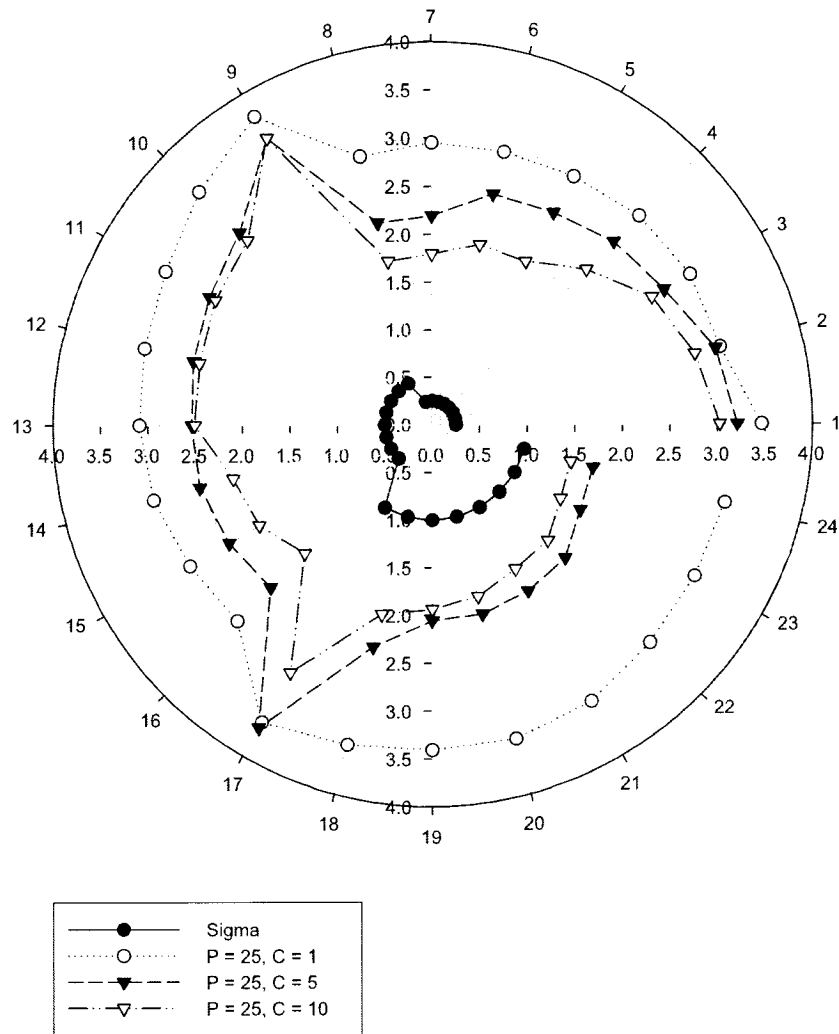


Figure 4.3: Subject-A parametric plot using 250 ms classification window

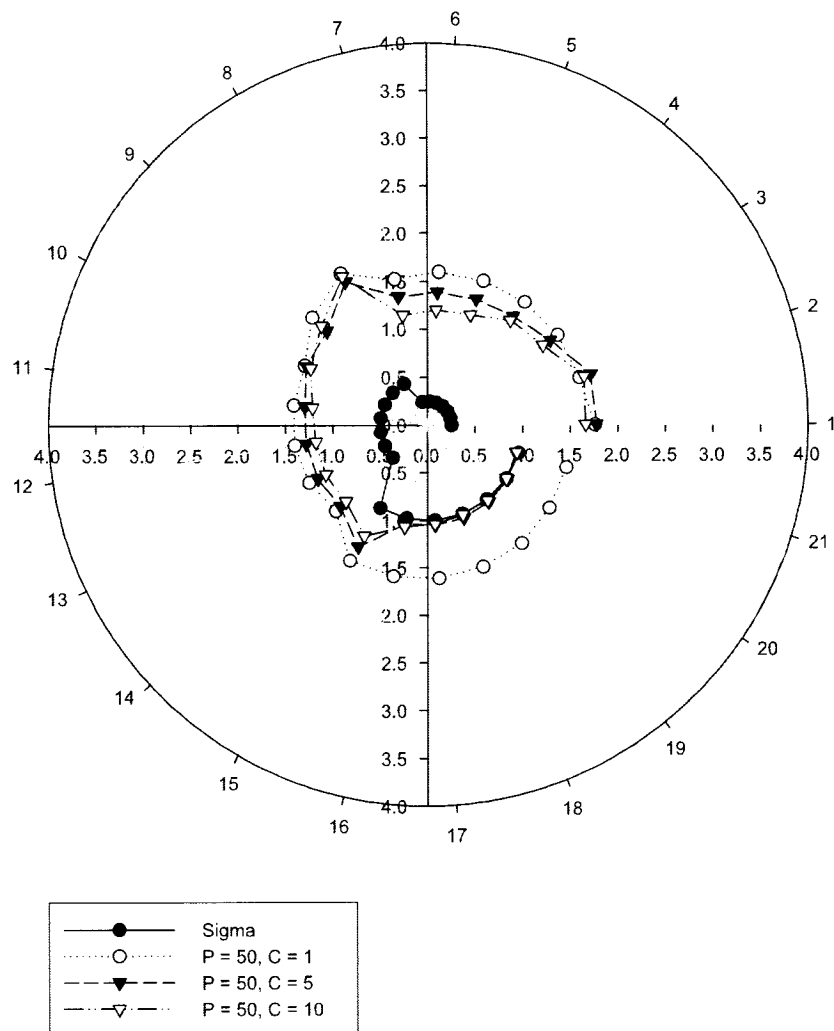


Figure 4.4: Subject-A parametric plot using 500 ms classification window

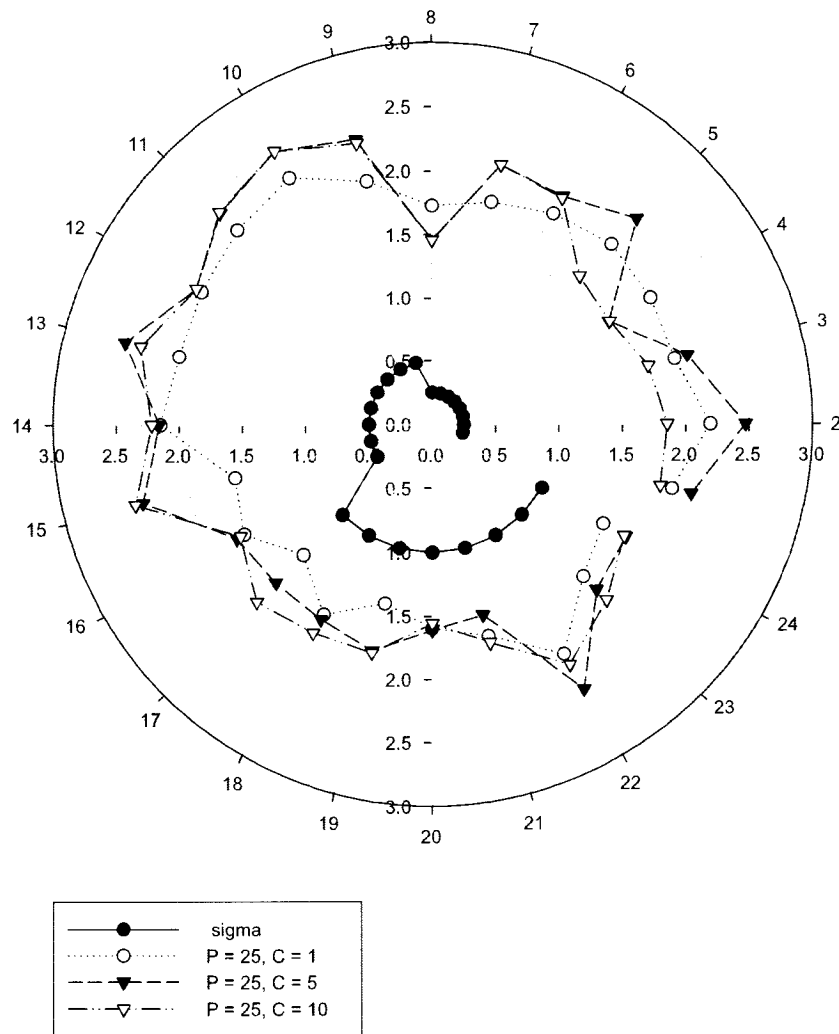


Figure 4.5: Subject-B parametric plot using 250 ms classification window

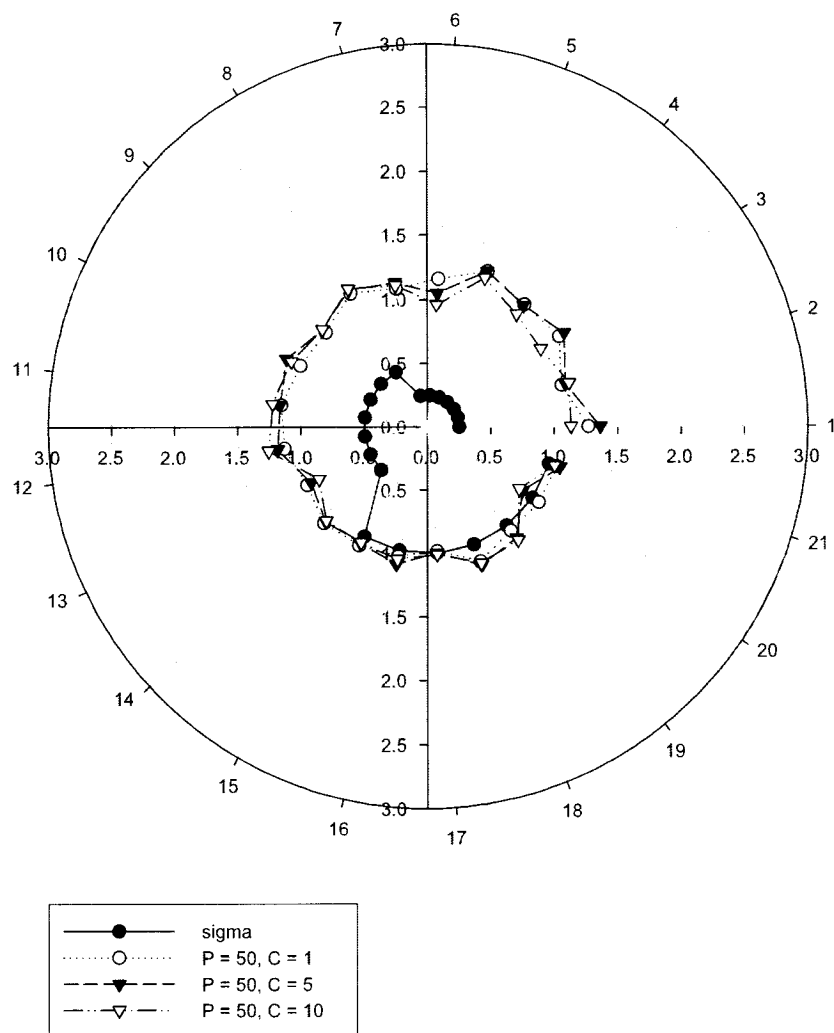


Figure 4.6: Subject-B parametric plot using 500 ms classification window

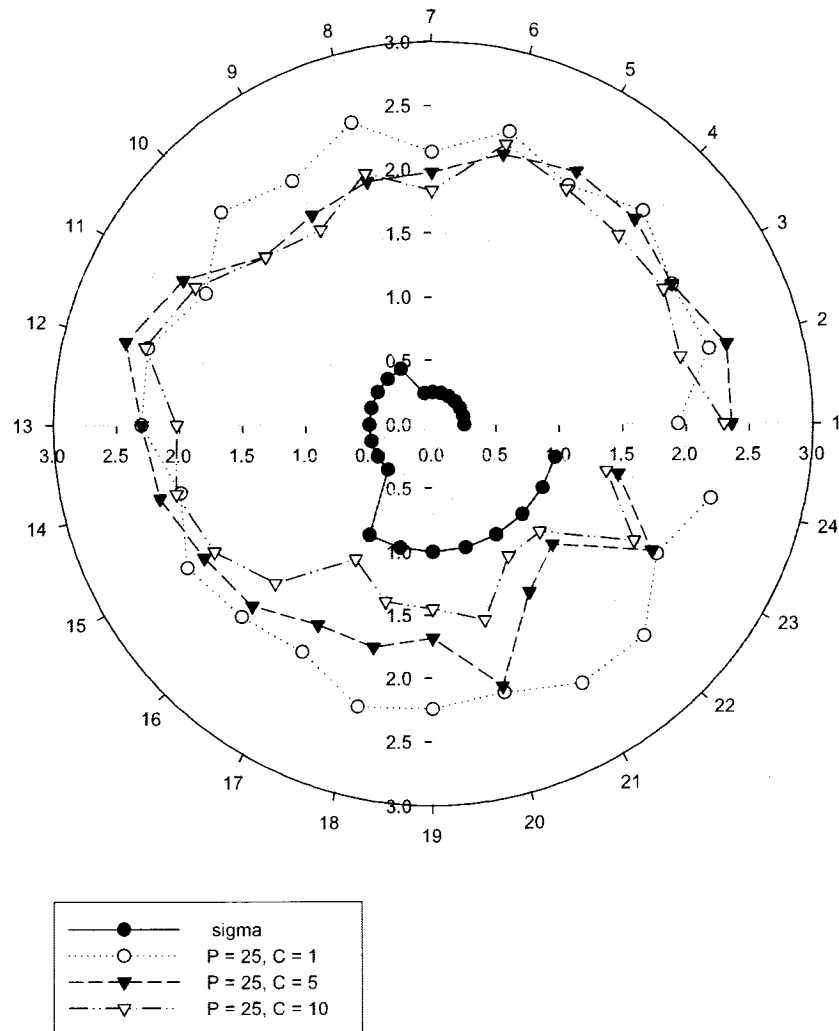


Figure 4.7: Subject-C parametric plot using 250 ms classification window

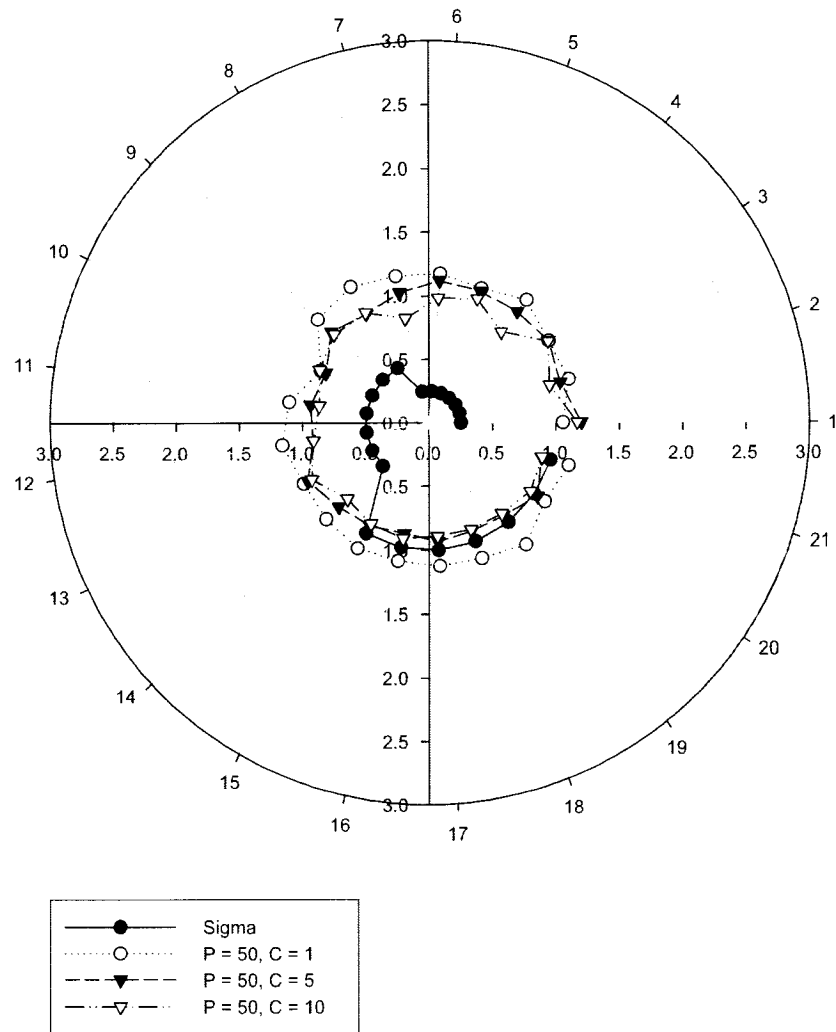


Figure 4.8: Subject-C parametric plot using 500 ms classification window

Table 4.3: Laplacian source density approximation minimum and maximum correct SVM classification (250 ms, $\sigma = 0.5$)

Subject	C	NSV(%)	Classifications	Correct(%)	$\frac{\text{correct classification}}{\text{no. of support vectors}}$
A_{min}	1	100.0	14501	79.1	0.79
A_{max}	1	95.5	14501	97.97	1.03
B_{min}	5	100.0	2688	54.28	0.54
B_{max}	5	66.0	2688	94.42	1.43
C_{min}	5	100.0	1673	63.72	0.64
C_{max}	5	65.0	1673	92.29	1.42

Table 4.4: Filtered θ vs. α Laplacian source density approximation minimum and maximum correct SVM classification (250 ms, $\sigma = 0.5$)

Subject	C	NSV(%)	Classifications	Correct(%)	$\frac{\text{correct classification}}{\text{no. of support vectors}}$
A_{max}	1	98.5	14501	6.76	0.07
A_{max}	1	46.5	14501	98.97	2.12
B_{min}	5	99.0	2688	13.39	0.14
B_{max}	5	40.0	2688	94.42	2.36
C_{min}	5	99.5	1673	39.39	0.40
C_{max}	5	36.0	1673	92.29	2.56

Table 4.5: Filtered α vs. β Laplacian source density approximation minimum and maximum correct SVM classification (250 ms, $\sigma = 0.5$)

Subject	C	NSV(%)	Classifications	Correct(%)	$\frac{\text{correct classification}}{\text{no. of support vectors}}$
A_{min}	1	99.0	14501	6.43	0.06
A_{max}	1	43.5	14501	98.97	2.28
B_{min}	5	98.0	2688	24.22	0.25
B_{max}	5	31.5	2688	94.42	3.00
C_{min}	5	97.5	1673	24.33	0.25
C_{max}	5	35.0	1673	92.29	2.64

Table 4.6: Filtered $\alpha\beta$ vs. γ Laplacian source density approximation minimum and maximum correct SVM classification (250 ms, $\sigma = 0.5$)

Subject	C	NSV(%)	Classifications	Correct(%)	$\frac{\text{correct classification}}{\text{no. of support vectors}}$
A_{min}	1	98.5	14501	10.05	0.10
A_{max}	1	36.5	14501	98.97	2.71
B_{min}	5	97.0	2688	28.98	0.30
B_{max}	5	32.5	2688	93.68	2.88
C_{min}	5	97.5	1673	22.95	0.24
C_{max}	5	32.5	1673	92.29	2.84

Chapter 5

Discussion, Conclusion, and Recommendations

The research proposed was to investigate the usage of electrophysiological response for the interface and control of a computing device. The application for this work was the autonomous augmentation of audio perception with a digital hearing aid as the data processing device. Using our model, the device would be capable of autonomously modifying the speech signal based on the identification of electrophysiological response, or an affective state. We studied the speech communication channel from production to perception and examined several electrophysiological attributes which lent themselves to being measured by a computing device adorned about the ear. The selected attributes were the motion of the eye (electrooculogram) and the activity of the brain (electroencephalogram). Harnessing the eye measurement for control was demonstrated effective, but visual adaptation could not be controlled or corrected; thus this method was postponed for future research. The measurement and use of brain current for the control of a computer (brain-computer-interfacing)

can be traced back approximately 30 years to the research of Vidal *et al.* Since then there have been a few notable examples of functional BCI by Wolpaw *et al* [20, 32], McFarland *et al* [25, 32], and Birbaumer *et al* [28, 32]. However, those methods of BCI depended upon operant conditioning and significant, if not full, cognitive focus. The model we proposed employed the post-“learned” and innate characteristics that remain from the damaged attribute or are associated with it. In effect, the operant conditioning for our model is performed *in situ*. Given the nature of measuring brain activity it is difficult to employ signal averaging techniques to reduce “noise” when the response may be aperiodic, thus averaging may only dilute the signal’s presence. Instead, our model’s focus was to identify an electrophysiological/affective state using single trials. The single trial identification of an affective state is not a trivial task, but it has the potential for significant speed of response.

Reviewing the three assumptions on which our model is based:

1. Emotional responses, or affective patterns, can be probed using observable bioelectric signals, in particular using the fluctuations of electroencephalographic potentials from the human scalp.
2. All meaningful electroencephalographic phenomena should be viewed as a complex structure of elementary rhythms that have correlation with underlying processes.
3. Although operant conditioning procedures could increase the reliability and stability of these time signatures and patterns, the loss of a normal or innate attribute would invoke a reliable and measurable affective pattern.

The results from our model analysis are very encouraging. By determining a good set of parameters, our support vector machine generated a very

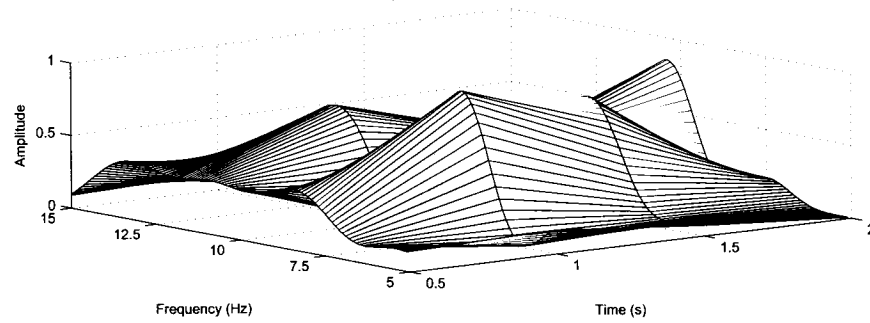
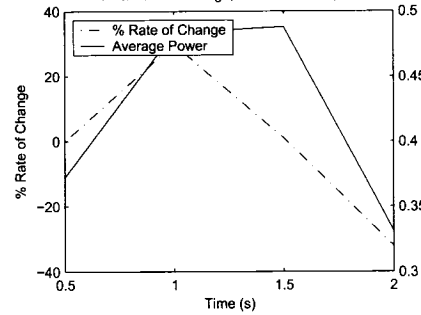
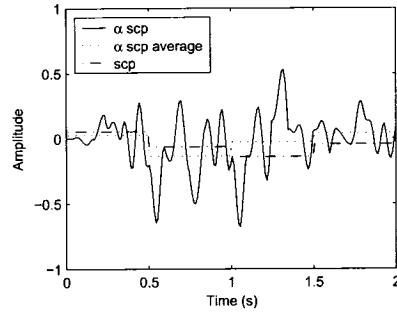
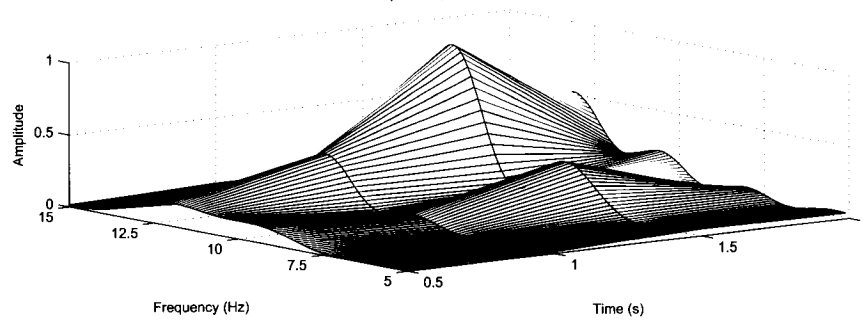
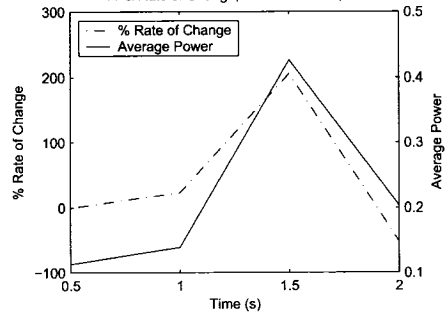
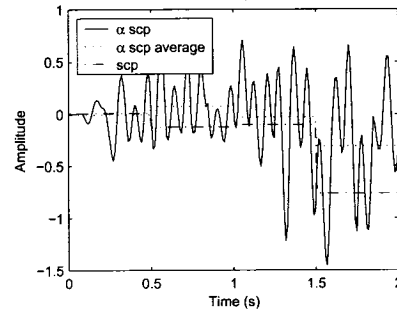
high percentage of correct classification ($>90\%$). In reference to our model assumptions, we have validated that emotional responses (affective patterns) can be measured using bioelectric signals and that the loss of an innate attribute is sufficient to produce a reliable and measurable response without explicit operant conditioning, or subject training of the BCI. However, our second assumption, although well documented in brain research literature, will require further investigation for validation in our research. The data reduction method of source density estimation resulted in similar classification results, but with increased computation cost. The filtering of specific frequency components for the training and testing of the support vector machine (SVM) classifier produced excellent results, but those results do not significantly differ from the non-filtered raw EEG training and testing data. Given the successful percentage of classification of each (raw EEG, raw Laplacian, filtered Laplacian), the choice of which is better suited for online implementation will be based on the capabilities of the target platform.

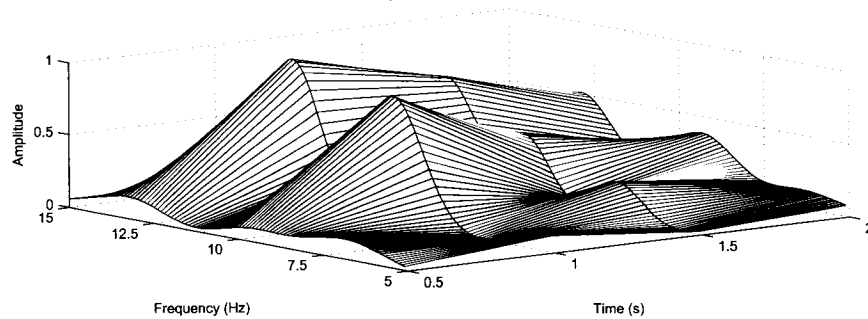
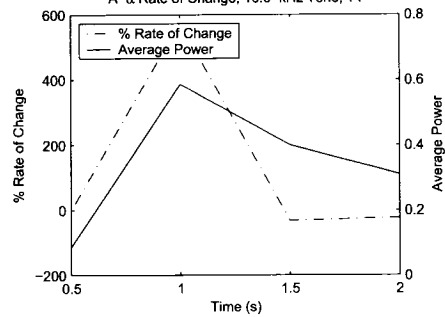
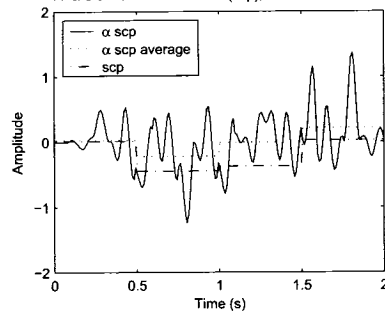
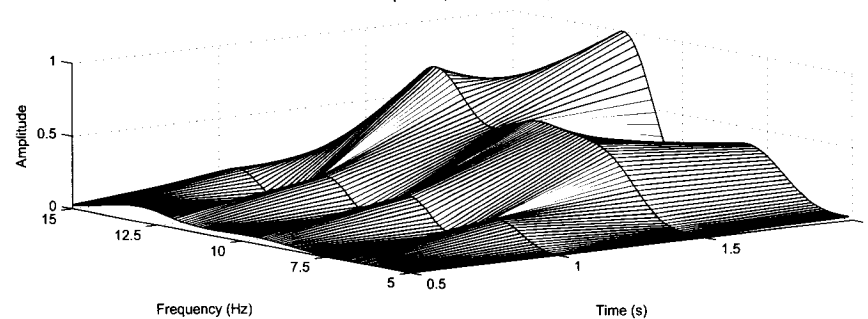
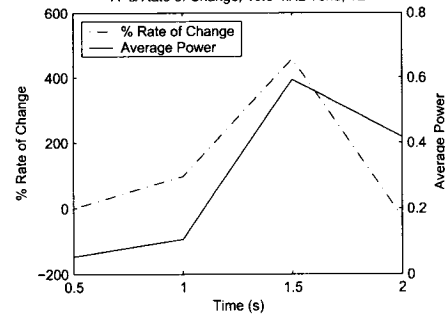
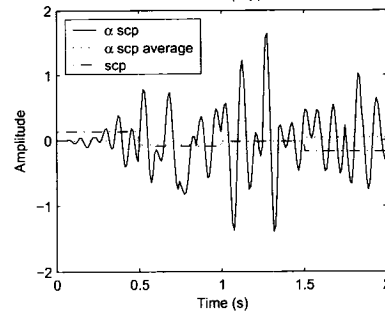
This research has successfully proven the efficacy of autonomous single trial identification of affective states as an alternative or additional method of hearing prosthetic control. The model successfully demonstrates the concept of a double feedback mechanism and the method of bidirectional communication between the man and the machine; cybranetics.

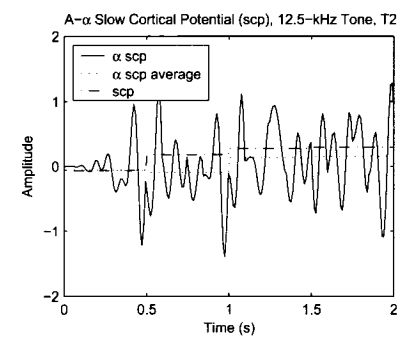
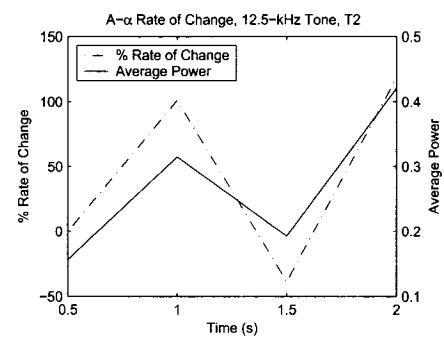
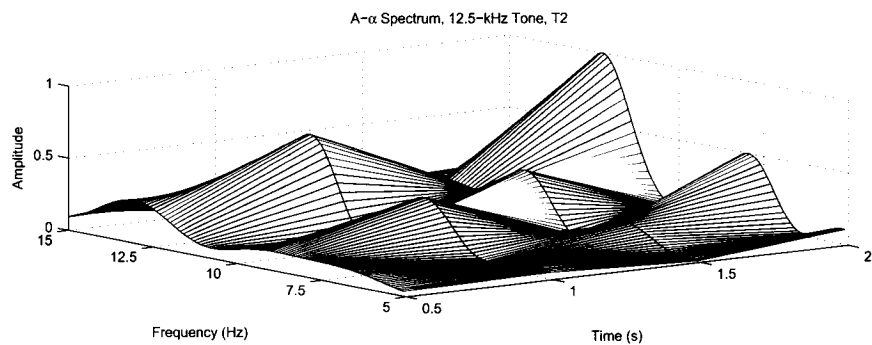
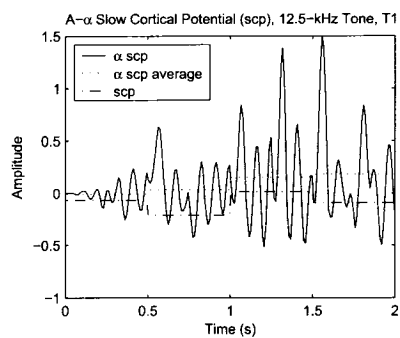
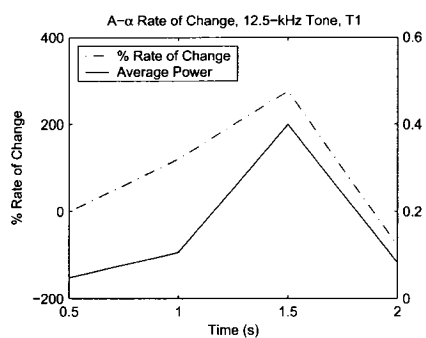
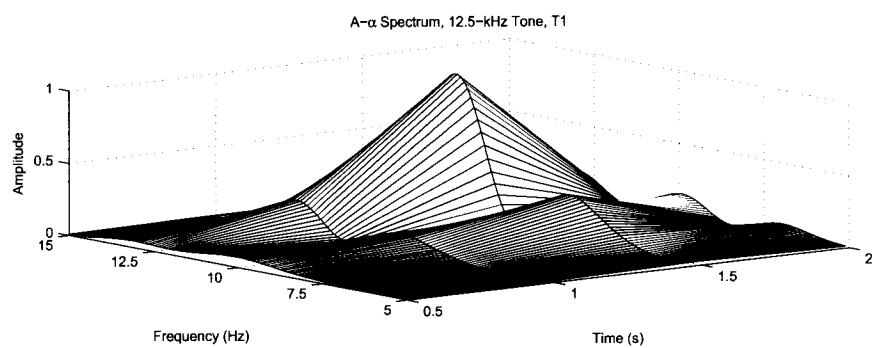
Recommendations for refining this research are to focus on increasing the communication bandwidth and information content. Neglecting the overhead of target platform processing, the information transfer rate of the present model was 1 bit / 250 ms; 4 bits/second or 240 bits/minute. A recent survey of BCI [30] information transfer rates stated a maximum of 5 – 25 bits/minute. However the comparison is not adequate because the survey of BCI research is primarily for the conscious control of a computer's cursor for the selection

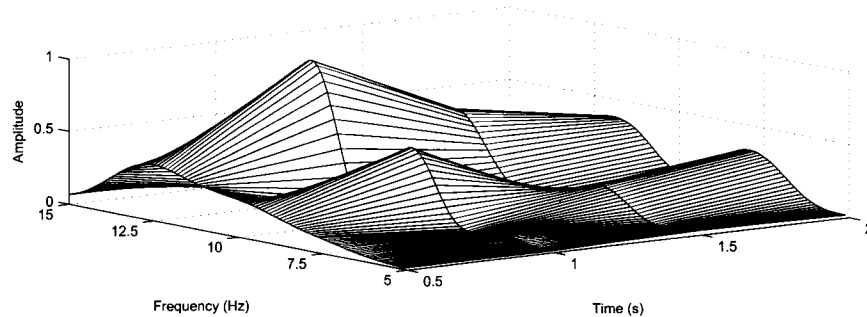
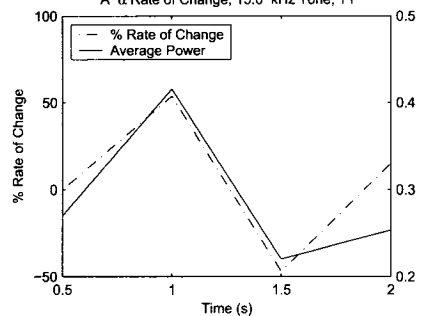
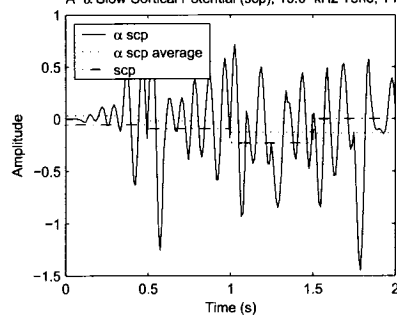
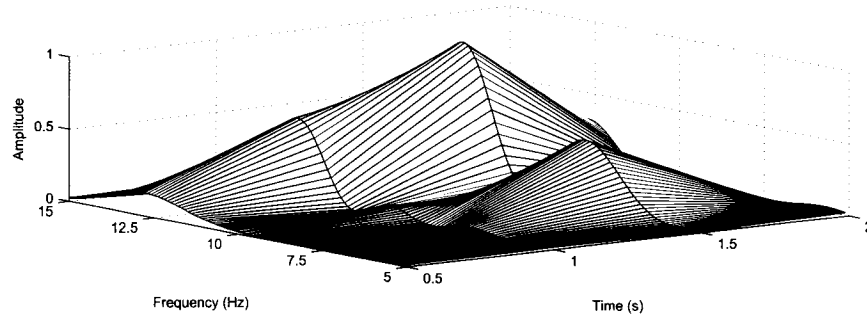
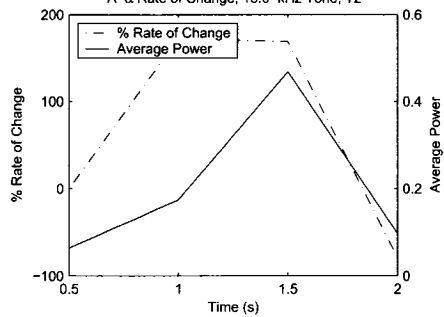
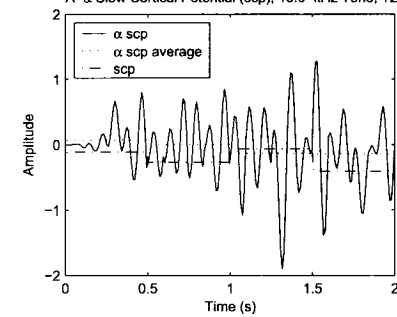
of symbols or letters. Our model is novel in that respect, but limited as well. The next step of this research would be to investigate if our affective state classification can be extended to two- or three-bits for the selection of an affective quadrant or octant employing the same concepts used in synchronous sequential digital logic design to create an affective state machine (SASM). To provide a contextual awareness it may be necessary to use parallel information channels (e.g. direction of visual gaze) and parallel support vector machines as inputs to the synchronous affective state machine.

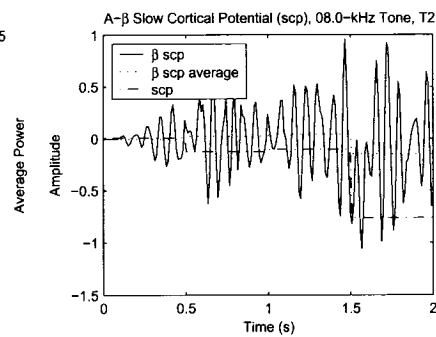
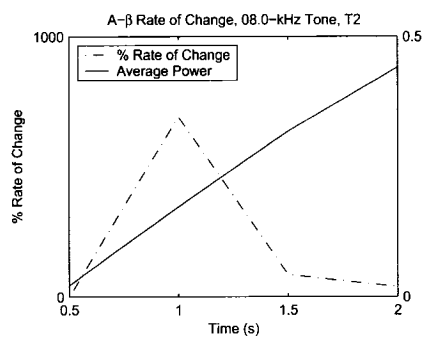
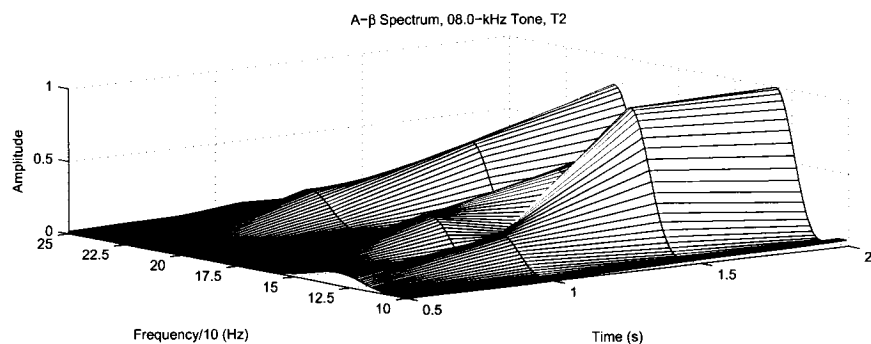
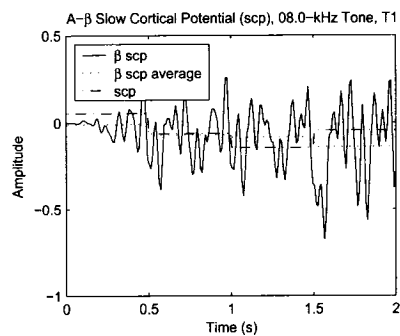
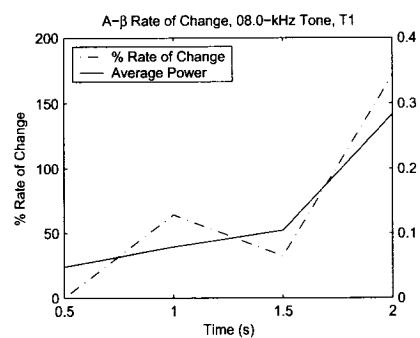
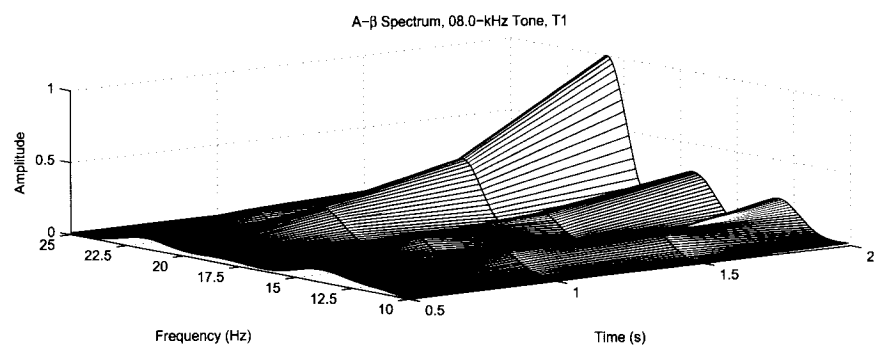
Appendix A: Subject A Experimental Results

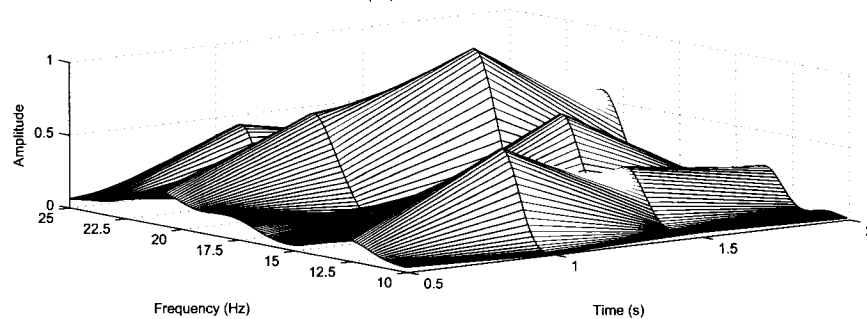
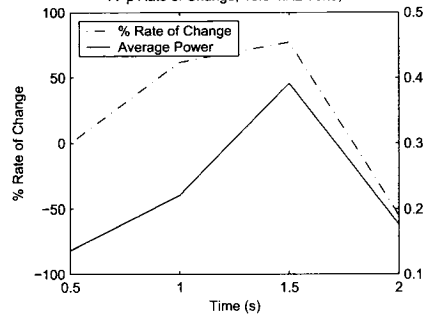
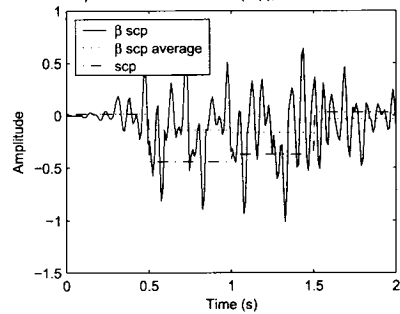
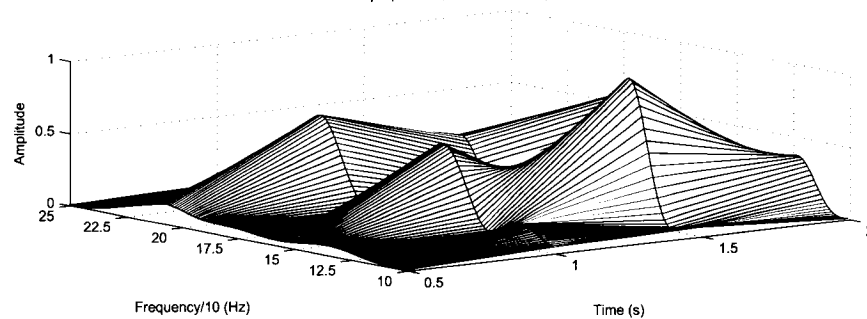
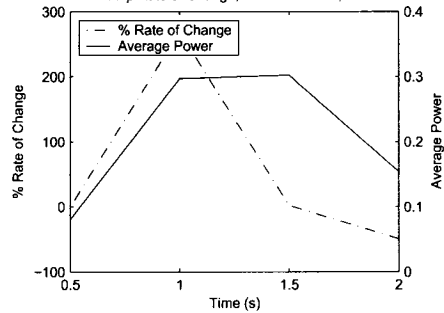
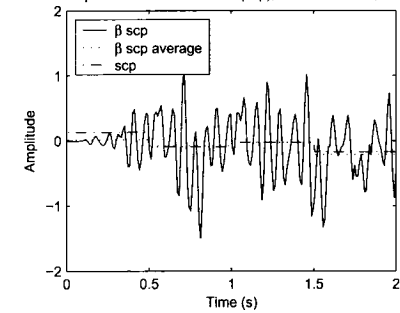
A- α Spectrum, 08.0-kHz Tone, T1A- α Rate of Change, 08.0-kHz Tone, T1A- α Slow Cortical Potential (scp), 08.0-kHz Tone, T1A- α Spectrum, 08.0-kHz Tone, T2A- α Rate of Change, 08.0-kHz Tone, T2A- α Slow Cortical Potential (scp), 08.0-kHz Tone, T2

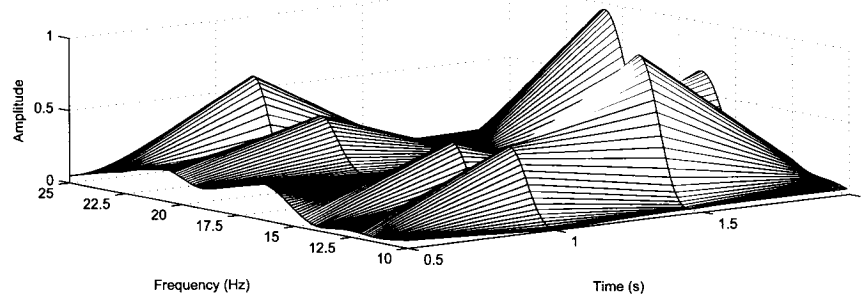
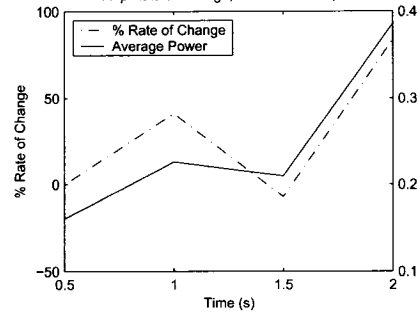
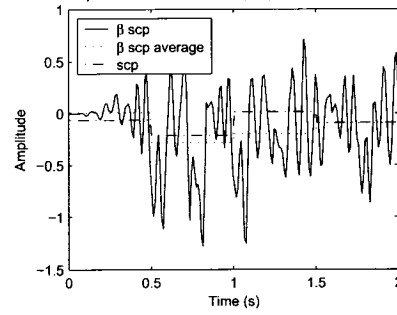
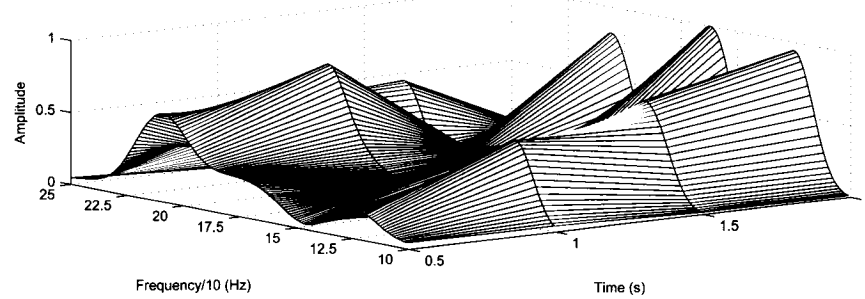
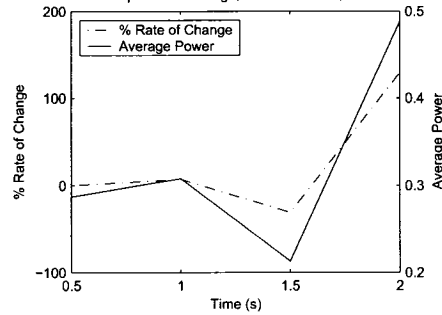
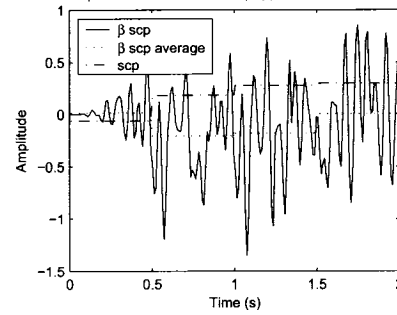
A- α Spectrum, 10.0-kHz Tone, T1A- α Rate of Change, 10.0-kHz Tone, T1A- α Slow Cortical Potential (scp), 10.0-kHz Tone, T1A- α Spectrum, 10.0-kHz Tone, T2A- α Rate of Change, 10.0-kHz Tone, T2A- α Slow Cortical Potential (scp), 10.0-kHz Tone, T2

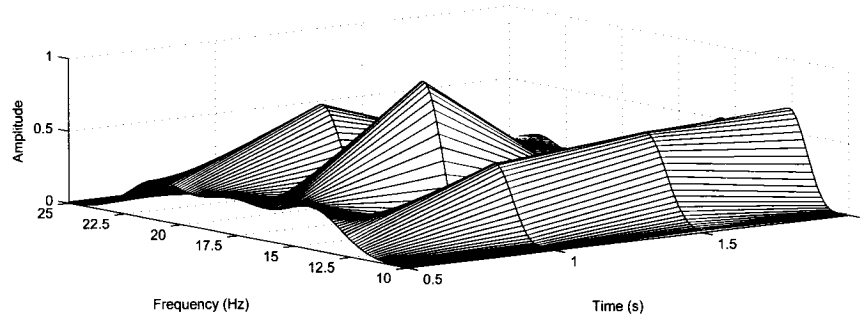
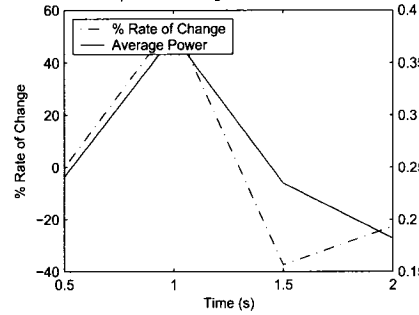
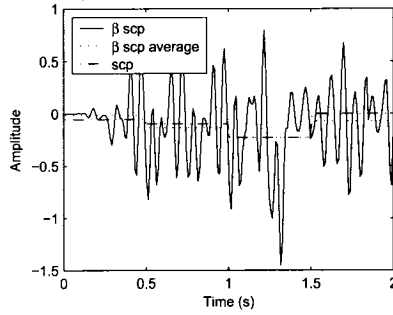
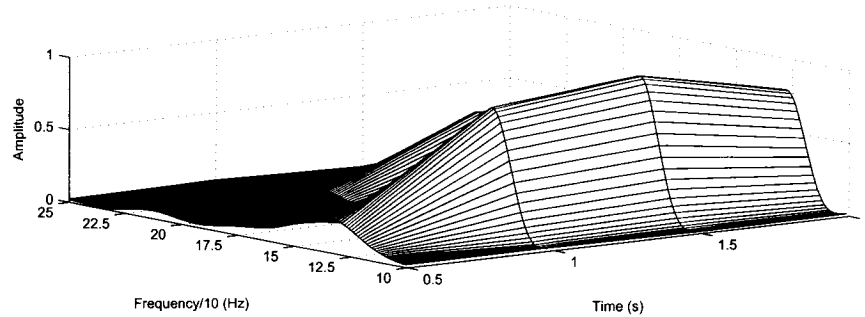
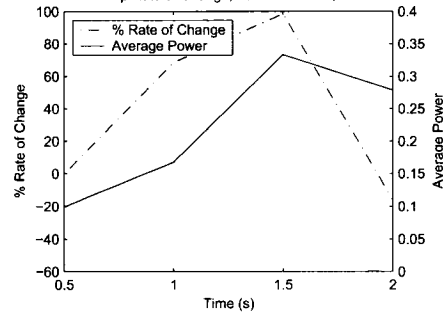
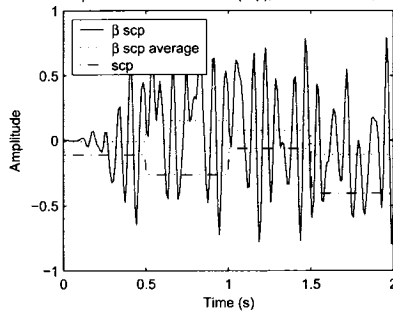


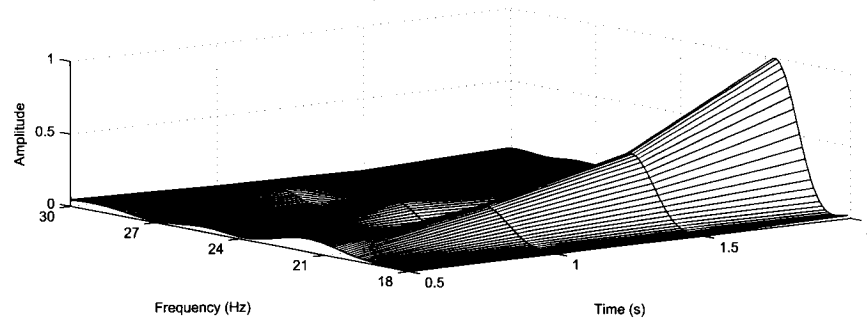
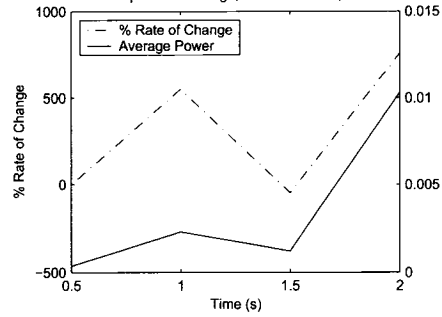
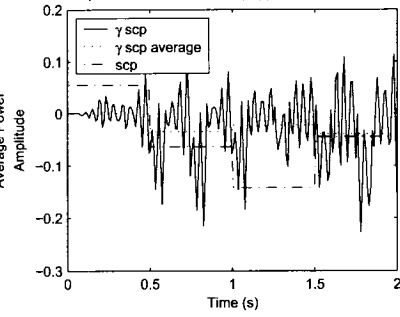
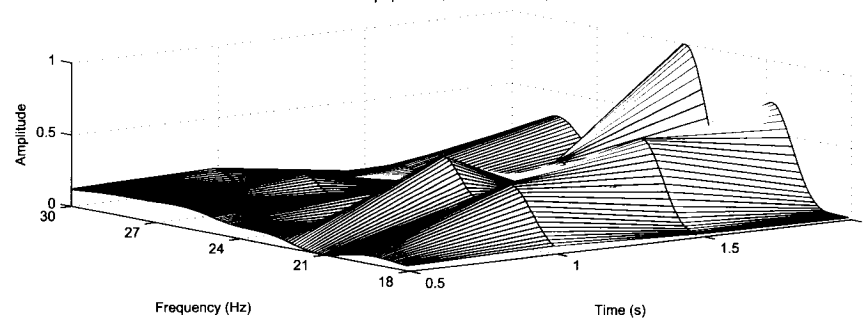
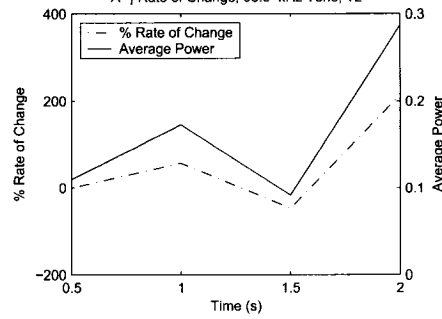
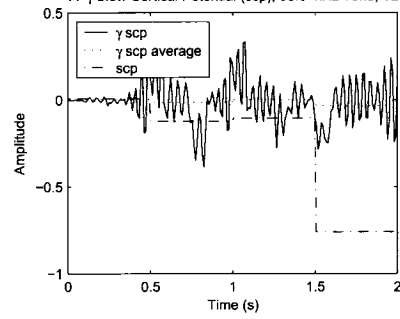
A- α Spectrum, 15.0-kHz Tone, T1A- α Rate of Change, 15.0-kHz Tone, T1A- α Slow Cortical Potential (scp), 15.0-kHz Tone, T1A- α Spectrum, 15.0-kHz Tone, T2A- α Rate of Change, 15.0-kHz Tone, T2A- α Slow Cortical Potential (scp), 15.0-kHz Tone, T2

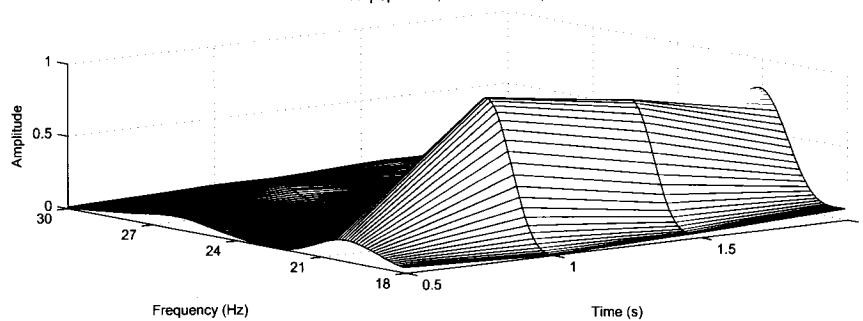
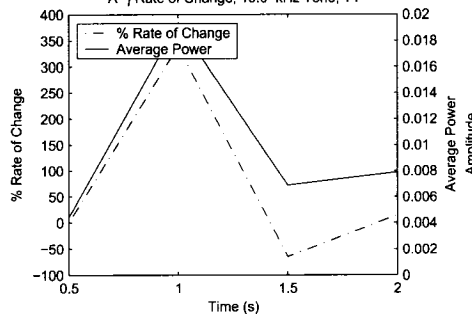
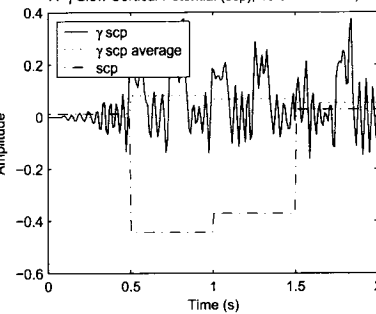
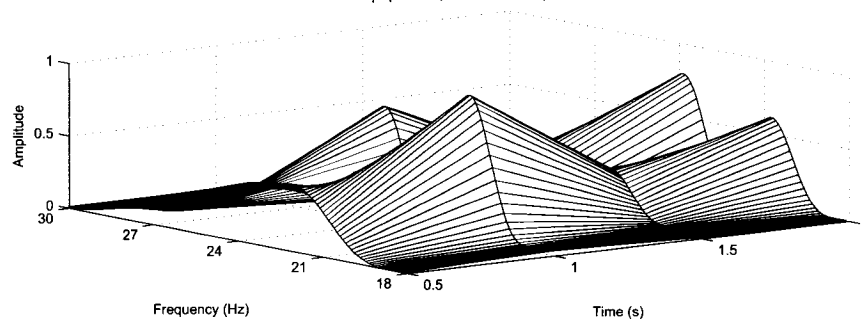
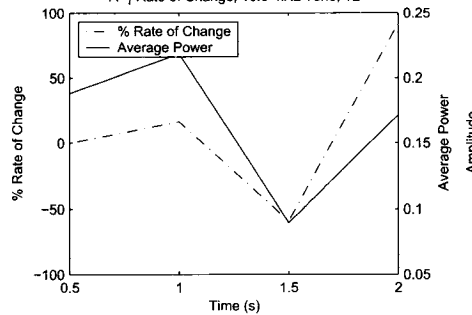
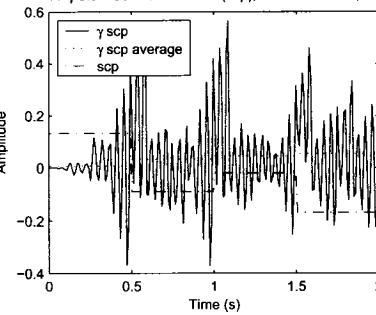


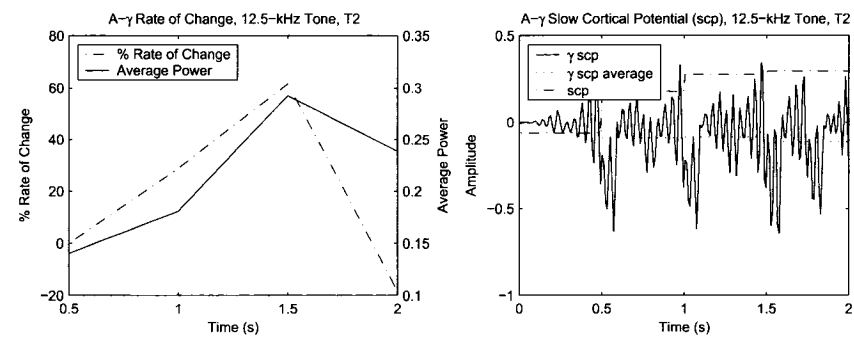
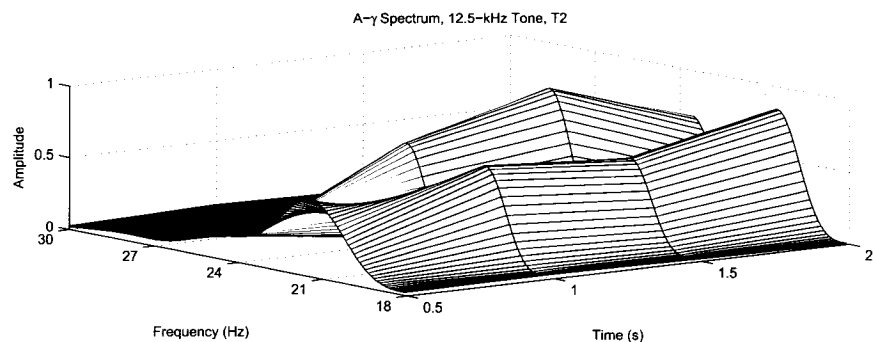
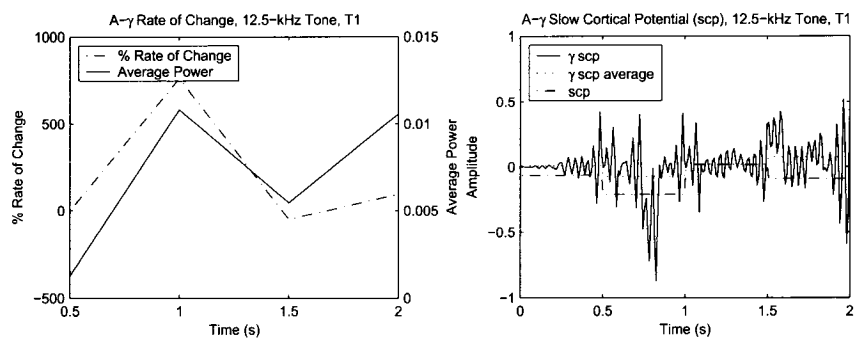
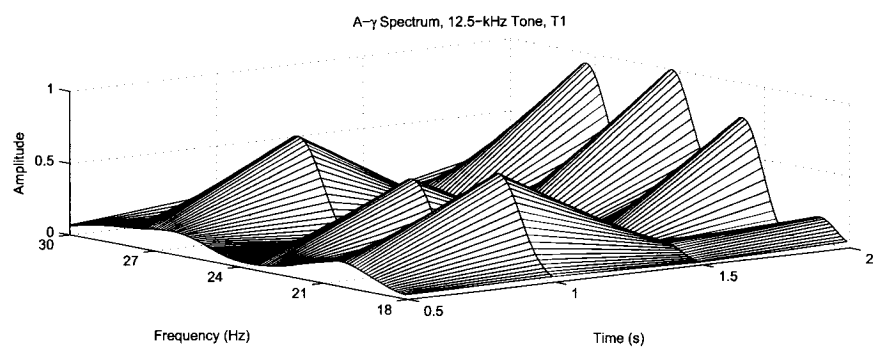
A- β Spectrum, 10.0-kHz Tone, T1A- β Rate of Change, 10.0-kHz Tone, T1A- β Slow Cortical Potential (scp), 10.0-kHz Tone, T1A- β Spectrum, 10.0-kHz Tone, T2A- β Rate of Change, 10.0-kHz Tone, T2A- β Slow Cortical Potential (scp), 10.0-kHz Tone, T2

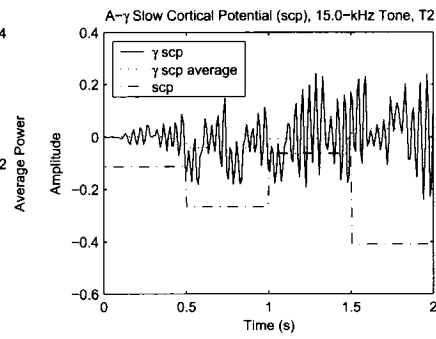
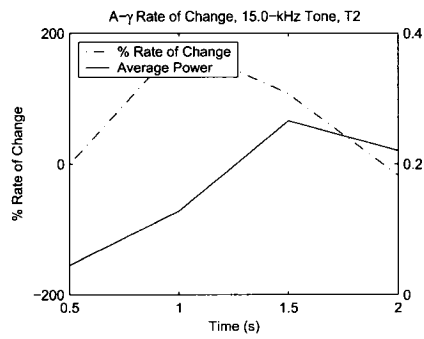
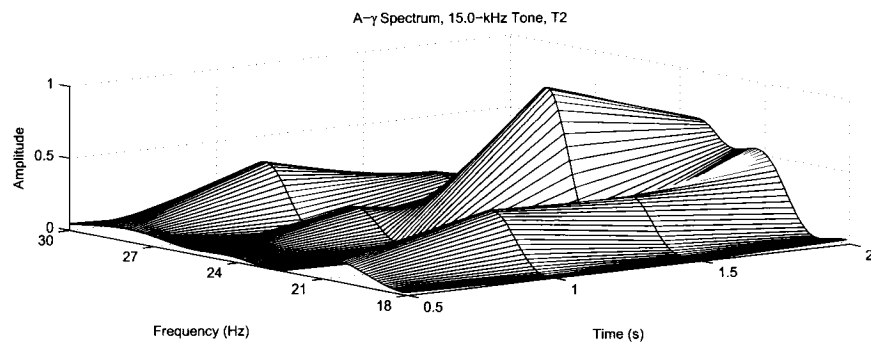
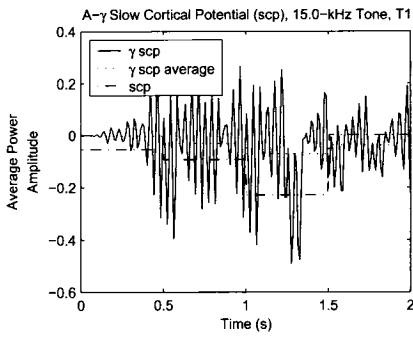
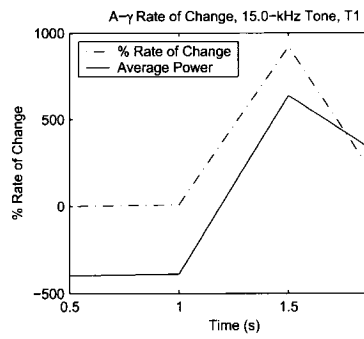
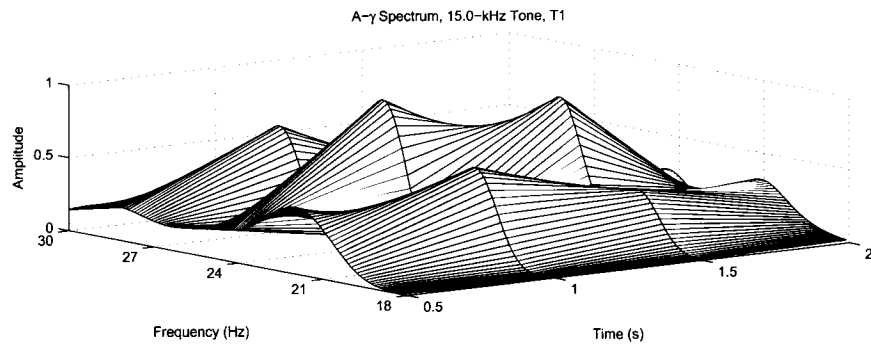
A- β Spectrum, 12.5-kHz Tone, T1A- β Rate of Change, 12.5-kHz Tone, T1A- β Slow Cortical Potential (scp), 12.5-kHz Tone, T1A- β Spectrum, 12.5-kHz Tone, T2A- β Rate of Change, 12.5-kHz Tone, T2A- β Slow Cortical Potential (scp), 12.5-kHz Tone, T2

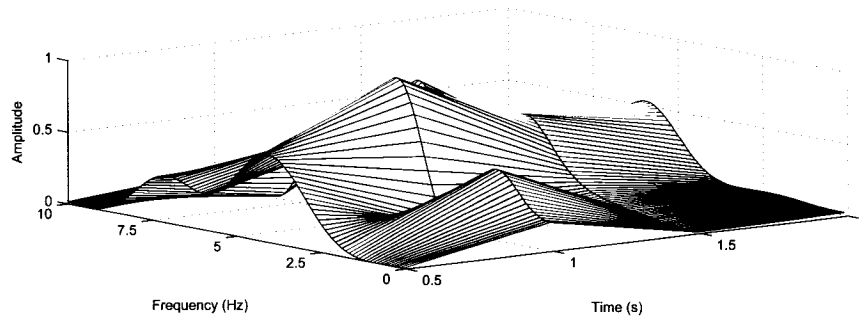
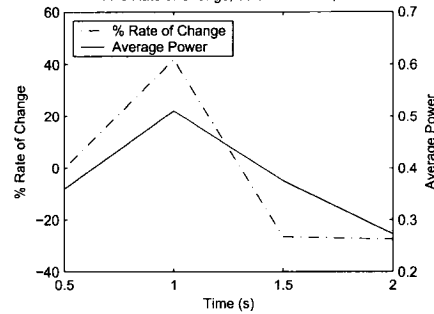
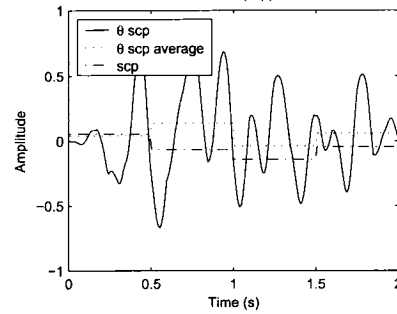
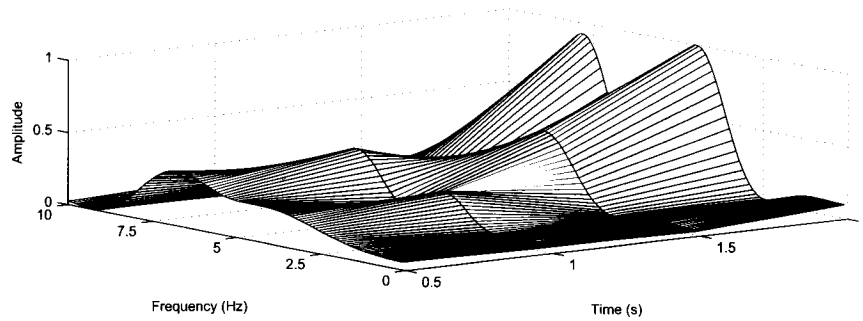
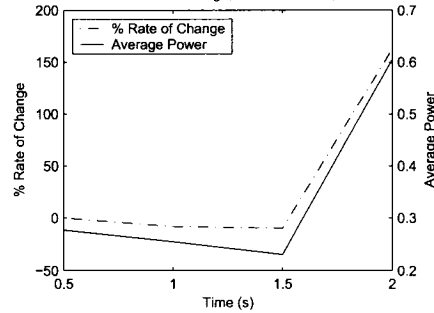
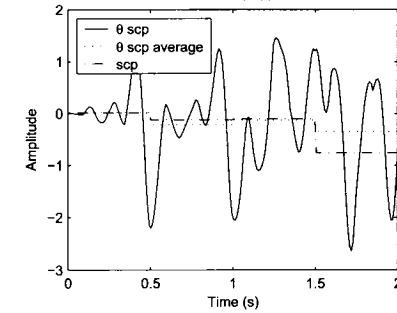
A- β Spectrum, 15.0-kHz Tone, T1A- β Rate of Change, 15.0-kHz Tone, T1A- β Slow Cortical Potential (scp), 15.0-kHz Tone, T1A- β Spectrum, 15.0-kHz Tone, T2A- β Rate of Change, 15.0-kHz Tone, T2A- β Slow Cortical Potential (scp), 15.0-kHz Tone, T2

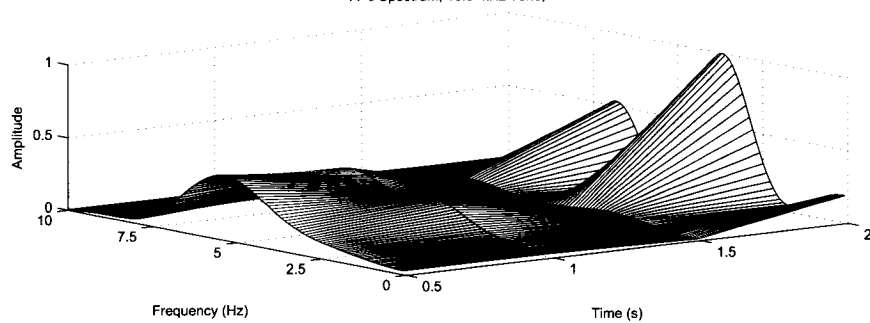
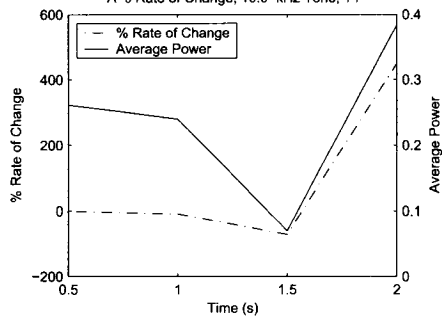
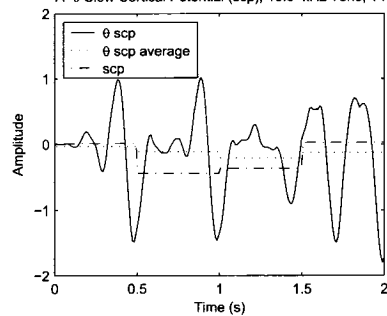
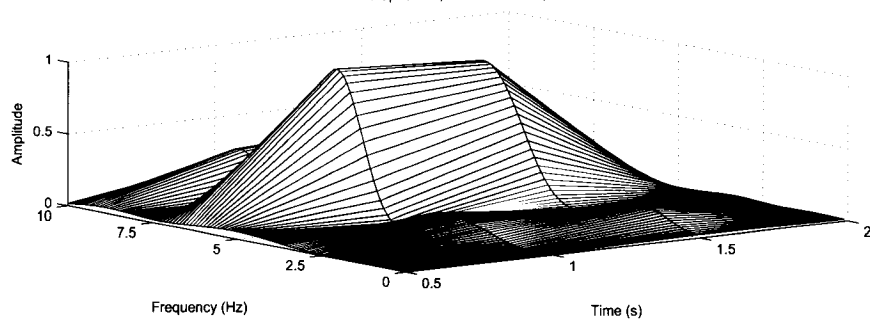
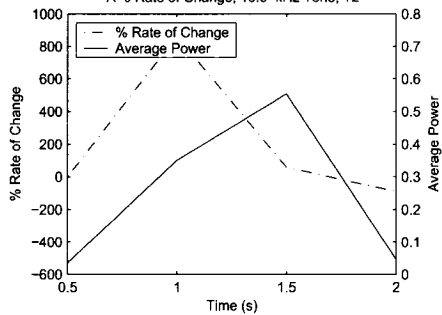
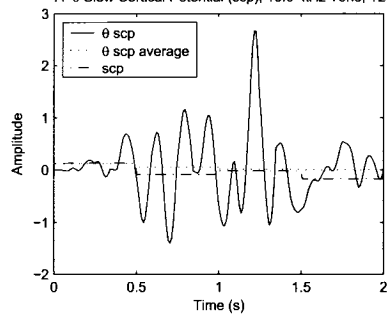
A- γ Spectrum, 08.0-kHz Tone, T1A- γ Rate of Change, 08.0-kHz Tone, T1A- γ Slow Cortical Potential (scp), 08.0-kHz Tone, T1A- γ Spectrum, 08.0-kHz Tone, T2A- γ Rate of Change, 08.0-kHz Tone, T2A- γ Slow Cortical Potential (scp), 08.0-kHz Tone, T2

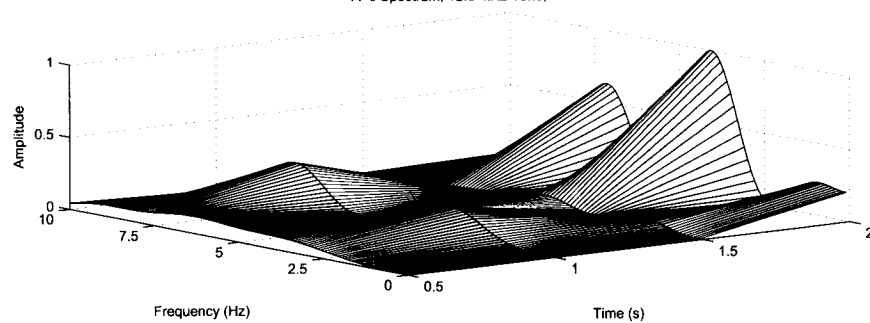
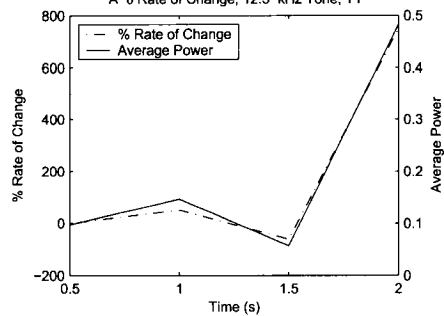
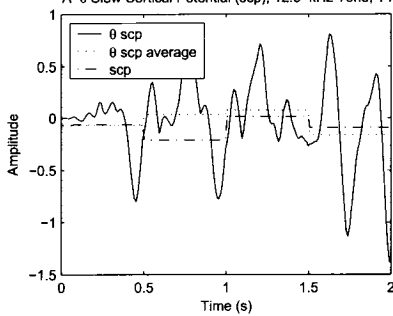
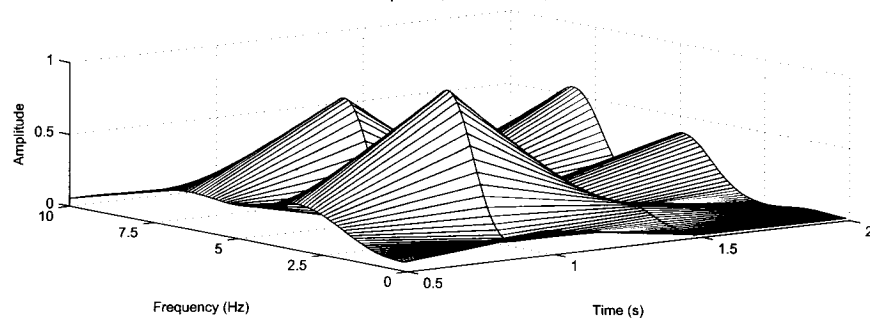
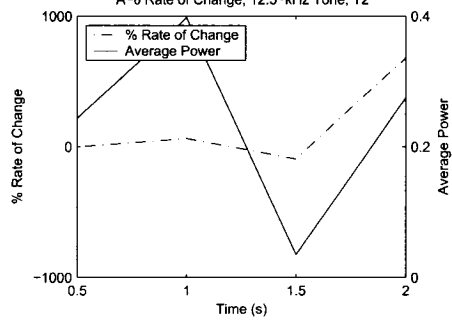
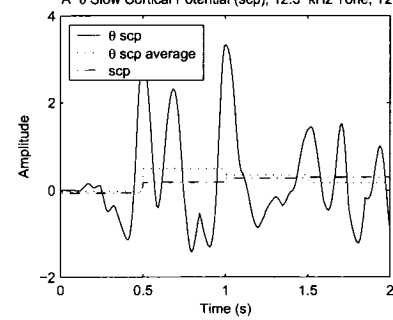
A- γ Spectrum, 10.0-kHz Tone, T1A- γ Rate of Change, 10.0-kHz Tone, T1A- γ Slow Cortical Potential (scp), 10.0-kHz Tone, T1A- γ Spectrum, 10.0-kHz Tone, T2A- γ Rate of Change, 10.0-kHz Tone, T2A- γ Slow Cortical Potential (scp), 10.0-kHz Tone, T2

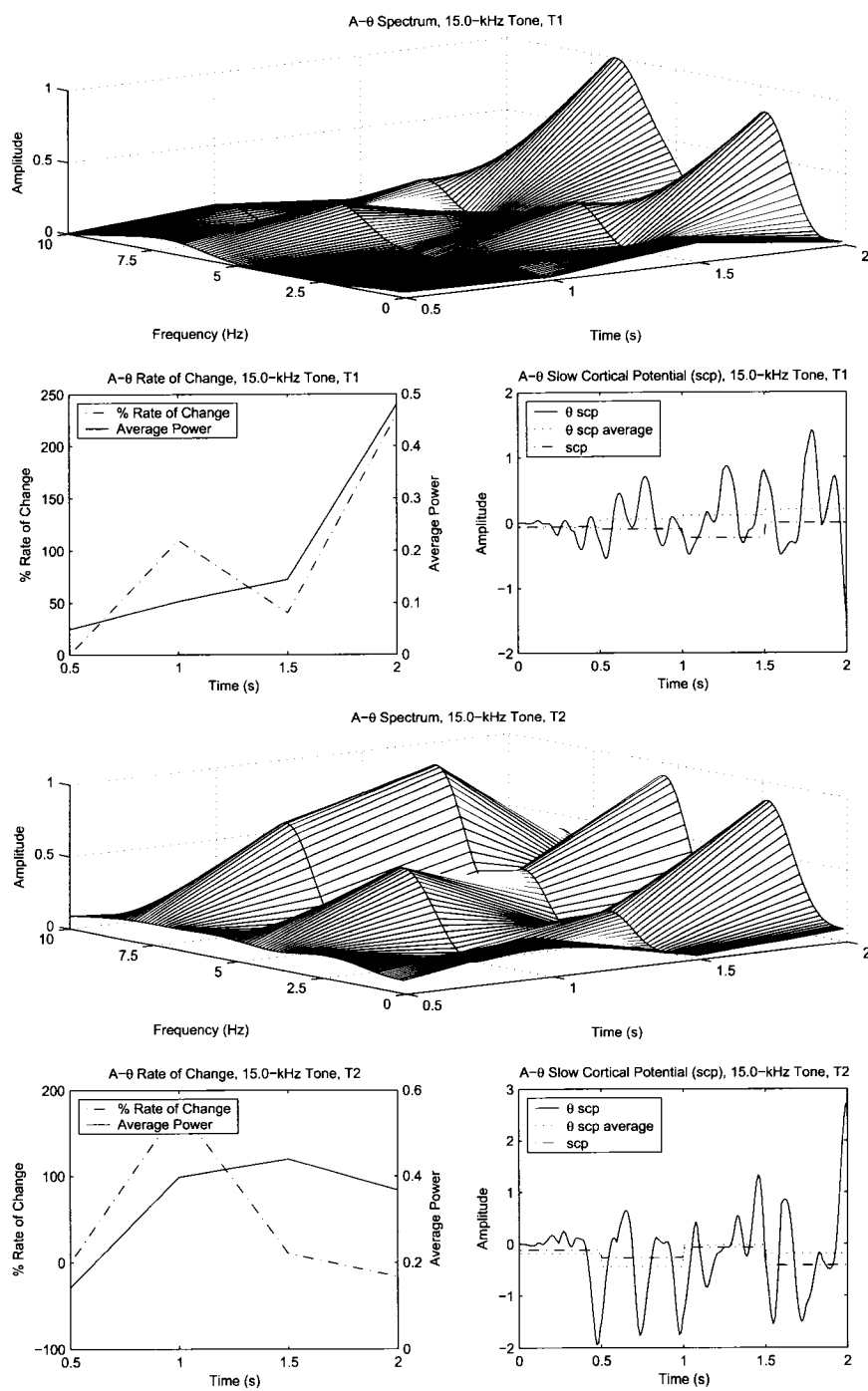


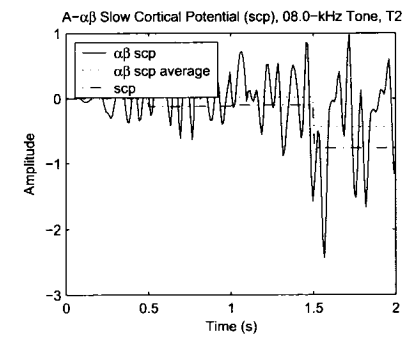
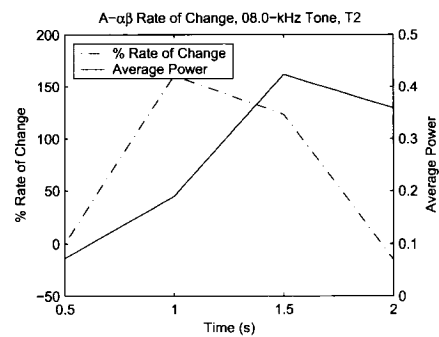
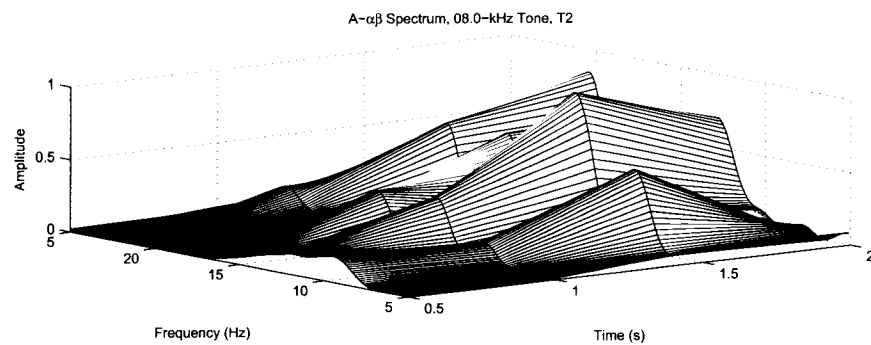
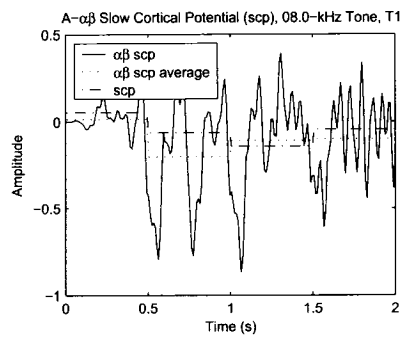
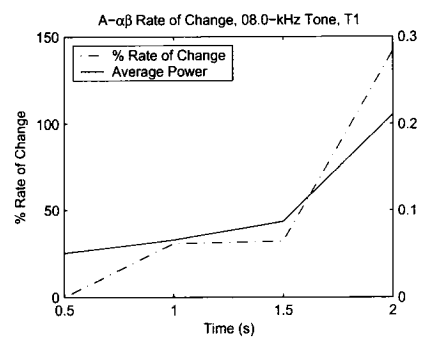
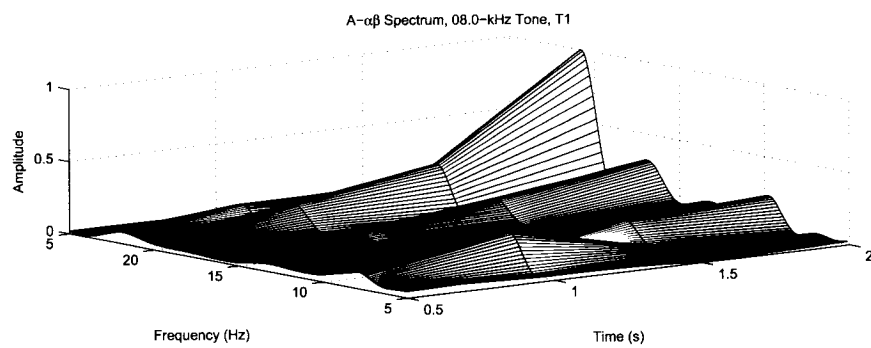


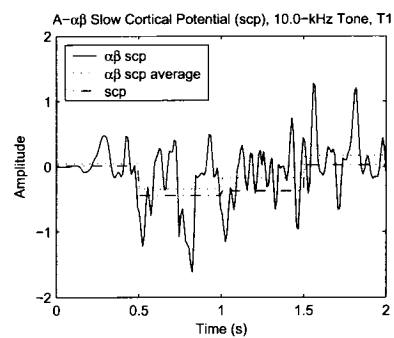
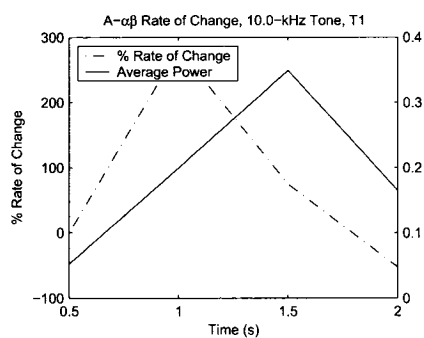
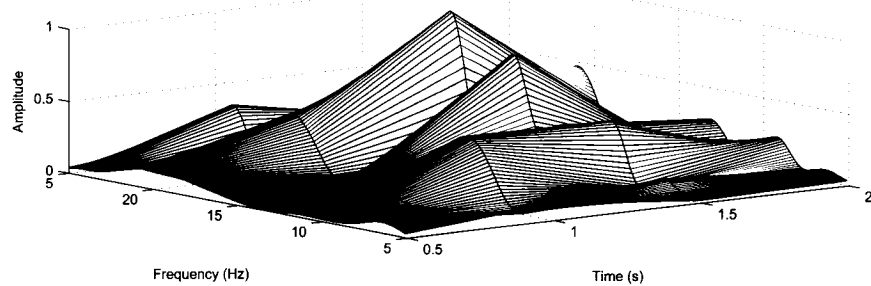
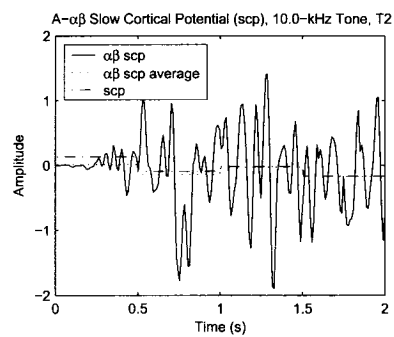
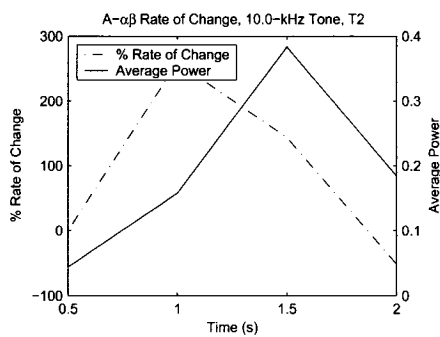
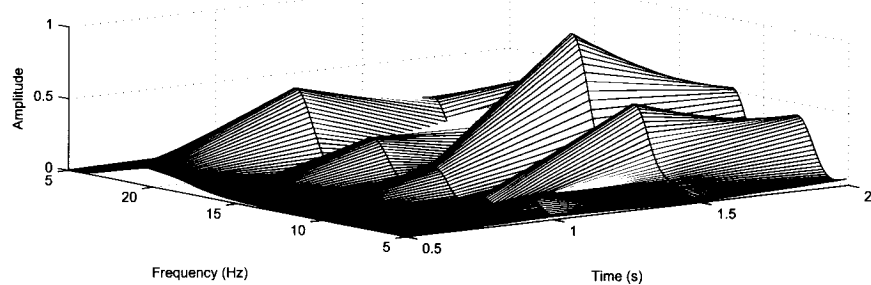
A- θ Spectrum, 08.0-kHz Tone, T1A- θ Rate of Change, 08.0-kHz Tone, T1A- θ Slow Cortical Potential (scp), 08.0-kHz Tone, T1A- θ Spectrum, 08.0-kHz Tone, T2A- θ Rate of Change, 08.0-kHz Tone, T2A- θ Slow Cortical Potential (scp), 08.0-kHz Tone, T2

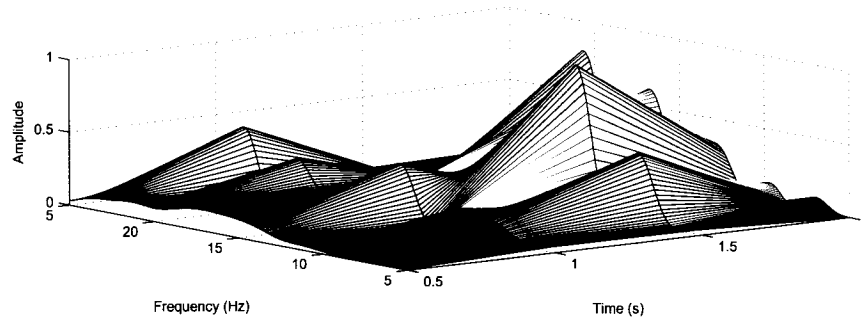
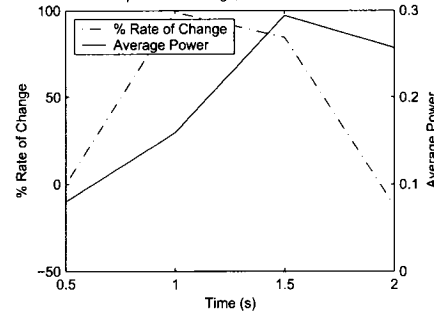
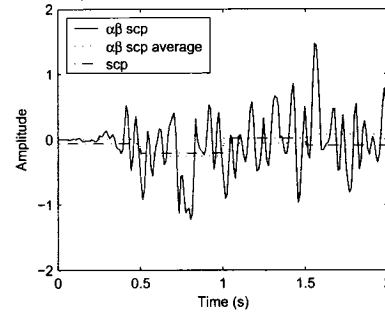
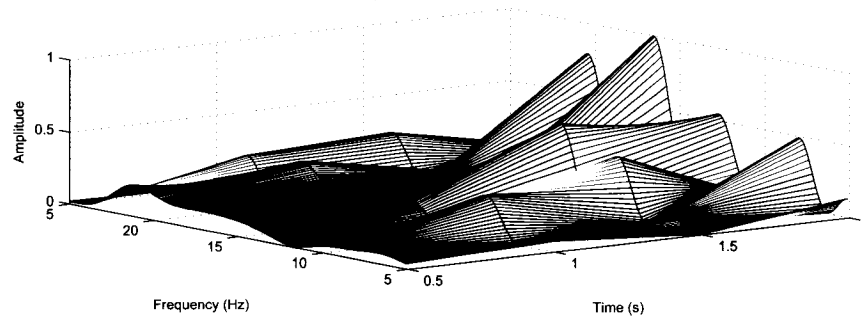
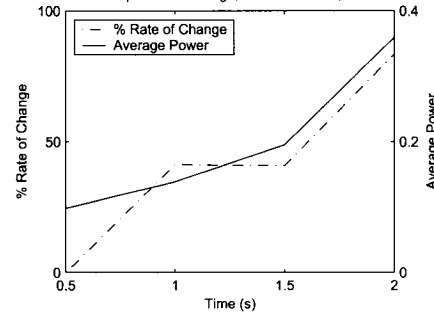
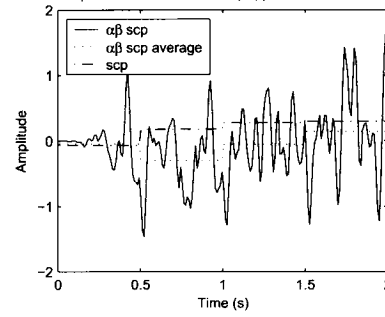
A- θ Spectrum, 10.0-kHz Tone, T1A- θ Rate of Change, 10.0-kHz Tone, T1A- θ Slow Cortical Potential (scp), 10.0-kHz Tone, T1A- θ Spectrum, 10.0-kHz Tone, T2A- θ Rate of Change, 10.0-kHz Tone, T2A- θ Slow Cortical Potential (scp), 10.0-kHz Tone, T2

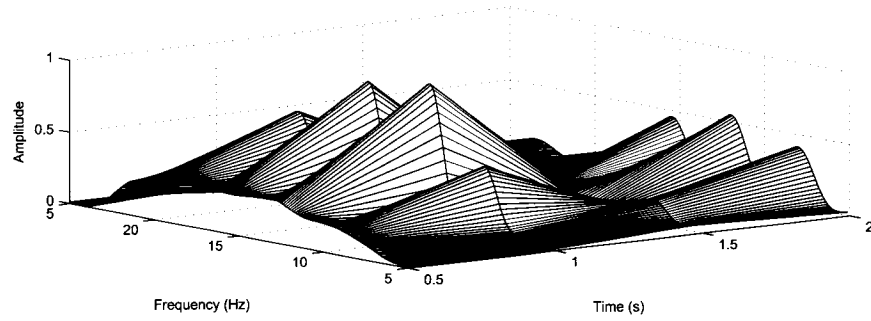
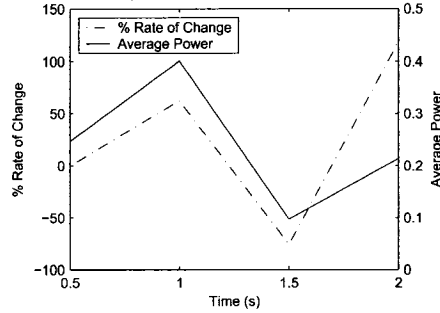
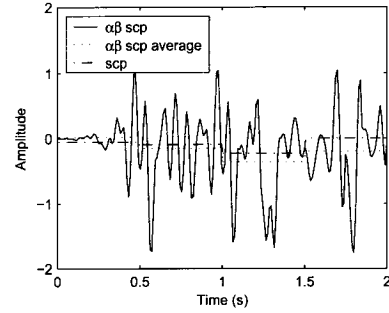
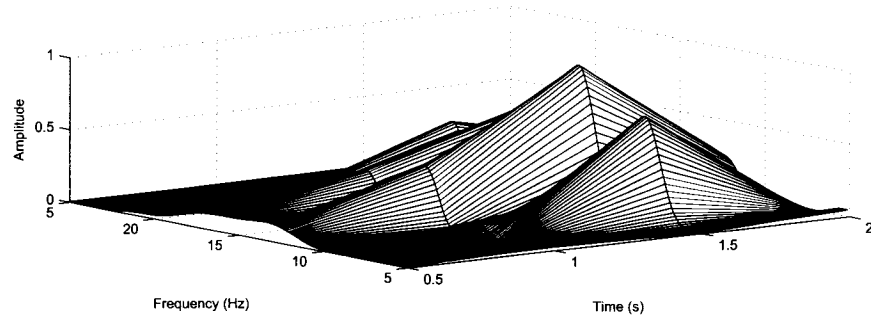
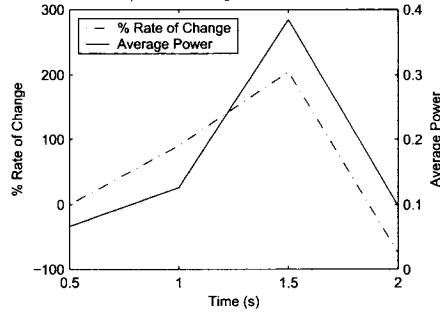
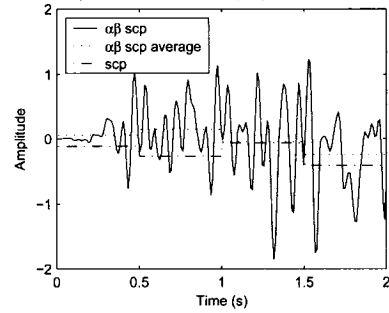
A- θ Spectrum, 12.5-kHz Tone, T1A- θ Rate of Change, 12.5-kHz Tone, T1A- θ Slow Cortical Potential (scp), 12.5-kHz Tone, T1A- θ Spectrum, 12.5-kHz Tone, T2A- θ Rate of Change, 12.5-kHz Tone, T2A- θ Slow Cortical Potential (scp), 12.5-kHz Tone, T2



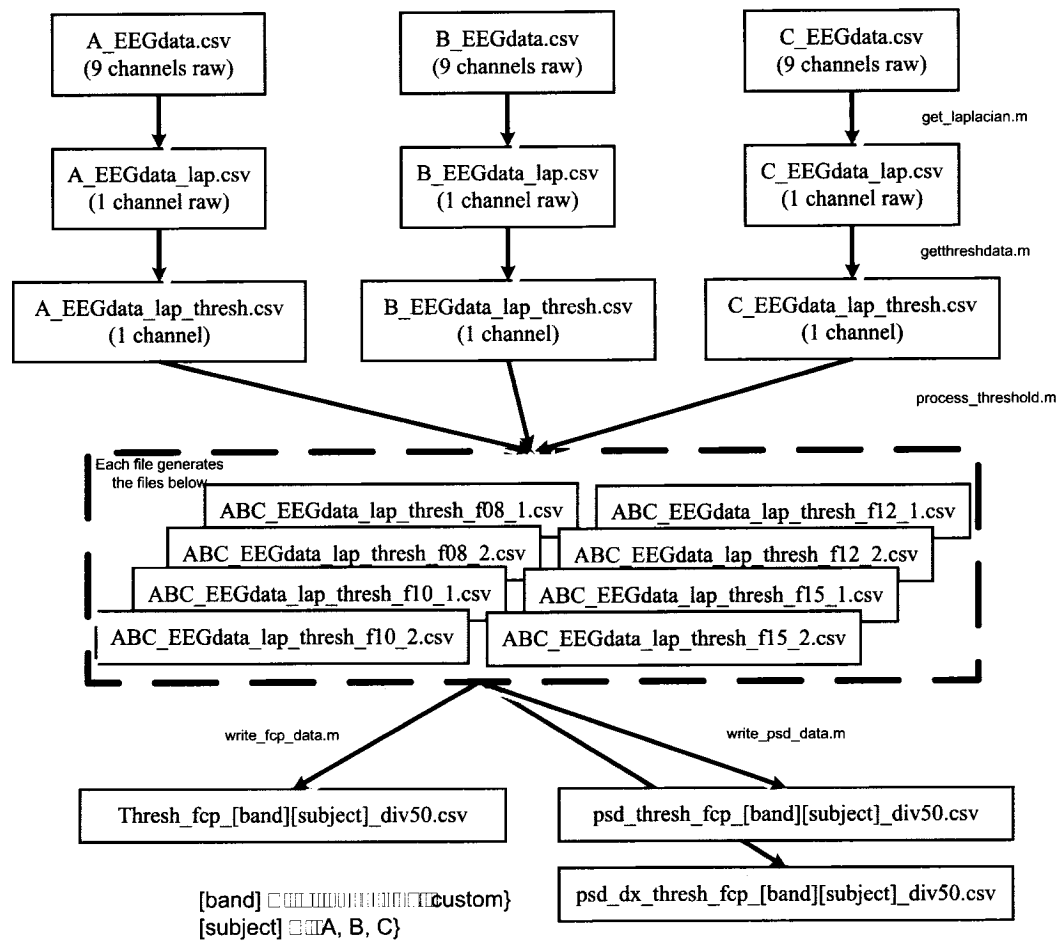


A- $\alpha\beta$ Spectrum, 10.0-kHz Tone, T1A- $\alpha\beta$ Spectrum, 10.0-kHz Tone, T2

A- $\alpha\beta$ Spectrum, 12.5-kHz Tone, T1A- $\alpha\beta$ Rate of Change, 12.5-kHz Tone, T1A- $\alpha\beta$ Slow Cortical Potential (scp), 12.5-kHz Tone, T1A- $\alpha\beta$ Spectrum, 12.5-kHz Tone, T2A- $\alpha\beta$ Rate of Change, 12.5-kHz Tone, T2A- $\alpha\beta$ Slow Cortical Potential (scp), 12.5-kHz Tone, T2

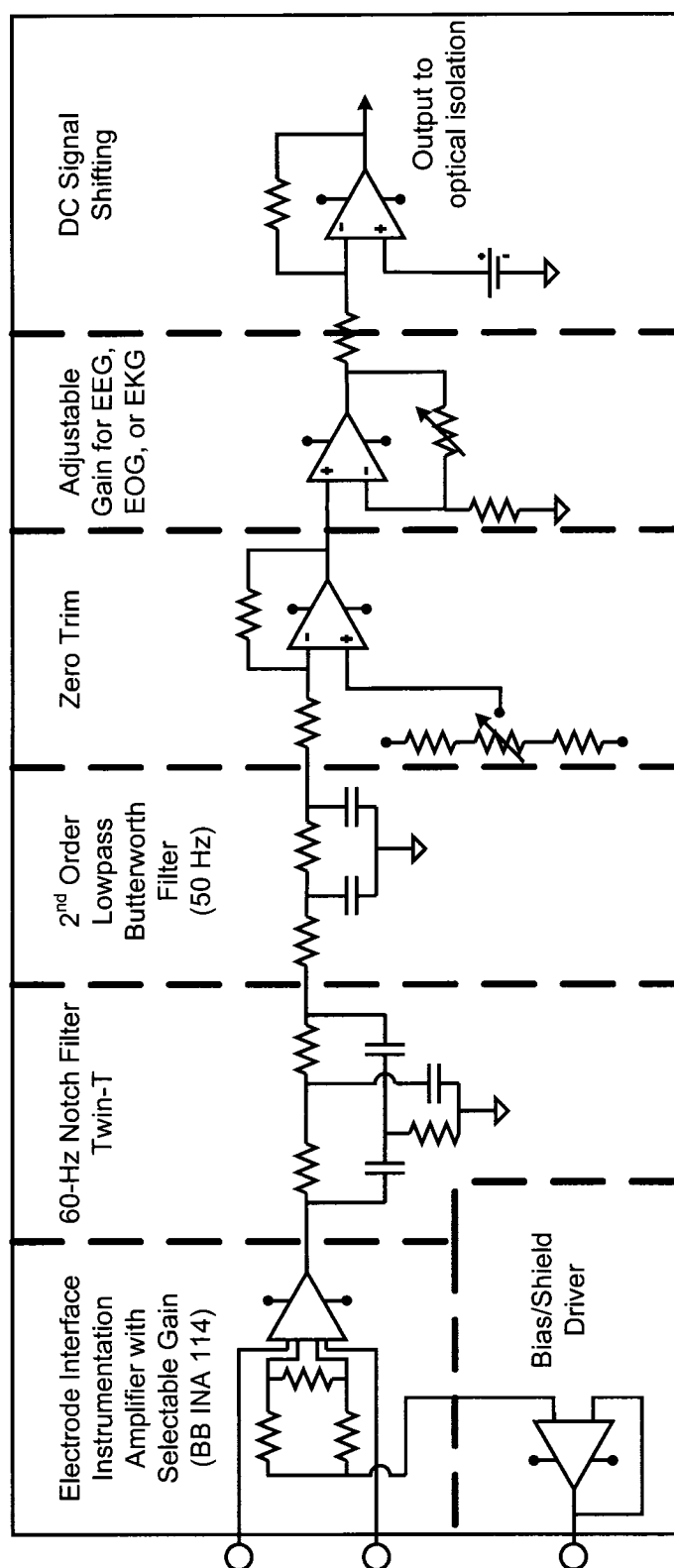
A- $\alpha\beta$ Spectrum, 15.0-kHz Tone, T1A- $\alpha\beta$ Rate of Change, 15.0-kHz Tone, T1A- $\alpha\beta$ Slow Cortical Potential (scp), 15.0-kHz Tone, T1A- $\alpha\beta$ Spectrum, 15.0-kHz Tone, T2A- $\alpha\beta$ Rate of Change, 15.0-kHz Tone, T2A- $\alpha\beta$ Slow Cortical Potential (scp), 15.0-kHz Tone, T2

Appendix B: Threshold Data Analysis Files



The number of files generated for threshold analysis = $8 * 54 = 432$ files

Appendix C: Single Channel Schematic of Electrophysiological Amplifier



Bibliography

- [1] T. Yagi, Y. Ito, H. Kanda, S. Tanaka, H. Watanabe, and Y. Uchikawa. Hybrid retinal implant: fusion of engineering and neuroscience. In *Proceedings of the 1999 IEEE International Conference on Systems, Man, and Cybernetics*, volume 4, pages 382–385, October 1999.
- [2] A. Mudry and L. Dodelé. History of the technological development of air conduction hearing aids. *The Journal of Laryngology & Otology*, 114:418–423, June 2000.
- [3] A. Maynard Engebretson. Benefits of Digital Hearing Aids. *IEEE Engineering in Medicine and Biology*, pages 238–248, April/May 1994.
- [4] Norbert Wiener. *Cybernetics*. M.I.T Press and John Wiley and Sons Inc., 2nd edition, 1961.
- [5] J. von Neumann. *The Computer and the Brain*. Yale Nota Bene, second edition, 2000.
- [6] D. C. Engelbart. *Vistas in Information Handling*, chapter A Conceptual Framework for the Augmentation of Man’s Intellect, pages 1–29. Spartan Books, Washington, DC, 1963.
- [7] D. C. Engelbart and W. K. English. A Research Center for Augmenting Human Intellect. In *AFIPS Conference Proceedings of the 1968 Fall Joint Computer Conference*, volume 33, pages 395–410, San Francisco, CA, USA, December 1968.
- [8] D. C. Engelbart. Intellectual Implications of Multi-Access Computer Networks. In *Proceedings of the Interdisciplinary Conference on Multi-Access Computer Networks*, Austin, TX, USA, April 1970.
- [9] D. C. Engelbart. Toward Augmenting the Human Intellect and Boosting our Collective IQ. *Communications of the ACM*, 38(8):30–33, August 1995.

- [10] D. C. Engelbart. *A History of Personal Workstations*, chapter The Augmented Knowledge Workshop, pages 185–236. ACM Press, New York, 1988.
- [11] W. K. English, D. C. Engelbart, and Melvyn L. Berman. Display-Selection Techniques for Text manipulation. *IEEE Transactions on Human Factors in Electronics*, HFE-8(1):5–15, March 1967.
- [12] Jacques J. Vidal. Toward Direct Brain-Computer Communication. *Annual Review of Biophysics and Bioengineering*, 2:157–180, 1973.
- [13] J. J. Vidal. Real-Time Detection of Brain Events in EEG. *Proceedings of the IEEE*, 65(5):633–641, May 1977.
- [14] Kenneth A. Kooi, Richard P. Tucker, and Robert E. Marshall. *Fundamentals of Electroencephalography*. Harper and Row, 2nd edition, 1978.
- [15] S. Deutsch and A. Deutsch. *Understanding the Nervous System: An Engineering Perspective*. IEEE Press, 1992.
- [16] B. H. Brown, R. H. Smallwood, D. C. Barber, P. V. Lawford, and D. R. Hose. *Medical Physics and Biomedical Engineering*. Medical Physics. Institute of Physics, 1999.
- [17] B. J. Fisch. *EEG Primer: Basic Principles of Digital and Analog EEG*. Elsevier, third revised and enlarged edition, 1999.
- [18] Joseph J. Carr and John M. Brown. *Introduction to Biomedical Equipment Technology*. Prentice Hall, 4th edition, 2001.
- [19] L. A. Farwell and E. Donchin. Talking off the top of your head: toward a menatl prosthesis utilizing event-related brain potentials. *Electroencephalography and Clinical Neurophysiology*, 70:510–523, 1988.
- [20] Jonathan R. Wolpaw, Dennis J. McFarland, Gregory W. Neat, and Catherine A. Forneris. An EEG-Based Brain-Computer Interface for Cursor Control. *Electroencephalography and Clinical Neurophysiology*, (78):252–259, 1991.
- [21] J. R. Wolpaw and D. J. McFarland. Multichannel eeg-based brain-computer communication. *Electroencephalography and Clinical Neurophysiology*, 90:444–449, 1994.

- [22] T. M. Vaughan, J. R. Wolpaw, and E. Donchin. EEG-Based Communication: Prospects and Problems. *IEEE Transactions on Rehabilitation Engineering*, 4(4):425–430, December 1996.
- [23] J. R. Wolpaw, D. Flotzinger, G. Pfurtscheller, and D. J. McFarland. Timing of EEG-Based Cursor Control. *Journal of Clinical Neurophysiology*, 14(6):529–538, November 1997.
- [24] D. J. McFarland, A. T. Lefkowitz, and J. R. Wolpaw. Design and Operation of an EEG-Based Brain-Computer Interface with Digital Signal Processing Technology. *Behaviour Research Methods, Instruments, and Computers*, 29(3):337–345, 1997.
- [25] L. A. Miner, D. J. McFarland, and J. R. Wolpaw. Answering Questions With an Electroencephalogram-Based Brain-Computer Interface. *Arch Phys Med Rehabil*, 79:1029–1033, September 1998.
- [26] C. Guger, W. Harkam, C. Hertnaes, and G. Pfurtscheller. Prosthetic control by an eeg-based brain-computer interface (bci). In *Proc. AAATE 5th European Conference for the Advancement of Assistive Technology*, pages 3–6, Düsseldorf, Germany, November 1999.
- [27] N. Birbaumer, N. Ghanayim, T. Hinterberger, I. Iversen, B. Kotchoubey, A. Kubler, J. Perelmouter, E. Taub, and H. Flor. A Spelling Device for the Paralyzed. *Nature*, 398:297–298, March 1999.
- [28] N. Birbaumer, A. Kubler, N. Ghanayim, T. Hinterberger, J. Perelmouter, J. Kaiser, I. Iversen, B. Kotchoubey, N. Neumann, and H. Flor. The Thought Translation Device (TTD) for Completely Paralyzed Patients. *IEEE Transactions on Rehabilitation Engineering*, 8(2):190–192, June 2000.
- [29] J. Perelmouter and N. Birbaumer. A binary spelling interface with random errors. *IEEE Transactions on Rehabilitation Engineering*, 8(2):227–232, June 2000.
- [30] J. R. Wolpaw, N. Birbaumer, W. J. Heetderks, D. J. McFarland, P. H. Peckham, G. Schalk, L. A. Quatrano, C. J. Robinson, and T. M. Vaughan. Brain-Computer Interface Technology: A Review of the First International Meeting. *IEEE Transactions on Rehabilitation Engineering*, 8(2):164–173, June 2000.

- [31] J. R. Wolpaw, D. J. McFarland, and T. M. Vaughan. Brain-computer interface research at the wadsworth center. *IEEE Transactions on Rehabilitation Engineering*, 8(2):222–226, June 2000.
- [32] J. R. Wolpaw, N. Birbaumer, D. J. McFarland, G. Pfurtscheller, and T. M. Vaughan. Brain-Computer Interfaces for Communication and Control. *Clinical Neurophysiology*, 113:767–791, 2002.
- [33] B. Blankertz, K. R. Muller, G. Curio, T. M. Vaughan, G. Schalk, J. R. Wolpaw, A. Schogl, C. Neuper, G. Pfurtscheller, T. Hinterberger, M. Schroder, and N. Birbaumer. The BCI Competition 2003: Progress and Perspectives in Detection and Discrimination of EEG Single Trials. *IEEE Transactions on Biomedical Engineering*, 51(6):1044–1051, June 2004.
- [34] J. F. Borisoff, S. G. Mason, A. Bashashati, and G. E. Birch. Brain-computer interface design for asynchronous control applications: Improvements to the lf-asd asynchronous brain switch. *IEEE Transactions on Biomedical Engineering*, 51(6):985–992, June 2004.
- [35] G. E. Fabiani, D. J. McFarland, J. R. Wolpaw, and G. Pfurtscheller. Conversion of eeg activity into cursor movement by brain-computer interface (bci). *IEEE Transactions on Neural Systems and Rehabilitation Engineering*, 12(3):331–338, September 2004.
- [36] T. Hinterberger, S. Schmidt, N. Neumann, J. Mellinger, B. Blankertz, G. Curio, and N. Birbaumer. Brain-Computer Communication and Slow Cortical Potentials. *IEEE Transactions on Biomedical Engineering*, 51(6):1011–1018, June 2004.
- [37] G. Schalk, D. J. McFarland, T. Hinterberger, N. Birbaumer, and J. R. Wolpaw. Bci2000: A general-purpose brain-computer interface (bci) system. *IEEE Transactions on Biomedical Engineering*, 51(6):1034–1043, June 2004.
- [38] R. Scherer, G. R. Müller, C. Neuper, B. Graimann, and G. Pfurtscheller. An asynchronously controlled eeg-based virtual keyboard: Improvement of the spelling rate. *IEEE Transactions on Biomedical Engineering*, 51(6):979–984, June 2004.
- [39] M. Tregoubov and N. Birbaumer. On the building of binary spelling interfaces for augmentative communication. *IEEE Transactions on Biomedical Engineering*, 52(2):300–305, February 2005.

- [40] N. Birbaumer and A. Öhman, editors. *The Structure of Emotion*. Hogrefe & Huber, 1993.
- [41] R. W. Picard and J. Healy. Affective Wearables. *Personal Technologies*, pages 231–240, 1997.
- [42] R. W. Picard. *Affective Wearables*. M.I.T Press and John Wiley and Sons Inc., 1997.
- [43] R. W. Picard and G. Cosier. Affective Intelligence. *BT Technol J*, 14(4), October 1997.
- [44] R. W. Picard. Human-computer coupling. *Proceedings of the IEEE*, 86:1803–1807, August 1998.
- [45] J. Healey and R. W. Picard. Digital Processing of Affective Signals. In *Proceedings of the ICASSP*, 1998.
- [46] J. Healey, J. Seger, and R. W. Picard. Quantifying Driver Stress: Developing a System for Collecting and Processing Bio-Metric Signals in Natural Situations. In *Proceedings of the Rocky Mountain Bio-Engineering Symposium (RMBS)*, April 1999.
- [47] T. Starner, J. Weaver, and A. Pentland. A wearable computer based american sign language recognizer. In *Digest of Papers, First International Symposium on Wearable Computers (ISWC)*, pages 130–137, October 1997.
- [48] T. Starner and M. Gandy. The Gesture Pendant: A Self-Illuminating, Wearable, Infrared Computer Vision System for Home Automation Control and Medical Monitoring. *International Symposium on Wearable Computing*, pages 87–94, 2000.
- [49] T. Starner. The Challenges of Wearable Computing: Part 1. *IEEE Micro*, pages 44–52, July-August 2001.
- [50] T. Starner. The Challenges of Wearable Computing: Part 2. *IEEE Micro*, pages 54–67, July-August 2001.
- [51] T. Starner. Wearable Computers: No Longer Science Fiction. *Pervasive Computing*, pages 86–88, January-March 2002.
- [52] T. E. Starner. Wearable Agents. *Pervasive Computing*, pages 90–92, April-June 2002.

- [53] T. E. Starner. The Role of Speech Input in Wearable Computing. *Pervasive Computing*, pages 89–93, July–September 2002.
- [54] T. E. Starner. Attention, Memory, and Wearable Interfaces. *Pervasive Computing*, pages 88–91, October–December 2002.
- [55] S. Mann. Eudaemonic Computing (‘Underwearables’). *International Symposium of Wearable Computers*, page 177, June 1997.
- [56] S. Mann. Humanistic Computing: “WearComp” as a New Framework and Application for Intelligent Signal Processing. *Proceedings of the IEEE*, 86(11):2123–2149, November 1998.
- [57] S. Mann. Wearable computing: Toward humanistic intelligence. *IEEE Intelligent Systems*, pages 10–15, May/June 2001.
- [58] T. Starner. Human-Powered Wearable Computing. *IBM Systems Journal*, 35(3& 4):618–629, 1996.
- [59] E. R. Post, M. Reynolds, M. Gray, J. Paradiso, and N. Gershenfeld. Intrabody Buses for Data and Power. *IEEE Transactions*, pages 52–55, June 1997.
- [60] T. Starner and Y. Maguire. A Heat Dissipation Tutorial for Wearable Computers. In *Proceedings of the Third International Symposium on Wearable Computers (ISWC)*, pages 140–148, 1998.
- [61] T. G. Zimmerman. Personal Area Networks: Near-Field IntraBody Communication. *IBM Systems Journal*, 35(3 and 4):609–617, 1996.
- [62] Victoria T. Nasman, Gloria L. Calhoun, and Grant R. McMillan. *Head Mounted Displays: Designing for the User*, chapter Chapter 10 - Brain Actuated Control and HMDs, pages 285–312. Optical and Electro-Optical Engineering Series. McGraw-Hill, 1997.
- [63] K. S. Jones, M. S. Middendorf, G. Calhoun, and G. McMillan. Evaluation of an Electroencephalographic-Based control device. *Proceedings of the Human Factors and Ergonomics Society 42nd Annl. Meeting*, 1:491–495, October 1998.
- [64] M. S. Middendorf, G. McMillan, G. Calhoun, and K. S. Jones. Brain-computer interfaces based on the steady-state visual evoked response. *IEEE Transactions on Rehabilitation Engineering* [see also *IEEE Trans.*

on *Neural Systems and Rehabilitation Engineering*], 8(2):211–214, June 2000.

- [65] M. J. Zieniewixz, D. C. Johnson, D. C. Wong, and J. D. Flatt. The Evolution of Army Wearable Computers. *Pervasive Computing*, pages 30–40, October–December 2002.
- [66] Steve Ditlea. The PC goes ready-to-wear. *IEEE Spectrum*, pages 35–39, October 2000.
- [67] D. Marculescu, R. Marculescu, S. Park, and S. Jayaraman. Ready to Wear. *IEEE Spectrum*, 40(10):28–32, October 2003.
- [68] E. Jovanov, A. O. Lords, D. Raskovic, P. G. Cox, R. Adhami, and F. Andrasik. Stress monitoring using a distributed wireless intelligent sensor system. *IEEE Engineering in medicine and Biology*, 22(3):49–55, 2003.
- [69] E. Waterhouse. New horizons in ambulatory electroencephalography. *IEEE Engineering in medicine and Biology*, 22(3):74–79, 2003.
- [70] M. Manto, M. Topping, M. Soede, J. Sanchez-Lacuesta, W. Harwin, J. Pons, J. Williams, S. Skaarup, and L. Normie. Dynamically responsive intervention for tremor suppression. *IEEE Engineering in medicine and Biology*, 22(3):120–132, 2003.
- [71] J. J. Collins and C. J. De Luca. Random Walking During Quiet Standing. *The American Physical Society*, 73(5):764–767, August 1994.
- [72] R. Barea, L. Boquete, M. Mazo, and E. López. System for assisted mobility using eye movements based on electrooculography. *IEEE Transactions on Neural Systems and Rehabilitation Engineering*, 10(4):209–218, December 2002.
- [73] J. Cavuoto. Neural engineering’s image problem. *IEEE Spectrum*, pages 32–37, April 2004.
- [74] D. J. Weber, R. B. Stein, K. M. Chan, G. E. Loeb, F. J. R. Richmond, R. Rolf, K. James, and S. L. Chong. Bionic walkade for correcting foot drop. *IEEE Transactions on Neural Systems and Rehabilitation Engineering*, 13(2):242–246, June 2005.
- [75] *Neural Prostheses for Restoration of Sensory and Motor Function*. Methods and New Frontiers in Neuroscience. CRC Press, 2000.

- [76] T. E. Doyle, Z. Kucеровsky, and W. D. Greason. The digital hearing aid, wearable computing, and electrophysiological response. *Joint Proceedings of the 39th Annual Rocky Mountain Bioengineering Symposium and the 39th International ISA Biomedical Sciences Instrumentation Symposium*, RMBS 38/ISA 419:129–134, April 2002.
- [77] A. E. Pavlik, J.T Inglis, M. Lauk, L. Oddsson, and J. J. Collins. The effects of stochastic galvanic vestibular stimulation on human postural sway. *Experimental Brain Research*, 124:273–280, 1999.
- [78] Margit Gföhler and Peter Lugner. Cycling by Means of Functional Electrical Stimulation. *IEEE Transactions on Rehabilitation Engineering*, 8(2):233–243, June 2000.
- [79] *Hearing Aids: A Manual for Clinicians*. Lippincott - Raven, 1996.
- [80] Noam Chomsky. *Language and Problems of Knowledge*. The Managua Lectures. The MIT Press, 1988.
- [81] L. R. Rabiner. *Digital Processing of Speech Signals*. Prentice-Hall, 1978.
- [82] T. Parsons. *Voice and Speech Processing*. McGrawHill, 1986.
- [83] D. B. Fry. *The Physics of Speech*. Cambridge Textbooks in Linguistics. Cambridge University Press, 1979.
- [84] R. L. Schow and M. A. Nerbonne. *Introduction to Aural Rehabilitation*. Perspectives in Audiology Series. Pro-Ed, 1989.
- [85] S. Rosen. Presbycusis study of a relatively noise-free population in the sudan. *Transactions of the American Otological Society*, 50:135 – 152, 1962.
- [86] R. Grant (clinical audiologist). Audiological evaluation, May 2001.
- [87] R. Gao, S. Basseas, D. T. Bargiotas, and L. H. Tsoukalas. Next-generation hearing prosthetics. *IEEE Robotics and Automation Magazine*, pages 21–25, March 2003.
- [88] B. G. Frankel. *Adult-Onset Hearing Impairment: Social and Psychological Correlates of Adjustment*. PhD thesis, Department of Epidemiology and Biostatistics, Faculty of Science, University of Western Ontario, London, Ontario, 1981.

- [89] D. A. Ramsdell. *Hearing and Deafness*. Holt, Rinehart and Winston, 4th edition, 1978.
- [90] H. Myklebust. *The Psychology of Deafness*. Grune and Straton, 2nd edition, 1964.
- [91] A. Vonlanthen. *Hearing Instrument Technology: for the hearing health-care professional*. Independent, 1st edition, 1995. ISBN 3-274-00089-2.
- [92] Philipos C. Loizou. Introduction to Cochlear Implants. *IEEE Engineering in Medicine and Biology*, pages 32–42, January/February 1999.
- [93] H. G. McAllister, N. D. Black, and N. Waterman. Hearing Aids - a development with digital signal processing devices. *Computing and Control Engineering Journal*, pages 283–291, December 1995.
- [94] Thomas E. Doyle. A Study of Frequency Shifting for the Application of Informtaion Retention. Geophysics (gp504b) Digital Filtering Independent Project, University of Western Ontario, Geophysics Department, University of Western Ontario, March 1998.
- [95] Jean Babel, Nicolas Stangos, Silvio Korol, and Micheline Spiritus. *Ocular Electrophysiology*. Georg Thieme Publishers, 1977.
- [96] Robert M. Stern, William J. Ray, and Karen S. Quigley. *Psychophysiological Recording*. Oxford University Press, 2001.
- [97] Kenneth Hugdahl. *Psychophysiology*. Harvard University Press, 1995.
- [98] Kenshiro Uenoyama, Noriko Uenoyama, and Iwao Iinuma. Vector-Electro-Oculography and Its Clinical Application: Two-Dimensional Recording of Eye Movements. *British Journal of Ophthalmology*, 48(6):318–329, June 1964.
- [99] K. Sauve. Gamma-band synchronous oscillations: Recent evidence regarding their functional significance. *Consciousness and Cognition*, 8:213–224, 1999.
- [100] C. H. Vanderwolf. Are neocortical gamma waves related to conciousness? *Brain Research*, 885:217–224, 2000.
- [101] E. T. Richey and Richard Namon. *EEG Instrumentation and Technology*. Charles C. Thomas, 1976.

- [102] John S. Ebersole and Samuel L. Bridgers. *Ambulatory EEG Monitoring*, chapter Chapter 4 - Montage Design for Cassette EEG. Raven Press, 1989.
 - [103] L. R. Rabiner and B. Gold. *Theory and Application of Digital Signal Processing*, chapter The Theory and Approximation of Finite Duration Impulse Response Digital Filters, pages 75–204. Prentice Hall, 1975.
 - [104] R. G. Lyons. *Understanding Digital Signal Processing*, chapter Appendix H. Prentice Hall, 2nd edition, 2004.
 - [105] J. G. Proakis and D. G. Manolakis. *Digital Signal Processing Principles, Algorithms, and Applications*, chapter Appendix C. Prentice Hall, 3rd edition, 1996.
 - [106] D. M. Mackay. On-line source-density computation with minimum of electrodes. *Electroencephalography and Clinical Neurophysiology*, 56(4):696–698, 1983.
 - [107] D. M. MacKay. Source density analysis of scalp potentials during evaluated action. *Experimental Brain Research*, 54(1):73–85, 1984.
 - [108] D. Regan. *Human Brain Electrophysiology: Evoked Potentials and Evoked Magnetic Fields in Science and Medicine*. Elsevier, 1989.
 - [109] D. J. Mcfarland, L. M. McCane, S. V. David, and J. R. Wolpaw. Spatial filter selection for eeg-based communication. *Electroencephalography and clinical Neurophysiology*, 103:386 – 394, 1997.
 - [110] B. D. Mensh, J. Werfel, and H. S. Seung. Bci competition 2003 — data set ia: combining gamma-band power with slow cortical potentials to improve single trial classification of electroencephalographic signals. *IEEE Transactions on Biomedical Engineering*, 51(6):1052–1056, 2004.
 - [111] J. H. Mathews and K. D. Fink. *Numerical Methods Using Matlab*. Pearson, 4 edition, 2004.
 - [112] S. C. Chapra and R. P. Canale. *Numerical Methods for Engineers*. McGrawHill, 4 edition, 2002.
 - [113] D. J. Klass. Guidelines for clinical practice & facility standards: Electroencephalography. Technical report, College of Physicians and Surgeons of Ontario, September 2000.
-

- [114] Dan Jones. Personal communications, 2001.
- [115] Alan V. Oppenheim, Ronald W. Schafer, and John R. Buck. *Discrete-Time Signal Processing*. Signal Processing Series. Prentice Hall, 1999.
- [116] A. I. Belousov, S. A. Verzhakov, and J. vonFrese. A flexible classification approach with optimal generalisation performance: support vector machines. *Chemometrics and Intelligent Laboratory Systems*, 64:15 – 25, 2002.
- [117] K. Müller, S. Mika, G. Rätsch, K. Tsuda, and B. Schölkopf. An introduction to kernel-based learning algorithms. *IEEE Transactions on Neural Networks*, 12(2):181 – 202, March 2001.
- [118] V. Kecman. Support vector machine basics. Technical report, The University of Auckland, School of Engineering, April 2004.

Vita

NAME:	Thomas E. Doyle, P.Eng
PLACE OF BIRTH:	Toronto (East York), Ontario, Canada
YEAR OF BIRTH:	1972
POST-SECONDARY EDUCATION AND DEGREES:	University of Western Ontario London, Ontario 1997-1998 M.E.Sc. University of Western Ontario London, Ontario 1991-1997 B.E.Sc. (Electrical Engineering) University of Western Ontario London, Ontario 1993-1997 B.Sc. (Computer Science)
HONOURS AND AWARDS:	Ontario Graduate Scholarship and the Ontario Graduate Scholarship for Science and Technology Awarded by the Provincial Government of Ontario 1999-2003 Special University Scholarship Awarded by the University of Western Ontario 1998 - 1999
RELATED EXPERIENCE:	Lecturer - Engineering Computation Department of Electrical and Computer Engineering McMaster University 2003 - 2006 Graduate Teaching and Research Assistant University of Western Ontario 1997 - 2003 Research and Development Engineer PlasSep Limited 1997 - 1998